

EDITORIAL BOARD

Editor-in-Chief

I.V. Krivtsun E.O. Paton Electric Welding Institute, Kyiv, Ukraine

Deputy Editor-in-Chief

S.V. Akhonin E.O. Paton Electric Welding Institute, Kyiv, Ukraine

Deputy Editor-in-Chief

L.M. Lobanov E.O. Paton Electric Welding Institute, Kyiv, Ukraine

Editorial Board Members

O.M. Berdnikova E.O. Paton Electric Welding Institute, Kyiv, Ukraine
Chang Yunlong School of Materials Science and Engineering, Shenyang University of Technology, Shenyang, China
V.V. Dmitrik NTUU «Kharkiv Polytechnic Institute», Kharkiv, Ukraine
Dong Chunlin China-Ukraine Institute of Welding of Guangdong Academy of Sciences, Guangzhou, China
M. Gasik Aalto University Foundation, Finland
A. Gumenyuk Bundesanstalt für Materialforschung und –prüfung (BAM), Berlin, Germany
V.V. Knysh E.O. Paton Electric Welding Institute, Kyiv, Ukraine
V.M. Korzhyk E.O. Paton Electric Welding Institute, Kyiv, Ukraine
V.V. Kvasnytskyi NTUU «Igor Sikorsky Kyiv Polytechnic Institute», Kyiv, Ukraine
Yu.M. Lankin E.O. Paton Electric Welding Institute, Kyiv, Ukraine
S.Yu. Maksymov E.O. Paton Electric Welding Institute, Kyiv, Ukraine
Yupiter HP Manurung Smart Manufacturing Research Institute, Universiti Teknologi MARA, Shah Alam, Malaysia
M.O. Pashchin E.O. Paton Electric Welding Institute, Kyiv, Ukraine
Ya. Pilarczyk Welding Institute, Gliwice, Poland
V.D. Poznyakov E.O. Paton Electric Welding Institute, Kyiv, Ukraine
U. Reisingen Welding and Joining Institute, Aachen, Germany
I.O. Ryabtsev E.O. Paton Electric Welding Institute, Kyiv, Ukraine
V.M. Uchanin Karpenko Physico-Mechanical Institute, Lviv, Ukraine
Yang Yongqiang South China University of Technology, Guangzhou, China

Managing Editor

O.T. Zelnichenko International Association «Welding», Kyiv, Ukraine

Address of Editorial Board

E.O. Paton Electric Welding Institute, 11 Kazymyr Malevych Str. (former Bozhenko), 03150, Kyiv, Ukraine
Tel./Fax: (38044) 205 23 90, E-mail: journal@paton.kiev.ua
<https://patonpublishinghouse.com/eng/journals/tpwj>

State Registration Certificate 24933-14873 ПП from 13.08.2021

ISSN 0957-798X, DOI: <http://dx.doi.org/10.37434/tpwj>

Subscriptions, 12 issues per year:

\$384 — annual subscription for the printed (hard copy) version, air postage and packaging included;

\$312 — annual subscription for the electronic version (sending issues in pdf format or providing access to IP addresses).

Representative Office of «The Paton Welding Journal» in China:

China-Ukraine Institute of Welding, Guangdong Academy of Sciences

Address: Room 210, No. 363 Changxing Road, Tianhe, Guangzhou, 510650, China.

Zhang Yupeng, Tel: +86-20-61086791, E-mail: patonjournal@gwi.gd.cn

The content of the journal includes articles received from authors from around the world in the field of welding, metallurgy, material science and selectively includes translations into English of articles from the following journals, published by PWI in Ukrainian:

- Automatic Welding (<https://patonpublishinghouse.com/eng/journals/as>);
- Technical Diagnostics & Nondestructive Testing (<https://patonpublishinghouse.com/eng/journals/tdnk>);
- Electrometallurgy Today (<https://patonpublishinghouse.com/eng/journals/sem>).

CONTENTS

ORIGINAL ARTICLES

- L.M. Lobanov, M.O. Pashchyn, O.L. Mikhodui, A.A. Hryniuk, E.V. Ilyashenko, P.V. Goncharov, V.V. Savytskyi, Yu.M. Sydorenko, P.R. Ustymenko**
CALCULATED EVALUATION OF STRESS-STRAIN STATES OF WELDED JOINTS OF ALUMINIUM AMg61 ALLOY UNDER THE ACTION OF ELECTRODYNAMIC TREATMENT OF WELD METAL IN THE PROCESS OF FUSION WELDING* 3
- I.S. Gakh, B.O. Zaderiy, G.V. Zviagintseva, I.V. Honcharova, V.V. Kuprin, S.I. Chugunova**
STRUCTURE AND PROPERTIES OF WELDED JOINTS OF Ni₃Al INTERMETALLIC* 10
- L.V. Petrushynets, Yu.V. Falchenko, O.O. Novomlynets, V.E. Fedorchuk**
APPLICATION OF A LAYERED COMPOSITE MATERIAL BASED ON ALUMINIUM AND TITANIUM ALLOYS TO PRODUCE WELDED THREE-LAYER HONEYCOMB PANELS* 17
- T.B. Maidanchuk, V.M. Ilyushenko, A.M. Bondarenko, D.M. Stepchenko**
EFFECTIVENESS OF COMBINED GAS-SLAG PROTECTION AT MIG DEPOSITION OF COPPER ALLOYS ON STEEL* 23
- Yu.S. Borysov, A.L. Borysova, N.V. Vihilianska, O.P. Gryshchenko, Z.G. Ipatova, K.V. Yantsevych, M.A. Vasylykivska**
CORROSION RESISTANCE OF PLASMA COATINGS PRODUCED FROM COMPOSITE TiAl-BASED POWDERS WITH THE ADDITION OF NON-METALLIC REFRACTORY COMPOUNDS* 28
- Yu.M. Kuskov, V.M. Proskudin, V.A. Zhdanov, L.L. Okopnyk**
CURRENT-SUPPLYING MOULD IN ELECTROSLAG TECHNOLOGIES* 35
- S.V. Akhonin, V.O. Berezos, O.M. Pikulin, A.Yu. Severyn, O.O. Kotenko, M.M. Kuzmenko, L.D. Kulak, O.M. Shevchenko**
PRODUCING HIGH-TEMPERATURE TITANIUM ALLOYS OF Ti–Al–Zr–Si–Mo–Nb–Sn SYSTEM BY ELECTRON BEAM MELTING** 39
- V.V. Skryabinskyi, V.M. Nesterenkov, M.O. Rusynyk, A.V. Mykytchyk**
METALLURGICAL PROCESSES IN THE WELD METAL IN ELECTRON BEAM WELDING OF 01570 ALUMINIUM ALLOY** 46

*Translated Article(s) from «Automatic Welding», No. 7, 2022.

**Translated Article(s) from «Electrometallurgy Today», No. 2, 2022.

DOI: <https://doi.org/10.37434/tpwj2022.07.01>

CALCULATED EVALUATION OF STRESS-STRAIN STATES OF WELDED JOINTS OF ALUMINIUM AMg61 ALLOY UNDER THE ACTION OF ELECTRODYNAMIC TREATMENT OF WELD METAL IN THE PROCESS OF FUSION WELDING

L.M. Lobanov¹, M.O. Pashchyn¹, O.L. Mikhodui¹, A.A. Hryniuk¹, E.V. Ilyashenko¹, P.V. Goncharov¹, V.V. Savytskyi¹, Yu.M. Sydorenko², P.R. Ustymenko²

¹National Technical University of Ukraine “Igor Sikorsky Kyiv Polytechnic Institute”
37 Peremohy Prosp., 03056, Kyiv, Ukraine

²E.O. Paton Electric Welding Institute of the NASU
11 Kazymyr Malevych Str., 03150, Kyiv, Ukraine

ABSTRACT

The calculated evaluation of effect of impact interaction of the electrode-indenter with a welded plate of AMg61 alloy at its electrodynamic treatment (EDT) in the conditions of elevated temperatures was carried out. The solution of the problem was carried out in a flat two-dimensional Lagrangian statement based on a previously developed mathematical model using ANSYS/LS-DYNA software. The thermal cycle of welding was set by mechanical characteristics of AMg61 alloy at temperatures of 150 and 300 °C. The results of the calculation of residual stresses during impact action of the electrode-indenter at room and elevated temperatures in preliminary tensioned plates of AMg61 alloy of 3 mm thickness were presented. It is shown that the most acceptable temperature (from the studied temperature values) for the electrodynamic treatment of AMg61 alloy is 150 °C. Based on the results of the studies, it was found that the electrodynamic treatment of a welded joint specimen in the form of a plate preliminary loaded with elastic tension, leads to the transition of residual welding tensile stresses into compression stresses.

KEYWORDS: electrodynamic treatment, residual welding stresses, aluminium alloy, electric current pulse, impact interaction, finite-element model, electrode-indenter, elastic-plastic flow theory, fusion welding.

INTRODUCTION

The relevance of the problem of regulating residual welding stresses and strains in structures of aluminium alloys is caused by an increase in their use in various fields of mechanical engineering. Traditional technologies for reducing the level of residual welding stresses based on the mechanical or thermal effect on the welded joint metal is associated with significant difficulties [1, 2].

A challenging method of regulating stress-strain states of welded structures is electrodynamic treatment (EDT) of welded joints, whose efficiency in increasing the accuracy and service life of light alloys is proven in [3, 4]. In EDT, the weld metal is subjected to a volumetric electrodynamic effect, which initiates an electroplastic effect (EPE) in the treatment zone and, as a consequence, the relaxation of residual welding stresses [5].

The use of EDT, taking into account the features of the process of welding, is a new trend of engineering practice, which facilitates an expansion of the capabilities of the method. The study of measures aimed at improving the efficiency of the EDT process is relevant, one of which is the accompanying heating

of the electric-pulse effect zone, which, according to data [6], stimulates the mechanisms for relaxation of tensile stresses of low-carbon steel specimens.

The realization of EDT technology in the process of welding contributes to more intensive relaxation of welding stresses as a result of EDT as compared to the treatment of the weld metal at room temperature. It should be noted that until now, the theoretical and experimental studies of the effect of heat from the source of welding heating on the efficiency of EDT use as a method of regulating residual welding stresses have not been carried out. The search for the optimal EDT mode in the conditions of welding is associated with the experimental evaluation of electrophysical and mechanical characteristics of the material being treated. An alternative solution to the problem is the mathematical modeling of the EDT process, which allows evaluating the evolution of stress-strain states of welded joints as a result of EDT [7–9]. This is relevant for optimizing the technology of metal structure treatment in the conditions of their welding.

The aim of the work is the calculated evaluation of stress-strain states of metal materials under the effect of EDT in the process of welding (at elevated temperatures).

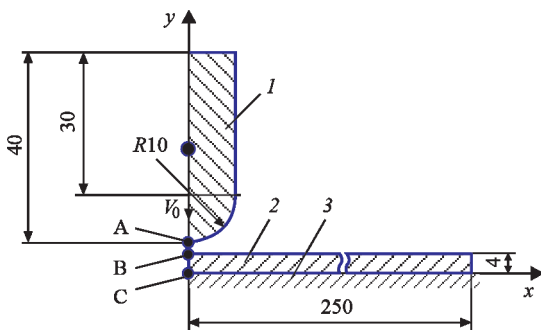


Figure 1. Calculation scheme of the process of dynamic loading of the plate during EDT: 1 — electrode-indenter; 2 — treated specimen; 3 — absolutely rigid base; A — point on the outer surface of the indenter-electrode; B — point on the outer surface of the plate; C — point on the back surface of the plate; V_0 — speed of movement of the indenter-electrode [11]

MATHEMATICAL MODEL AND DISCUSSION OF CALCULATION RESULTS

Modeling of stress-strain states of welded joints as a result of EDT in the conditions of elevated temperatures is performed using a simplified two-dimensional (2D) flat statement. The calculation scheme of the problem of the process of impact interaction of the electrode-indenter with the plates [7] is presented in Figure 1. The solution of the problem was performed with the use of ANSYS/LS-DYNA software. To construct a finite-element mesh, a flat two-dimensional finite element SOLID 162 in the form of a rectangle was used. Computer modeling was performed on the base of a Lagrangian approach using a moving finite-element mesh, which is rigidly related to the environment and deforms together with it [10, 11].

The presence of a geometric symmetry of the electrode 1 and the plate 2, being in impact interaction, allows considering only half of their cross-section in the calculation scheme with a simultaneous imposition of boundary conditions.

These conditions include the imposition of a prohibition on the movement of nodes of a finite-element mesh (FEM) of the bodies located on the symmetry axis, in the horizontal direction X . Leaning of a welded joint against an absolutely rigid base 3 (Figure 1) was considered, which in the mathematical statement is equivalent to the prohibition of FEM-nodes on the movement in the vertical direction Z , which belong to

the lower surface of the plate 2, which contacts with the desktop 3.

For numerical modeling, a continuous model of elastic-plastic environment (of a plate) under study was used. This allowed recording the laws of mass conservation, amount of movement and energy in the form of differential equations in partial derivatives. To study the processes associated with large plastic deformations of the environment, the theory of plastic flow was used, considering plastic deformation of a solid body as a state of movement on the base of respective Prandtl–Reuss ratios [7].

As an experimental metal material of a welded plate, AMg61 alloy of Al–Mg system was used.

In the mathematical statement, the behavior of the plate materials (aluminium AMg61 alloy) and the electrode-indenter (M1 copper) under the action of external pulse load was described using the ideal elastic-plastic model of the material [9–11]. This model in the library of ANSYS/LS-DYNA software materials is called PLASTIC-KINEMATIC.

The thermal effect was applied on the plate by variation of the values of elasticity modulus E and yield strength σ_y of AMg61 alloy at the values of temperature $T = 150$ and 300 °C. The mechanical characteristics of the metal materials involved in modeling at different values of temperature T are given in Table 1.

The choice of T values is predetermined by modeling the use of EDT in combination with the process of welding, where the specified T values correspond to the location of the electrode-indenter along the weld line at a distance L_{EDT} behind the source of welding heating (Figure 2). Modeling of the stress state was also performed for the values of E and σ_y at $T = 20$ °C with the aim of comparing the EDT efficiency after weld cooling (at $T = 20$ °C, line 1) and in the process of welding ($T = 150$ and 300 °C, lines 2, 3).

According to the results of previous experimental studies, it was found that the electrode-indenter received a value $V_0 = 5$ m/s, and its temperature in the process of welding did not exceed 20 °C [7]. Therefore, the properties of the electrode-indenter at its contact interaction with the plate were set exclusively for $T = 20$ °C (Table 1, line 4).

Table 1. Mechanical characteristics of structural elements of EDT model of AMg61 alloy in the process of welding

Number	Structural element of the model	Material	Density ρ , kg/m ³	Poisson's ratio, μ	T , °C	Modulus of elasticity E , GPa	Yield strength σ_y , MPa	Relative elongation δ , %
1	Plate of 300×200×3 mm	AMg61	640	0.34	20	71	150	22
2					150	60	120	40
3					300	55	50	55
4	Electrode of 15 mm diameter	M1	8940	0.35	20	128	300	6

The choice of T values is predetermined by the results of [12], where the mechanism of EDT action on the relaxation of stresses $\Delta\sigma$ of the plane specimens of AMg61 alloy during their load with longitudinal (along the main axis of the specimen) tension σ_0 was studied. The work shows that the maximum values $\Delta\sigma$ that determined the efficiency of treatment were achieved during tension of the specimens to $\sigma_0 = \sigma_y$.

Welding heating creates thermal expansion of metal in the treatment zone. According to the data of Table 1, at an increase in T , the values of elasticity σ_y of AMg61 alloy decrease, and plasticity δ increase. This, based on the results [12], contributes to intensification of the process of relaxation $\Delta\sigma$ of residual welding stresses at lower values σ_y at a constant energy level E_{EDT} of electrodynamic action. I.e., at $E_{EDT} = \text{const}$, the values $\Delta\sigma$ have an inverse dependence on σ_y . The relaxation mechanisms are based on the synergy of the electroplasticity effect and superposition of the wave of elastic stresses from EDT with the field of residual welding stresses [3, 12].

The justification of the choice of the range T was based on the following provisions. At $T = 150^\circ\text{C}$ (Table 1, line 2), AMg61 alloy maintains elastic properties, that makes the contribution of the elastic wave of stresses to the relaxation of stress states dominant as compared to the electroplastic component. At $T = 300^\circ\text{C}$ (Table 1, line 3), the opposite is observed, i.e. AMg61 alloy has high plasticity at low elasticity. This makes the plastic component in the process of stress relaxation dominant. Modeling of stress states at different T values allows optimizing the conditions of thermal effect on the action of EDT in the process of welding.

Welding stresses in the plane of the plate were modeled by setting the values of longitudinal σ_x (along the axis x in Figure 1) and transverse σ_y (along the normal to the axis x) components of tensile stresses. The values σ_x and σ_y were respectively accepted equal to σ_y and $0.5\sigma_y$ of AMg61 alloy at $T = 20, 150$ and 300°C . The result of modeling is the distribution of components σ_x and σ_y of temporary and residual stresses over the thickness of the plate in the points B, C between them after its dynamic loading along the axis z , as is shown in Figure 3. The distribution of temporary and residual σ_x and σ_y was modeled at a distance of 5 mm from the line B–C on both surfaces of the plate and between them. This allowed determining the nature of EDT action distribution from the line B–C over the thickness of the plate.

The distribution of stresses σ_x and σ_y along the line B–C (Figure 3) and at a distance of 5 mm from it after EDT at $T = 20, 150$ and 300°C were considered.

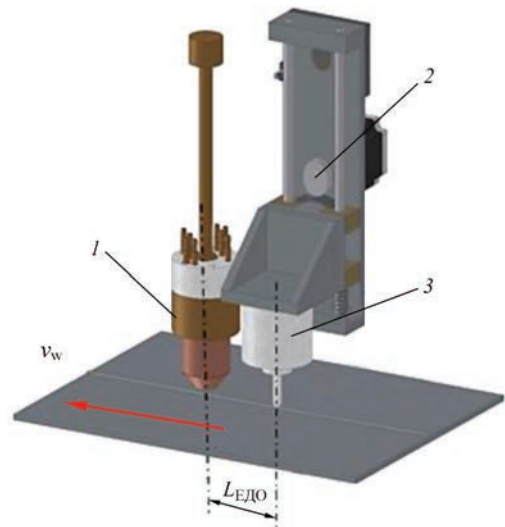


Figure 2. Scheme of EDT in the process of welding: v_w — welding direction; 1 — welding torch; 2 — eccentric; 3 — electrode device of EDT; L_{EDT} — distance between the axes of electrodes for welding and EDT

Figure 3 shows the results of modeling distribution of stresses σ_x and σ_y in the form of axonometric surfaces in the cross-section of the plates $\delta = 3$ mm at the moment of completion (instant patterns) of the EDT contact action at a temperature $T = 20, 150$ and 300°C . Figure 3 shows the values of stresses along the line between the points B and C and at a distance of 5 mm from the line B–C. Analyzing the results of Figure 3 in general, it is possible to see the dominance of compression stresses throughout the whole considered temperature range both on the section B–C (i.e., along the contact action line) and at a distance of 5 mm from it.

The temperature effect on the plates of AMg61 alloy in the conditions of contact interaction with the indenter causes certain features of the formation of stress-strain states of the specimens to be considered below.

Figure 4 presents distribution of stresses σ_x along the line between the points B and C (Figure 1) of the plates of AMg61 alloy $\delta = 3$ mm after EDT at a variation of temperature effect T . The feasibility of studying the component σ_x is associated with its dominant effect on service characteristics of welded joints [2].

In Figure 4, *a, b* it can be seen that near the middle of the plane of the plate ($z = \delta/2$), an increase in the values σ_x in relation to stresses in the points B and C occurs. This is explained by the effect of reflection of stress wave at EDT from the absolute rigid base 3 (see Figure 2). The mathematical model of the reflection mechanism and verification of the results of the calculation at $T = 20^\circ\text{C}$ is considered in [11].

Using the data from Table 1, the analysis not of the absolute values of stresses σ_x and σ_y was carried out, but those derived with respect to σ_y . This, given the dependence $\sigma_y = f(T)$, allowed carrying out the correct

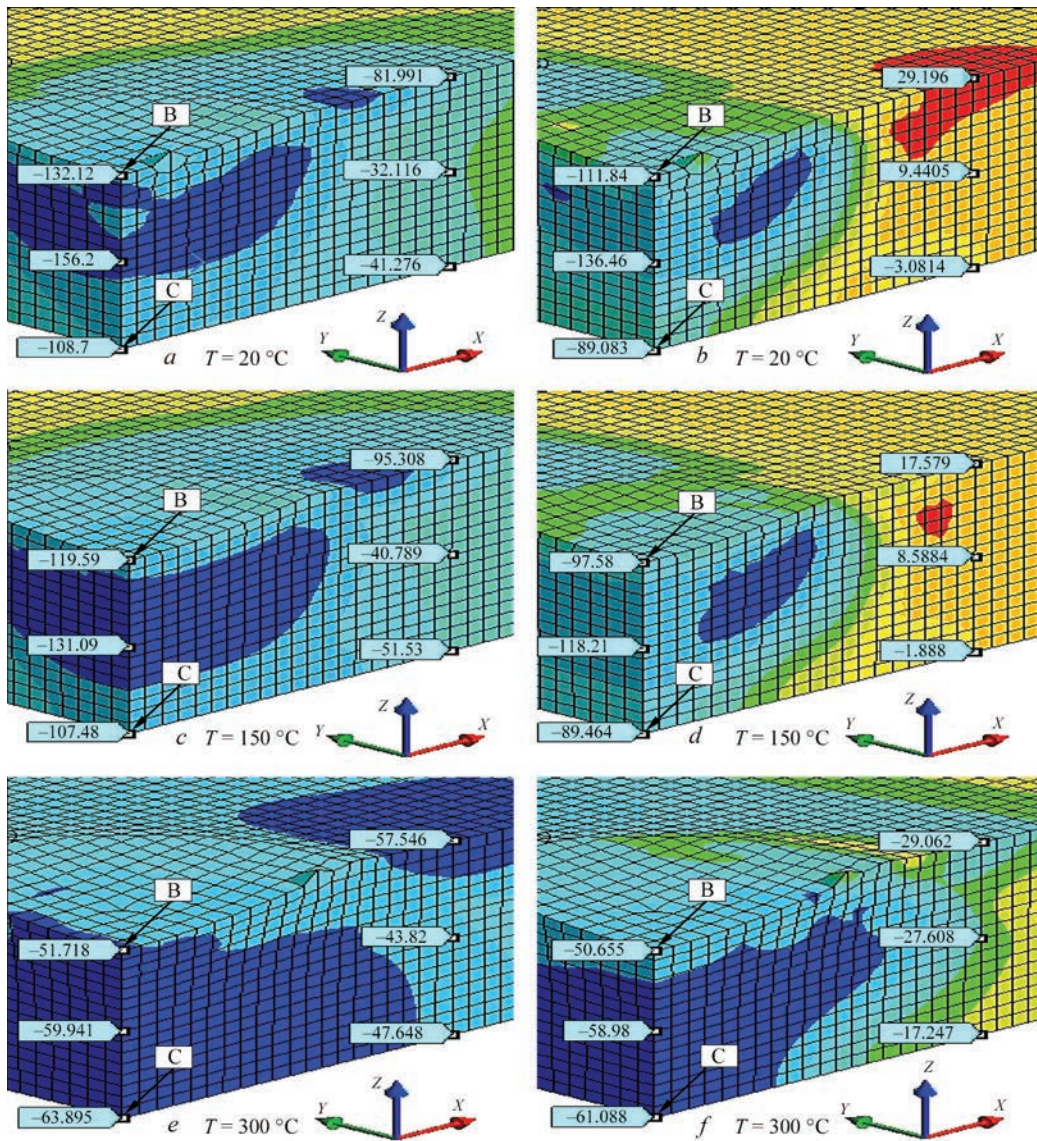


Figure 3. Instantaneous patterns of calculated distribution of values (MPa) of components of stresses σ_x , σ_y in the plate of AMg61 alloy $\delta = 3$ mm at the moment of completion of the EDT action along the line between the points B and C (Figure 2) and at a distance of 5 mm from the line B–C: *a* — σ_x at $T = 20$ °C; *b* — σ_y at $T = 20$ °C; *c* — σ_x at $T = 150$ °C; *d* — σ_y at $T = 150$ °C; *e* — σ_x at $T = 300$ °C; *f* — σ_y at $T = 300$ °C

comparative evaluation of the effect of variations of T values on EDT efficiency.

At 20 °C along the line B–C, the values σ_x and σ_y of compression stresses in the point B are higher than in the point C (Figure 3, *a*, *b*). Thus, in the point B, σ_x reaches the values $-0.88\sigma_y$ and in the point C $-0.75\sigma_y$ and σ_y in the point B reaches $-0.74\sigma_y$ and $-0.6\sigma_y$ in the point C. At the area of the cross-section, which corresponds to half of the thickness of the plate (further — area $\delta/2$), σ_x and σ_y reach the values, respectively $-\sigma_y$ (Figure 4, *a* for σ_x) and $-0.9\sigma_y$. I.e., the area near the middle of the plate ($z = \delta/2$) is subjected to the maximum effect of σ_x and σ_y stresses after EDT at $T = 20$ °C.

While removing from the line B–C by 5 mm, a decrease in stresses and a change in the nature of their distribution over the thickness of the plate is observed (Figure 3, *a*, *b*). Thus, the compression σ_x

reaches $-0.55\sigma_y$ in the point B and $-0.27\sigma_y$ — in the point C. In the area $\delta/2$, σ_x reach $-0.2\sigma_y$. At the same time, while removing by 5 mm from the line B–C, σ_y are tensile, which reach $0.2\sigma_y$ in the point B, monotonously reduced to $0.06\sigma_y$ in the point $\delta/2$ and almost to zero in the point C.

An increase in the treatment temperature to 150 °C (Figure 3, *c*, *d*) has a positive effect (as compared to $T = 20$ °C) on the value and the nature of distribution of compression stresses in the cross-section of the plate. At the same time, the area of action of compression stresses σ_x on the cross-section of the plate is slightly larger than the area of action at $T = 20$ °C (Figure 3, *a*, *b*). In the point B, compression σ_x and σ_y , as well as at $T = 20$ °C, are larger than on the reverse one. Thus, in the point B, the values σ_x and σ_y reach respectively $-\sigma_y$ and $-0.8\sigma_y$ of AMg61 alloy at

$T = 150\text{ }^{\circ}\text{C}$ and -0.95 and $-0.77\sigma_y$ during cooling to $T = 20\text{ }^{\circ}\text{C}$ (Figure 4, *b* for σ_x). In the point $\delta/2$, the values σ_x and σ_y reach σ_y for temperatures $T = 150$ and $20\text{ }^{\circ}\text{C}$. In the point B, σ_x reach $-0.85\sigma_y$, $\sigma_y = -0.71\sigma_y$ at $T = 150\text{ }^{\circ}\text{C}$ and $\sigma_x = -0.89\sigma_y$, and $\sigma_y = -0.74\sigma_y$ at $T = 20\text{ }^{\circ}\text{C}$ (Figure 4, *b* for σ_x).

While removing by 5 mm from the line B–C, as in the previous case, the compression stresses on the facial side of the plate are higher than the absolute value unlike on the side of the backing plate. At $T = 150\text{ }^{\circ}\text{C}$, the maximum compression values σ_x in the point B reach $-0.8\sigma_y$ (Figure 3, *c*) and during cooling to $20\text{ }^{\circ}\text{C}$, they reach $-0.75\sigma_y$. At $T = 150$ and $20\text{ }^{\circ}\text{C}$, the maximum values of tensile σ_y on the contact surface reach $0.15\sigma_y$. On the area $\delta/2$, the values of compression σ_x reach $-0.34\sigma_y$, and tensile σ_y , respectively, $0.07\sigma_y$ for temperatures 150 and $20\text{ }^{\circ}\text{C}$. In the point C, the compression σ_x reach $-0.43\sigma_y$ and σ_y are close to zero in the considered temperature range. The distribution of σ_y over the cross-section of the plate increases slightly, as compared to the results of Figure 3, *b*. While comparing the values σ_x while removing by 5 mm from the line B–C at $T = 20$ and $150\text{ }^{\circ}\text{C}$, it can be seen that the thermal effect contributes to the formation of greater compression stresses than after EDT at room temperature.

As compared to EDT at $T = 20\text{ }^{\circ}\text{C}$, it can be seen that an increase in the treatment temperature to $300\text{ }^{\circ}\text{C}$ (Figure 3, *e, f*) promotes the distribution of compression stresses over the thickness of the plate and reduction of their values as compared to the results at $T = 20$ and $150\text{ }^{\circ}\text{C}$ (Figure 3, *a–d*). In the point B, the values of σ_x and σ_y of compression stresses, unlike the previous variants, are lower than in the point C and reach $-\sigma_y$ at $T = 300\text{ }^{\circ}\text{C}$ and $-0.44\sigma_y$ during cooling to $T = 20\text{ }^{\circ}\text{C}$ (Figure 4, *c* for σ_x). In the point $\delta/2$, compression σ_x and σ_y reach the values $-\sigma_y$ for $T = 300\text{ }^{\circ}\text{C}$ and $-0.54\sigma_y$ for $T = 20\text{ }^{\circ}\text{C}$. In the point C, compression σ_x and σ_y reach $-\sigma_y$ at $T = 300\text{ }^{\circ}\text{C}$ and $-0.5\sigma_y$ at $T = 20\text{ }^{\circ}\text{C}$. At the same time, the area of action of

Table 2. Relative values of stress components σ_x and σ_y in the plate of AMg61 alloy $\delta = 3$ after EDT at the variation of values of temperature T of its accompanying heating

Number	$T, \text{ }^{\circ}\text{C}$	Line B–C						5 mm from the line B–C					
		σ_x			σ_y			σ_x			σ_y		
		B, $\times\sigma_y$	$\delta/2, \times\sigma_y$	C, $\times\sigma_y$	B, $\times\sigma_y$	$\delta/2, \times\sigma_y$	C, $\times\sigma_y$	5 mm from the B $\times\sigma_y$	5 mm from the $\delta/2 \times\sigma_y$	5 mm from the C $\times\sigma_y$	5 mm from the B $\times\sigma_y$	5 mm from the $\delta/2 \times\sigma_y$	5 mm from the C $\times\sigma_y$
1	20	-0.88	-1.0	-0.75	-0.74	-0.9	-0.6	-0.55	-0.2	-0.27	0.2	0.06	0
2	150	-1.0	-1.0	-0.85	-0.8	-1.0	-0.71	-0.8	-0.34	-0.43	0.15	0.07	0
3	20 after cooling from $T = 150\text{ }^{\circ}\text{C}$	-0.95	-1.0	-0.89	-0.77	-1.0	-0.74	-0.75	-0.34	-0.43	0.15	0.07	0
4	300	-1.0	-1.0	-1.0	-1.0	-1.0	-1.0	-1.0	-0.88	-1.0	-0.6	-0.54	-0.34
5	20 after cooling from $T = 300\text{ }^{\circ}\text{C}$	-0.44	-0.54	-0.5	-0.44	-0.54	-0.5	-0.49	-0.38	-0.41	-0.24	-0.24	-0.14

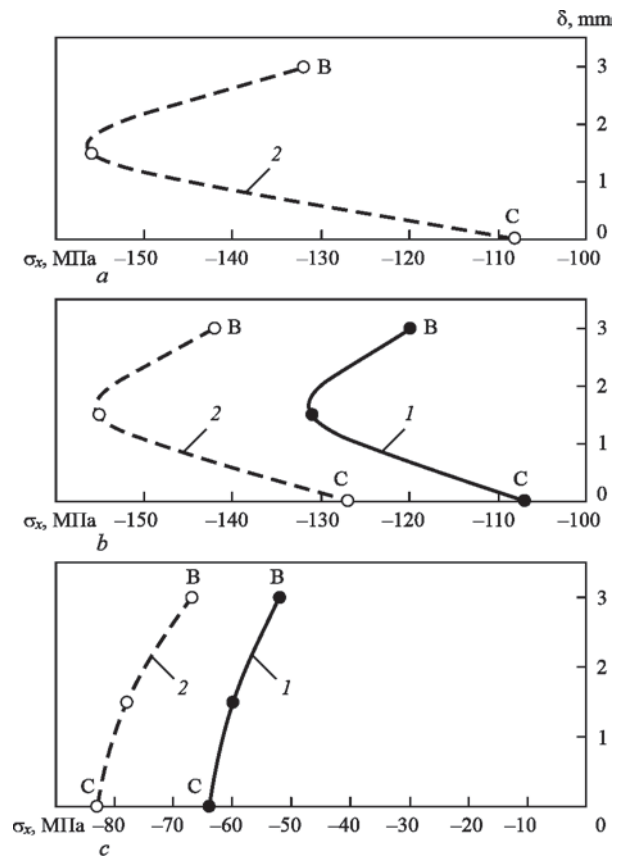


Figure 4. Stresses σ_x along the line between the points B and C (Figure 2) of plates of AMg61 alloy $\delta = 3$ mm after EDT at a temperature T and cooling to $T = 20\text{ }^{\circ}\text{C}$, where the curve 1 — σ_x (instantaneous) at the moment of completion of contact interaction at elevated temperatures; curve 2 — σ_x at room temperature: *a* — $T = 20\text{ }^{\circ}\text{C}$; *b* — 150; *c* — 300

stresses σ_x (Figure 3, *d*) over the cross-section of the plate three times increases as compared to the variant of EDT at $T = 20\text{ }^{\circ}\text{C}$ (Figure 3, *a*).

While removing by 5 mm from the line B–C, as in the previous variants of the calculation, the reduction of stresses (Figure 3, *e, f*) is determined. Thus, the maximum values of the compression σ_x in the point B reach $-\sigma_y$ at $T = 300\text{ }^{\circ}\text{C}$. During cooling to $T = 20\text{ }^{\circ}\text{C}$, the compression σ_x in the point B reach $-0.49\sigma_y$ (Figure 4, *c*). The stresses σ_y while removing by 5 mm

from the line B–C are compressive over the thickness of the plate in the range of T from 300 to 20 °C. On the surface near the point B at $T = 300$ °C, σ_y reach $-0.6\sigma_y$ and at $T = 20$ °C respectively $-0.24\sigma_y$.

In the point $\delta/2$, the compressions reach $-0.88\sigma_y$ at $T = 300$ °C and $-0.38\sigma_y$ at $T = 20$ °C (Figure 4, c). In the p $\delta/2$, the compressions σ_y reach the values $-0.54\sigma_y$ at $T = 300$ °C and $-0.24\sigma_y$ at $T = 20$ °C. On the surface near the point C, the compressions σ_x at $T = 300$ °C reach $-\sigma_y$, and at $T = 20$ °C they decrease to $-0.41\sigma_y$ (Figure 4, c). On the surface near the point C, compressions σ_y at $T = 300$ °C reach $-0.34\sigma_y$, and at $T = 20$ °C they also decrease to $-0.14\sigma_y$. Also, the distribution of σ_y across the cross-section of the plate increases significantly as compared to the results of Figure 3, b. When comparing the values of σ_y while removing by 5 mm from the line B–C at $T = 20$ and 300 °C, it should be noted that the thermal effect contributes to the expansion of the area of action of compressive stresses at a decrease in their values.

The results of modeling described above are summarized in Table 2. When comparing the lines 1 and 2 and 1 and 4, it can be seen that the thermal action, which accompanies EDT, initiates more instantaneous values of stresses (in relation to σ_y) at elevated temperatures as compared to σ_x and σ_y at $T = 20$ °C. This contributes to the formation of higher compressive stresses during cooling of the plate as compared to the stress state after EDT at $T = 20$ °C. When comparing the lines 1 and 3, it can be seen that EDT of the plates of AMg61 alloy $\delta = 3$ mm under the conditions of their thermoelastic heating (at $T = 150$ °C) is more effective than at $T = 20$ °C. However, at EDT at the temperature of thermoplasticity ($T = 300$ °C), high values of instantaneous stresses, which are comparable to σ_x and σ_y at $T = 150$ °C (respectively, lines 4 and 2), form significantly lower residual compressive stresses, which is seen at comparison of the lines 3 and 5. This fact can be explained by the fact that at low values σ_y at $T = 300$ °C (Table 1, line 3), relaxation processes take place less intensively than at elastic heating to $T = 150$ °C, which indicates the dominance of the elastic component in the formation of stress-strain states in EDT. This is confirmed by the results of [12], which proved that the most effective is EDT of plane specimens of AMg6 alloy, which were previously tensioned to σ_y . I.e., preheating of the specimens to $T = 150$ °C according to [12], contributes to the maximum efficiency of EDT.

CONCLUSIONS

1. It was proved that the use of electrodynamic treatment (EDT) of the weld metal, which is performed in a single process synchronously with fusion welding, is more effective as compared to separate EDT after

welding, which is expressed in a more optimal residual stress-strain state of a finished welded joint.

2. On the basis of the previously developed mathematical model of the impact interaction of the electrode-indenter with the welded plate of AMg61 alloy, a numerical calculated evaluation of its stress states as a result of EDT at elevated temperatures was carried out.

3. Using the mathematical model of the mechanism of impact interaction of the electrode-indenter with the welded plate during EDT in the conditions of elevated temperatures in a plane two-dimensional statement, modeling of stresses at an impact elastic-plastic action of the electrode-indenter at a temperature of 20, 150 and 300 °C in the plate of AMg61 alloy with the thickness of 3 mm was performed. It was established that the most satisfactory stress state (among investigated) corresponds to EDT at a temperature of 150 °C.

REFERENCES

- Madi, Y., Besson, J. (2014) *Effect of residual stresses on brittle fracture*. Mat. ECRS-9. UTT, Troyes, France.
- Masubuchi, K. (1980) *Analysis of welded structures*, Pergamon Press, Oxford, United Kingdom.
- Lobanov, L.M., Pashchyn, N.A., Kondratenko, I.P. et al. (2018) Development of post-weld electrodynamic treatment using electric current pulses for control of stress-strain states and improvement of life of welded structures. *Materials Performance and Characterization*, **7**, 4. DOI: <https://doi.org/10.1520/MPC20170092>. ISSN 2379-1365
- Lobanov, L.M., Pashchyn, M.O., Tymoshenko, O.M. et al. (2020) Increase in the life of welded joints of AMg6 aluminium alloy. *The Paton Welding J.*, **4**, 2–8. DOI: <https://doi.org/10.37434/as2020.04.01>
- Conrad H., Sprecher A. (1989) *The electroplastic effect in metals*. Elsevier Science Publishers B.V., Dislocations in Solids Ed. by F.R.N. Nabarro, 500–529.
- Stepanov, G.V., Babutskii, A.I., Mameev, I.A. (2004) High-density pulse current-induced unsteady stress-strain state in a long rod. *Strength of Materials*, **36**, 377–381. DOI: <https://doi.org/10.1023/B:STOM.0000041538.10830.34>
- Lobanov, L.M., Pashchyn, M.O., Mykhodui, O.L., Sydorenko, Yu.M. (2017) Effect of the indenting electrode impact on the stress-strain state of an AMg6 alloy on electrodynamic treatment. *Strength of Materials*, **49**(3), 369–380. DOI: <https://doi.org/10.1007/s11223-017-9877-1>
- Sydorenko, Y.M., Pashchyn, M.O., Mykhodui, O.L. et al. (2020) Effect of pulse current on residual stresses in AMg6 aluminium alloy in electrodynamic treatment. *Strength of Materials*, **52**(5), 731–737. DOI: <https://doi.org/10.1007/s11223-020-00226-2>
- Lobanov, L.M., Pashchin, N.A., Mikhodui, O.L., Sidorenko, Y.M. (2018) Electric pulse component effect on the stress state of AMg6 aluminium alloy welded joints under electrodynamic treatment. *Strength of Materials*, **50**(2), 246–253. DOI: <https://doi.org/10.1007/s11223-017-9862-8> 10
- <http://www.ansys.com/>
- Lobanov, L.M., Pashchyn, M.O., Mikhodui, O.L. et al. (2021) Modeling of stress-strain states of AMg6 alloy due to impact action of electrode-indenter in electrodynamic treatment. *The Paton Welding J.*, **6**, 2–11. DOI: <https://doi.org/10.37434/tpwj2021.06.01>

12. Lobanov, L.M., Pashchyn, M.O., Mikhodui, O.L. (2012) Influence of the loading conditions on the deformation resistance of AMg6 alloy during electrodynamic treatment. *Strength of Materials*, **44**, 472–479. DOI: <https://doi.org/10.1007/s11223-012-9401-6>

ORCID

L.M. Lobanov: 0000-0001-9296-2335
 M.O. Pashchyn: 0000-0002-2201-5137,
 O.L. Mikhodui: 0000-0001-6660-7540,
 E.V. Illyashenko: 0000-0001-9876-0320,
 P.V. Goncharov: 0000-0002-1980-2340

CONFLICT OF INTEREST

The Authors declare no conflict of interest

CORRESPONDING AUTHOR

M.O. Pashchyn

E.O. Paton Electric Welding Institute of the NASU
 11 Kazymyr Malevych Str., 03150, Kyiv, Ukraine.
 E-mail: svarka2000@ukr.net

SUGGESTED CITATION

L.M. Lobanov, M.O. Pashchyn, O.L. Mikhodui, A.A. Hryniuk, E.V. Illyashenko, P.V. Goncharov, V.V. Savytskyi, Yu.M. Sydorenko, P.R. Ustymenko (2022) Calculated evaluation of stress-strain states of welded joints of aluminium AMg61 alloy under the action of electrodynamic treatment of weld metal in the process of fusion welding. *The Paton Welding J.*, **7**, 3–9.

JOURNAL HOME PAGE

<https://pwj.com.ua/en>

Received: 23.06.2022

Accepted: 15.09.2022

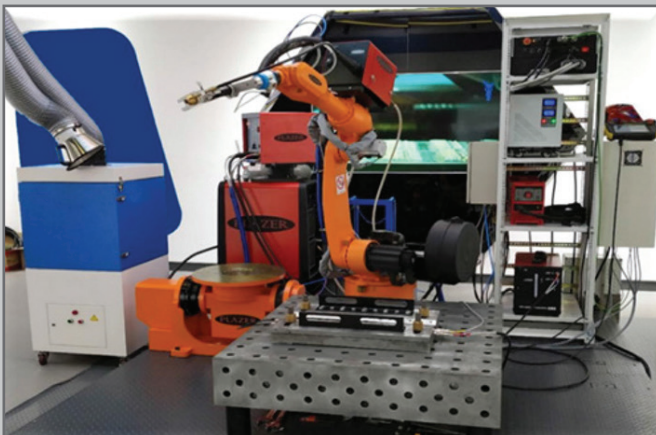
DEVELOPED in PWI

EQUIPMENT FOR ROBOTIC SPOT PLASMA WELDING ON ASYMMETRIC ALTERNATING CURRENT AND DIRECT CURRENT STRAIGHT POLARITY

Spot welding is performed by a plasma arc on alternating asymmetric current to join materials with a refractory oxide film on the surface (aluminum, magnesium and beryllium alloys) or on direct current of direct polarity to join materials without a refractory oxide film on the surface (low alloy steels, stainless and high strength steels, titanium, copper alloys). Spot joints are formed both without and with the use of filler wire feed.

The use of this equipment allows:

- ▶ to produce lightweight hollow structures (density is lower by 30–60 % compared to solid alloys), which consist of several sheets of high-strength aluminum and magnesium alloys with alternating sheets and truss (embossed) intermediate layers;
- ▶ welding sheets in a multilayer honeycomb panel with a thickness of 0.5 to 3.0 mm, welding sheets to a thinner corrugated filler, obtaining a honeycomb multilayer panel up to 4 meters wide and up to 12 meters long;
- ▶ to produce lightweight curvilinear panels by bending the first sheet of the panel according to a template, to obtain the required surface shape while ensuring high structural rigidity.



Robotic complex (left) and plasma torch (right) with a pneumatic clamping mechanism for spot plasma welding with direct and alternating asymmetric current of increased frequency



DOI: <https://doi.org/10.37434/tpwj2022.07.02>

STRUCTURE AND PROPERTIES OF WELDED JOINTS OF Ni₃Al INTERMETALLIC

I.S. Gakh¹, B.O. Zaderiy¹, G.V. Zviagintseva¹,
I.V. Honcharova², V.V. Kuprin², S.I. Chugunova²

¹E.O. Paton Electric Welding Institute of the NASU

11 Kazymyr Malevych Str., 03150, Kyiv, Ukraine. E-mail: gakh@paton.kiev.ua

²Frantsevych Institute for Problems of Materials Science of the NASU

3 Krzhyzhanovskiy Str., 03142, Kyiv, Ukraine. E-mail: irina@ipms.kiev.ua

ABSTRACT

Welded specimens of Ni₃Al intermetallic are the main strengthening phase of heat-resistant nickel alloys were taken as an example to define the main problems arising in fusion welding of this class of materials. Features of weld formation, structural and phase changes, and mechanical properties of the welded joints are considered. Conditions of crack initiation and methods to prevent them are determined. The effect of welding modes and heat treatment on the structure, strength and ductility characteristics was studied. Mechanical properties of welded joints in the temperature range of 20–1200 °C are assessed. Schemes and modes of welding and heat treatment are proposed, which allow preventing cracking and ensure an equal strength of welded joints and base metal at improvement of their ductility.

KEYWORDS: Ni₃Al intermetallic, welded joints, structure, mechanical properties, crack resistance, welding and heat treatment modes

INTRODUCTION

Today, in the creation of high-temperature industrial structures, including parts of a hot path in gas turbine engines, installations, multicomponent heat-resistant nickel alloys (HNA) based on the intermetallic Ni₃Al compound remain the most widely used materials. The volume fraction of Ni₃Al in the alloy can reach 85–90 % (for example, alloys of VKNA type), which provides its high serviceability and heat resistance of up to 1250 °C. The advantage of using intermetallics as a phase base of HNA is provided by its unique capabilities, such as high values of strength and elasticity, structural stability, that does not degrade when the temperature is increased, as well as limited rate of creep, recrystallization and corrosion [1–4]. At the same time, some of the mentioned advantages and features of the physical and mechanical characteristics contribute to deterioration of the alloy manufacturability, especially its weldability. Thus, high strength and modulus of elasticity, low ductility close to high temperatures, high coefficient of thermal expansion, low thermal conductivity contribute to the formation of significant welding stresses and cracks arising.

Considering the wide use of HNA in the aircraft, power, nuclear, metallurgical and other branches of industrial production, the problem of developing scientific and technological fundamentals of welding of modern perspective high alloys is acute.

Taking into account the predominant role of Ni₃Al intermetallic as the main strengthening phase of

HNA, the study of structural-phase changes and mechanical properties as a result of thermodeformation effect during welding will help to establish the physical fundamentals of weldability and strength in order to reasonably approach the development of technologies of welding industrial HNA.

RESEARCH METHODS

The studies were carried out with the use of plane specimens of Ni₃Al intermetallic, produced by the method of rapid cooling from the liquid state by pouring into a massive copper mold in a protective inert atmosphere.

In addition to the reasons mentioned above, the choice of the studied material — Ni₃Al intermetallic is predetermined by the need in excluding excitation of crystallization processes and phase transformations due to alloying elements of typical HNA. The need in a clear fixation of the intermetallic phase due to a high (~ 10³ °C/s) cooling rate of the melt determined the method of producing specimens.

The experiments were performed by electron beam welding (EBW) in vacuum, taking into account the advantages of EBW, in particular, possibilities of a wide control of heat input and heat distribution in the welding pool.

The specimens with a thickness of 1.5–2.0 mm and a size of 50×40 mm were welded. The specimens for welding and investigations were cut with the use of electric spark method and a subsequent grinding of cut places. The welding mode parameters were chosen from the standpoint of providing high-quality welds with a full

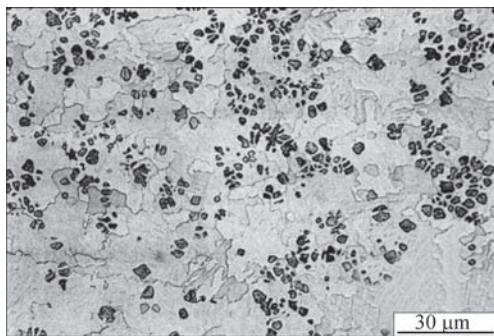


Figure 1. Microstructure of the initial material (Ni₃Al intermetallic), obtained by the method of hardening from the melt

penetration, taking into account the possibility of controlling thermal deformation processes in view of their effect on the tendency to crack formation.

The welding speed in the experiments varied in the range of 5–60 m/h. In order to limit the formation of cracks, preheating of the specimens with a beam was used. The range of heating temperatures during the studies was 400–800 °C.

The structure of the welded joints was detected by ion bombardment of the surface of the sections in an argon atmosphere with the further examination in the optical (NEOPHOT-32) and the electron scanning microscope (Jeol Superprob 733) with an X-ray analyzer. The phase composition of the specimens was determined in the DRON-UMI diffractometer in a monochromatic CuK α -radiation. The degree of a distant order η was evaluated from the ratio of integral intensities of diffraction peaks corresponding to the disordered face centered cubic lattice of a solid solution to the ordered one.

The mechanical characteristics were evaluated by the method of microindentation (“hot and cold”), testing of the plane specimens on three-point bending at room and elevated temperatures in the range of 200–1200 °C in the installation of the type INSTRON. The values of strength σ_p , yield $\sigma_{0.2}$ and ductility δ were determined during the destruction of upper fibers on the plane specimens with a section of 4×1.5 mm at a distance between the supports of 18 mm [5].

Microhardness at room temperature was determined using the PMT-3 hardness tester at a load of 2 N, at elevated temperatures (200–900 °C) in vacuum of 10⁻³ Pa in a modernized BIM-1C installation [6].

RESEARCH RESULTS

The initial material under study — Ni₃Al intermetallic produced by the method of hardening from the melt, is characterized by an equiaxial grain structure with a fine dendritic filling and the presence of separate metastable concentration configurations of a dendritic morphology (Figure 1). The performed micro-X-ray spectral analysis revealed a nonuniform distribution

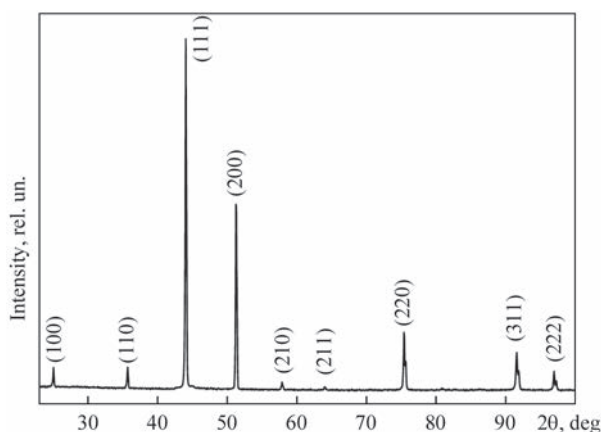


Figure 2. X-ray pattern from the surface of the specimen of Ni₃Al intermetallic in the initial state

of chemical components, which is most likely related to the mismatch in the process of cast formation of a peritectic point of the equilibrium diagram (Ni–Al) [7] with the region of the stoichiometric composition of Ni₃Al. The presence of such formations is associated with structural, mechanical and chemical heterogeneity, a significant discrepancy of microhardness values: from 2000–2500 MPa for the matrix to 3000–4000 MPa for the formations; low ductility of the material.

The X-ray analysis showed that in the initial material, both the presence of the ordered γ' -phase of Ni₃Al (Figure 2), as well as the disordered γ -phase, which was confirmed during fractographic examination of the specimens after plastic bending deformation (Figure 3).

Low ductility and toughness of fracture of intermetallic at low temperatures in combination with cast and welding stresses, chemical and structural heterogeneity, which contributes to an increased tendency to crack formation, is a well-known disadvantage of intermetallic alloys of a structural type L1₂, which include the investigated Ni₃Al. In welding of Ni₃Al specimens (as well as heat-resistant alloys on their base), the primary task is to prevent their arising.

One of the first methods of reducing the probability of crack formation is a preliminary heat treatment

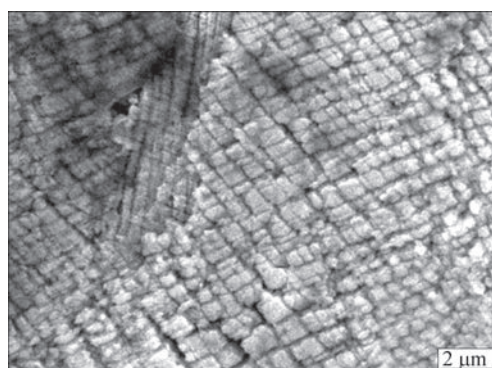


Figure 3. SEM-image of structure of Ni₃Al intermetallic after plastic deformation

Table 1. Mechanical properties during tests on bending of Ni₃Al intermetallic in the initial state and after heat treatment

State of the material	$\sigma_{0.02}$, MPa	$\sigma_{0.2}$, MPa	σ_p , MPa	δ , %	H_v , MPa
Initial	510	Brittle fracture	595	0,08	2450
Heat treatment of 1150 °C, 2 h	243	270	394	1,75	2100

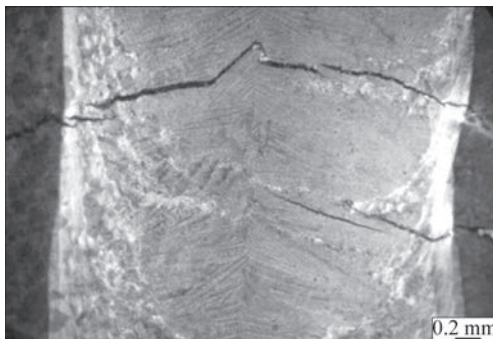
Table 2. Temperature and time parameters of cooling of weld metal of HNA with the content of Ni₃Al of more than 65 % for different welding speeds

v_w , m/h	$G \times R$, °C/s		R , mm/s	
	FL	Weld axis	FL	Weld axis
17	$3 \cdot 10^3$	25	0,4	5
40	$49 \cdot 10^3$	54	1	8
53	10^5	300	1,3	11

Note. R — rate of crystallization of weld pool metal; $G \times R$ — cooling rate; FL — area of the weld metal on the fusion line.

of welded metal, aimed at improving its ductility. The studies of the effect of heat treatment on the structure and properties of Ni₃Al showed that the optimal heat treatment (at 1150 °C during 2 h) led to an increase in the ductility due to an increase in the grain size (from 7 to 17 μm), and also contributed to dissolution of concentration configuration formations in the structure. The method of X-ray structural analysis revealed that this heat treatment leads to the maximum increase in the degree of orderness of Ni₃Al solid solution. Thus, a satisfactory complex (optimal ratio of strength and ductility) of mechanical properties of intermetallic at room temperature (Table 1) was obtained [8].

In [8] it is shown that when testing the specimens in a temperature range of 400–800 °C, the ductility δ is sharply reduced, almost to zero, which can be negatively manifested under unfavourable conditions, when the rise in welding stresses occur at the specified temperature interval, in maintaining or increasing the tendency to crack formation. Thus, preliminary heat treatment does not radically solve the problem of preventing cracking in welding of Ni₃Al intermetallic. The previous calculations [9] showed that in welding HNA at a speed of about 55 m/h, namely in this temperature range, a rise in welding stresses is observed.

**Figure 4.** Typical cracks in welding of alloys based on Ni₃Al intermetallic

The best result from the standpoint of preventing cracking is achieved as a result of control of the thermal cycle of welding, the value and nature of heat input and rigidity of welded joint. Technologically, this is performed by preheating, choosing the welding speed and concentration of welding beam energy as a result of its focusing and scanning. The thermomentering of welding process revealed that the rate of cooling of the weld metal in the temperature range of ductility failure (400–800 °C) is mainly determined by the welding speed and is approximately 300 °C/s at 12 m/h; 600 °C/s at 40 m/h; 155 °C/s at 53 m/h at the width of the weld, respectively 5.8; 4.6 and 2.8 mm.

The temperature and time parameters of cooling of the weld metal during crystallization and subsequent cooling vary throughout the cross-section and can reach approximately 10^5 °C/s depending on the conditions and parameters of the welding mode, which is shown on the example of variation in the rate from 17 to 53 m/h (Table 2).

Depending on the size and a certain combination of the mentioned thermal characteristics, both main longitudinal as well as transverse cracks may arise in the weld metal. More typical transverse cracks (Figure 4) arise at elevated (55–90 m/h) welding speeds, high specific power of the heating source in the welds of a small width. A decrease in the tendency to their formation due to an increased width of the weld is limited by the occurrence of the burn-throughs and the formation of axial crystallization cracks.

There is a narrow range of mode parameters and welding conditions, at which a high quality formation of welds without defects and the absence of cracks of both types are provided.

For the considered specimens, the realization of such conditions is achieved at a preheating of up to 600 °C, welding speed of 12–17 m/h, focusing and current of the welding beam, at which quality weld forma-

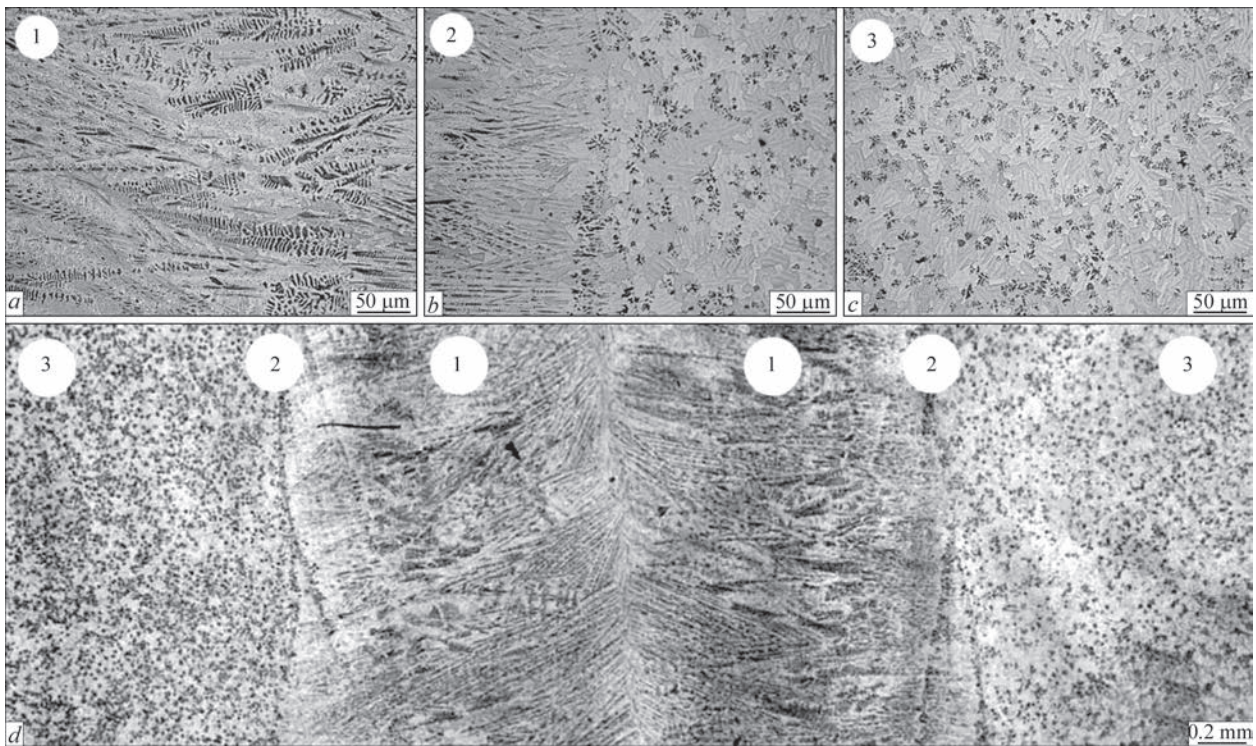


Figure 5. Microstructure of welded joint and individual areas of Ni₃Al intermetallic: *a* — weld metal (1); *b* — fusion zone (2); *c* — base metal (3); *d* — macrosection of welded joint

tion with a through penetration of 2.8–3.8 mm width is provided. Obviously, under such conditions, there is a low rate of increment, level and a uniform distribution of welding deformations and stresses, as well as the formation of a more homogeneous structure.

Taken into account a rather low ductility of intermetallics, the stochasticity of the influence of EBW parameters on the interaction of beam and welded metal, formation of a temperature field, the obtained conclu-

sions require correcting regarding each case of thickness, geometry of welded material, requirements to joint, etc. Thus, in welding of Ni₃Al intermetallic specimens of 1.5 mm thickness with preheating at a weld width of about 4 mm, produced at a welding speed of 12 m/h, longitudinal axial cracks and at 55 m/h, numerous transverse cracks arise. At the same time, at a thickness of 2 mm, welding speed of 12 m/h and weld width of about 4 mm, cracks were not observed.

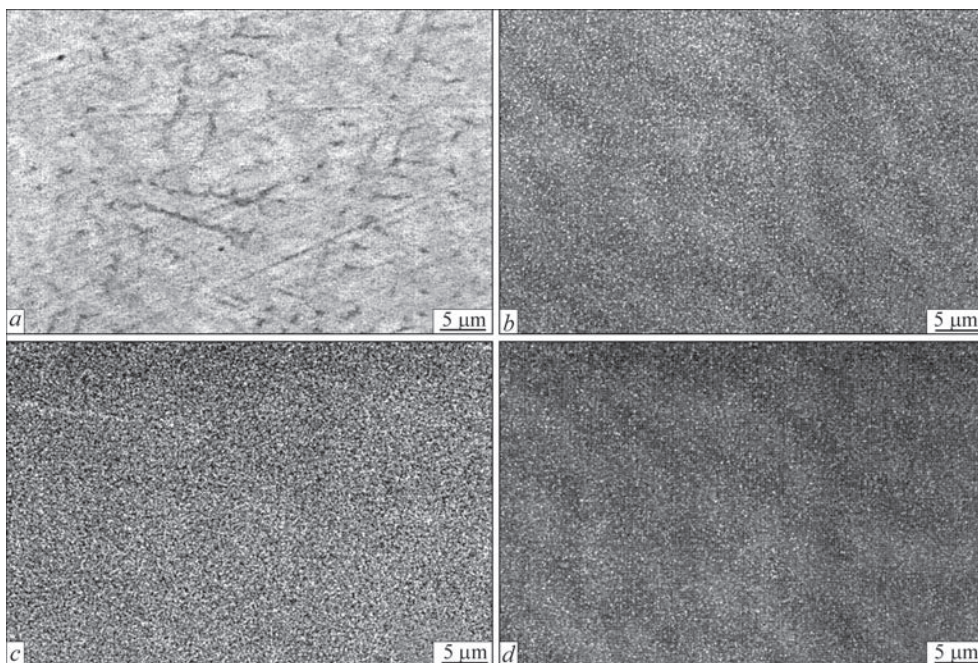


Figure 6. SEM-image of the surface of the weld of Ni₃Al: *a* — BEI (back electron image) mode and distribution of elements in the characteristic radiation of Al (*b*), Ni (*c*), Fe (*d*) obtained during micro- X-ray spectral analysis

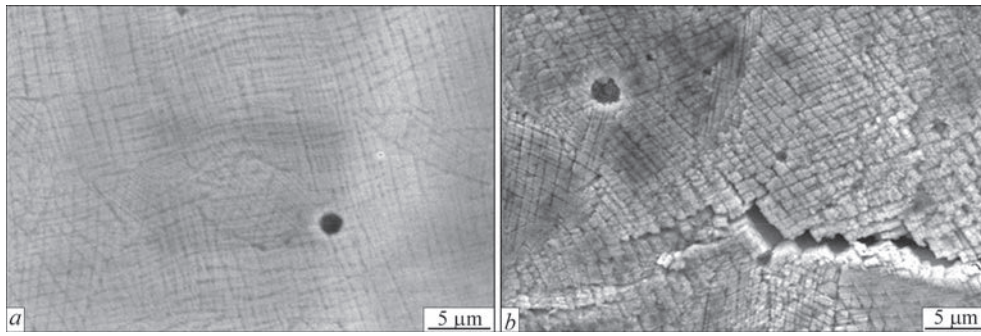


Figure 7. SEM-image of initial metal of Ni₃Al (a) and the surface of fracture of welded joint (b)

Table 3. Influence of heat treatment on mechanical properties (bending tests) of welded joints of Ni₃Al intermetallic. Welding in as-delivery state

Heat treatment	$\sigma_{0.02}$, MPa	$\sigma_{0.2}$, MPa	σ_t , MPa	δ , %	H_v , MPa	E , MPa
Without heat treatment	430	Brittle fracture	504	0,09	2500	2275
1100 °C, 2 h	323	Same	395	0,07	2270	–
1150 °C, 2 h	310	–”–	385	0,17	2300	–
1200 °C, 2 h	160	–”–	164	0,1	–	1714

Note. E , H_v — for heat-treated welded joints were not determined, and for welded joints in the initial state, the modulus and hardness were determined by the measurements of instrumental hardness; $\sigma_{0.02}$ is not a standard mechanical characteristics, that characterizes microductility and is determined by deformation of 0.02 % for comparing the materials subjected to brittle fracture; $\sigma_{0.2}$ is a standard characteristics at deformation of 0.2 % — yield strength, which cannot be determined from the diagram of our intermetallics, because the specimens are subjected to brittle fracture.

The structure of the welded joint of 2 mm thickness, produced maintaining the specified favourable conditions, is presented in Figure 5.

The X-ray spectral analysis of the weld metal showed that in the initial state of the material, the weld represents mainly an ordered intermetallic phase of Ni₃Al. The results of examinations by scanning electron microscopy with an X-ray microanalyzer showed that the main components and admixtures of the weld material are uniformly distributed (Figure 6). The size of the matrix and morphology of the γ' -phase are little different from the initial ones (Figure 7). A characteristic feature of the structure of the weld metal are columnar dendrites of a variable size (see Figure 5), orthogonally directed to the crystallization front of the welding pool, which in turn consist of small cellular elements. The difference in the

crystallization rates (see Table 2) and the temperature gradient over the cross-section of the welding pool leads to significant changes both in their sizes and morphology. Thus, near the fusion line, the distance between dendrites λ is 3–8, and near the axis of the weld is 5–9 μm . The difference between the morphology and sizes of the elements of the structure of the weld and the initial metal is mainly determined by the direction and intensity of heat removal in the process of crystallization. When forming a cast (initial metal), the heat removal is directed perpendicularly to its thickness; in crystallization of the weld it is directed orthogonally to the isotherm of the welding pool crystallization in the plane of the specimen. An increased dispersion of the structure of the base metal is associated with a higher rate of crystallization, and a change in the dispersion over the cross-section of the weld is associated with a change in the crystallization rate: from high near the fusion line to minimal, close to welding speed along the weld axis.

The considered peculiarities of the structure of welded joints are manifested in the certain way while determining the mechanical characteristics. Thus, the bending tests at room temperature (Tables 1, 3) indicate some reduction in strength and ductility as compared to intermetallic in the state of delivery.

The effect of the structural factor is also noticeable when evaluating the hardness of individual areas in the welded joint: base metal, heat-affected zone, areas of epitaxial growth, transitional area and near the weld axis (Figure 8).

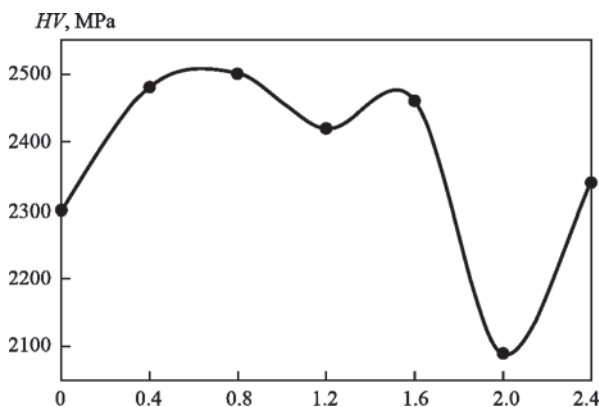


Figure 8. Distribution of hardness of individual areas of welded joint of Ni₃Al intermetallic

Table 4. Influence of heat treatment after preliminary stabilizing annealing of 1150 °C, 2 h and welding on mechanical properties (bending tests) of welded joints of Ni₃Al intermetallic

No.	Heat treatment	$\sigma_{0.02}$, MPa	$\sigma_{0.2}$, MPa	σ_t , MPa	δ , %
1*	1150 °C, 2 h	270	304	325	0.35
2	1150 °C, 5 h	–	290	345	1.2
3*	1150 °C, 10 h	245	270	310	1.58

*Material of other melting

At the same time, the methods of instrumental hardness showed that the integral values of ductility, hardness and Young modulus for the mentioned zones are close to each other [10].

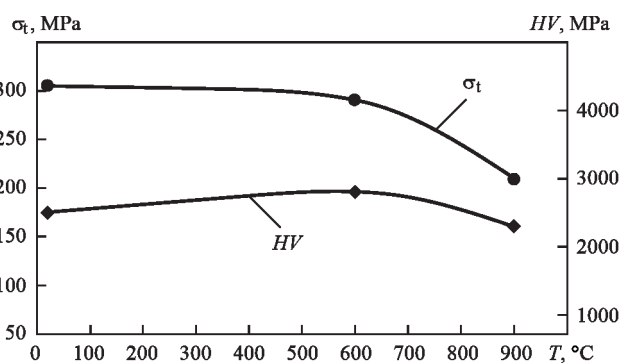
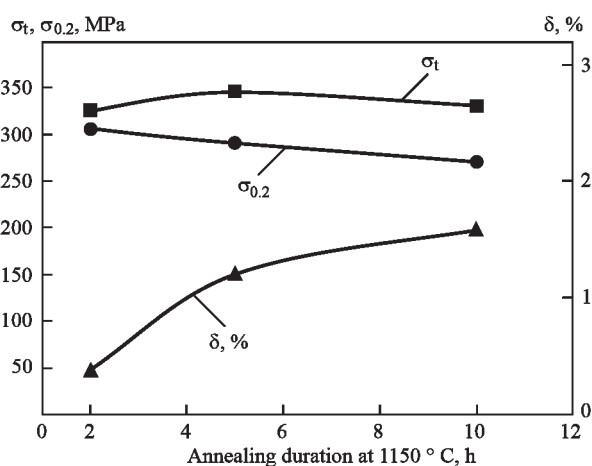
When the test temperature rises up to 900 °C, the hardness of the weld (2.1–2.4 GPa) is much exceeding the one for the base metal (1.6–1.8 GPa). As well as for the initial metal, the growth of H_v is also observed in the region of 600 °C (Figure 9).

Thus, as a result of welding, a less dispersed structure is formed, that varies over the weld width, which is also manifested in the reduction of its mechanical characteristics; here, the ductility index remains at the same low level as in the initial metal (see Tables 1, 3), i.e., the dispersion and morphology of the structure of the weld metal of Ni₃Al intermetallic is not optimal.

In view of these results, when studying welding of Ni₃Al intermetallic and alloys on its base, more attention should be paid to local changes in the structure of the weld metal, especially when studying the mechanism of crack formation, which are also most frequently originated in the areas of the weld with high hardness and dispersion of the structure (see Figure 5). The need in a separate consideration of the influence of structural changes in welding on the nature, mechanism of deformation and fracture of welded joints is also obvious.

In order to improve the indices of the structure, to obtain a satisfactory ratio of strength and ductility characteristics and to reduce residual stresses, a comprehensive study of the effect of heat treatment on the properties of welded joints was conducted. In this case, the heat treatment was carried out the same as for the initial metal in the temperature range of 800–1300 °C for 1–10 h.

As is seen from the results of mechanical tests (see Table 4, Figure 10), a satisfactory combination of values of σ_t , $\sigma_{0.2}$ and δ is achieved at annealing temperatures of 1150 °C. The optimal duration of heat treatment at the mentioned temperatures is 5 h (Figure 10). An increase in the duration to 10 h leads to a further growth in the ductility, but the strength characteristics begin to decrease more significantly. A more significant increase in the ductility of the welded joint as a result of heat treatment is achieved on the specimens,

**Figure 9.** Influence of test temperature on tensile strength σ_t and hardness H_v of the weld of Ni₃Al intermetallic**Figure 10.** Influence of annealing duration at 1150 °C on mechanical characteristics of welded joint of Ni₃Al intermetallic. Test temperature is 20 °C

which were preliminary treated before welding on the mode of 1150 °C during 2 h (Figure 10).

Thus, the implementation of the research results and proposed technological solutions in welding Ni₃Al intermetallic specimens allows preventing cracking and providing mechanical properties of welds at the level of the initial ones at a simultaneous increase in their ductility.

CONCLUSIONS

1. Ni₃Al intermetallic, which is the base of most modern HNA, is featured by an extremely low ductility and a high tendency to crack formation in fusion welding.

2. Prevention of crack formation in EBW of Ni₃Al intermetallic is achieved by combining the following technological means: heat treatment and preliminary heating of welded specimens, through penetration, reducing the rigidity of the joint, welding speed and heating concentrations. For specimens of 1.5–2.5 mm thickness, this is achieved at a preliminary annealing of 1150 °C during 2 h, preheating to about 600 °C, welding speed of 12–17 m/h and the welding beam current of ~ 15–20 mA in its sharp focusing, which provides a uniform through penetration and a high-quality formation of welds of ~ 3.0 mm width.

3. An increase in the ductility of welded joints while maintaining σ_p , $\sigma_{0.2}$, H_v and E at the level of the initial material is provided while maintaining the mentioned technological means of preventing crack formation, the use of postweld heat treatment of 1150 °C for 2 h. This provides the formation of the structure of 15–17 μm , which is close to the equiaxial grain with ordered quasi-cubic particles of the γ' -phase with the size of about 0.5–0.7 μm and the preservation of the stoichiometric composition of Ni_3Al intermetallic.

REFERENCES

1. Bazyleva, O.A., Arginbaeva, E.G., Turenko, E.Yu. (2013) High-temperature intermetallic alloys for GTE parts. *Aviats. Materialy i Tekhnologii*, **3**, 26–31 [in Russian].
2. Verin, A.S. (1997) Intermetallic Ni_3Al as the base of heat-resistant alloy. *MiTOM*, **5**, 70–73 [in Russian].
3. Lomberg, B.S., Ovsenyan, S.V., Bakradze, M.M., Mazalov, I.S. (2012) High-temperature heat-resistant nickel alloys for parts of gas-turbine engines. *Aviats. Materialy i Tekhnologii*, **5**, 52–57 [in Russian].
4. Kolobov, Yu.R., Kablov, E.N., Kozlov, E.V. et al. (2008) *Structure and properties of intermetallic materials with nano-phase strengthening*. Moscow, MISIS [in Russian].
5. Shaposhnikov, N.A. (1951) *Mechanical tests of metals*. Moscow, Mashgiz [in Russian].
6. Gudtsov, N.T., Lozinsky, I.G. (1952) Study of ageing process of metals and alloys by hardness measurement in vacuum heating. *Zh. Tekhnicheskoy Fiziki*, **22(8)**, 12–49 [in Russian].
7. Massalski, T.B., Murray, J.L., Bennett, L.H., Baker, H. (1986) Binary alloy phase diagrams. Metals Park, Ohio. *American Society for Metals*, **1**, 1002.
8. Milman, Yu.V., Chugunova, S.I., Goncharuk, V.A. et al. (2013) Structure and mechanical properties of rapid-quenched

intermetallic Ni_3Al . *Elektronnaya Mikroskopiya i Prochnost Materialov*, **19**, 78–85 [in Russian].

9. Yushchenko, K.A., Makhnenko, V.I., Savchenko, V.S., Chervyakov, N.O. (2006) *Investigation of thermal-deformation state of welded joints in stable austenitic steels and nickel alloys*: IIW Doc. IX-2224–06.
10. Mordel, L., Chugunova, S., Grinkevych, K. et al. (2013) The mechanical and tribological properties of welding joint of the Ni_3Al intermetallic. In: *Proc. of the 4th Int. Conf. on HighMat-Tech (Kyiv, Ukraine, October 7–11)*.

ORCID

I.S. Gakh: 0000-0001-8576-4234,
G.V. Zviagintseva: 0000-0002-6450-4887,
I.V. Honcharova: 0000-0001-7619-3572,
V.V. Kuprin: 0000-0002-4891-1810,
S.I. Chugunova: 0000-0001-9327-3072

CONFLICT OF INTEREST

The Authors declare no conflict of interest

CORRESPONDING AUTHOR

I.S. Gakh

E.O. Paton Electric Welding Institute of the NASU
11 Kazymyr Malevych Str., 03150, Kyiv, Ukraine.
E-mail: gakh@paton.kiev.ua

SUGGESTED CITATION

I.S. Gakh, B.O. Zaderiy, G.V. Zviagintseva,
I.V. Honcharova, V.V. Kuprin, S.I. Chugunova
(2022) Structure and properties of welded joints of
 Ni_3Al intermetallic. *The Paton Welding J.*, **7**, 10–16.

JOURNAL HOME PAGE

<https://pwj.com.ua/en>

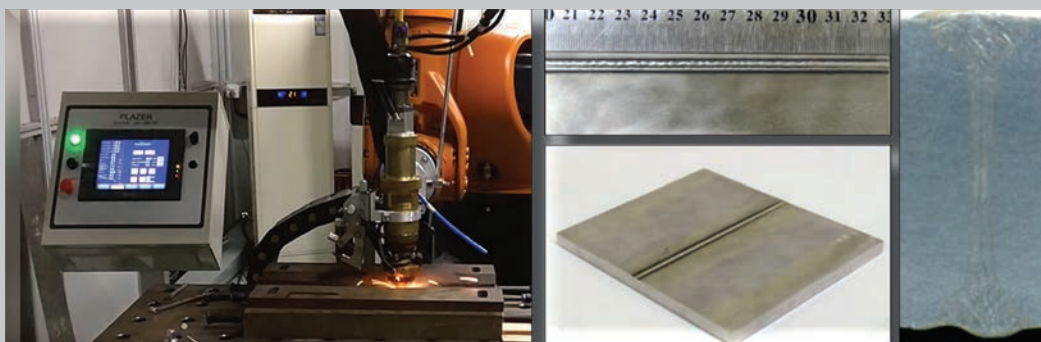
Received: 23.05.2022

Accepted: 15.09.2022

DEVELOPED in PWI

EQUIPMENT AND TECHNOLOGY FOR HIGH-SPEED HYBRID LASER-PLASMA WELDING

Hybrid laser-plasma welding implements the process of joint action of two heat sources (laser beam and plasma arc) into one weld pool, which increases the efficiency of absorption of laser beam energy by the welded metal. The equipment is designed to produce welded joints from aluminum and magnesium alloys, titanium, nickel and copper and other alloys, as well as low-alloy and alloy steels without and with filler wire feed.



APPLICATION OF A LAYERED COMPOSITE MATERIAL BASED ON ALUMINIUM AND TITANIUM ALLOYS TO PRODUCE WELDED THREE-LAYER HONEYCOMB PANELS

L.V. Petrushynets¹, Yu.V. Falchenko¹, O.O. Novomlynets², V.E. Fedorchuk¹

¹E.O. Paton Electric Welding Institute of the NASU
11 Kazymyr Malevych Str., 03150, Kyiv, Ukraine

²Chernigiv National Technological University
95 Shevchenko Str., 14035, Chernigiv, Ukraine. E-mail: oonl@ukr.net

ABSTRACT

The paper presents the results of studies on production of layered composite materials, based on aluminium and titanium alloys, by vacuum diffusion welding, with a broad range of specific weight values, which is achieved due to different layer ratio in each of the composites. Based on a layered composite material, a procedure was proposed for manufacture of three-layer honeycomb panels by vacuum diffusion welding. It is found that the average compressive strength of the three-layer panel with a filler from a layered composite material based on Al–Ti alloys is equal to 47.3 MPa, that is four times higher than the strength of similar honeycomb elements made from an aluminium alloy. It is shown that the layered material has higher thermal stability as compared to aluminium alloys. Specimen annealing at the temperature of 700 °C for 30 min does not lead to their early destruction or loss of shape.

KEYWORDS: aluminium, titanium, foil, joint, layered composite material, vacuum diffusion welding, three-layer honeycomb panels

INTRODUCTION

Three-layer aluminium panels with a honeycomb filler (Figure 1) have been widely used in aircraft and shipbuilding, construction and other industries due to their unique properties. At a relatively small weight, these structures are characterized by high values of strength and stiffness and, moreover, they have good vibration and radio technical characteristics, sound and thermal insulation properties. Such structures can be used as load-carrying elements in the wing, fuselage, floor, as well as thermal protection elements [1].

One of the methods to produce three-layer panels is vacuum diffusion welding (VDW) [2]. Welding of panels of aluminium alloys is recommended at temperatures higher than 500 °C. However, during heating, the modulus of elasticity of aluminium is rapidly reduced and, therefore, aluminium structures at temperatures of 250–300 °C and higher may lose stability, which causes a difficulty in producing three-layer honeycomb panels during their VDW.

It is possible to increase the resistance of a honeycomb filler in VDW of three-layer panels by the use of a more strength material, such as titanium, but its use as a filler will lead to a significant increase in the total mass of the structure, which when using products in the aircraft industry is not desirable.

In our opinion, the optimal variant between the minimum mass and the maximum strength of honeycomb structures is the use of layered composites. This

can significantly improve a number of properties, including specific stiffness and strength, fracture toughness, fatigue characteristics, impact characteristics, wear resistance, corrosion resistance and damping ability, provide an increased ductility of brittle materials and high stability of sizes [3].

In [4], the possibility of producing bimetal Al–Ti by VDW is confirmed.

It can be assumed that the use of layered composite materials (LCM), to which bimetals can also be attributed, can significantly improve the properties of honeycomb structures. Taking into account the possibility of wide regulation of the structure and composition of LCM at the stage of joint formation, studies on the manufacture of such materials is quite relevant. Taken this fact into account, the aim of the work is to develop the procedure of producing three-layer honeycomb panels by VDW from layered composites based on aluminium and titanium alloys.

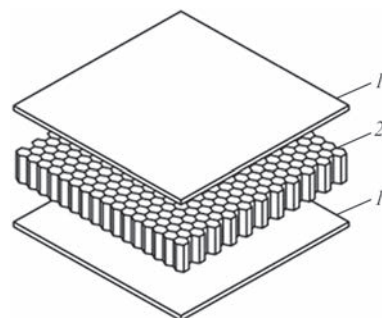


Figure 1. Scheme of a three-layer honeycomb panel: 1 — facial panel; 2 — honeycomb filler

Table 1. Chemical composition of AD1, AMg2 and VT1-0 alloys, wt.%

Alloy	Al	Ti	Fe	Si	Mn	Cu	Mg	Zn	Cr	Amount of impurities
AD1	Base	0.15	0.3	0.3	0.025	0.02	0.05	0.1	–	–
AMg2	Same	0.15	0.5	0.4	0.1–0.5	0.15	1.7–2.4	0.15	0.05	–
VT1-0	–	Base	0.025	0.10	–	–	–	–	–	0.35

RESEARCH PROCEDURES, MATERIALS

For studies, alloys of AD1 aluminium and VT1-0 titanium alloys in the form of foil respectively of 150 and 30 μm thickness were used. For lids, aluminium AMg2 alloy of 1 mm thickness or LCM based on aluminium and titanium of 480 μm thickness were used. The chemical composition of aluminium and titanium alloys used for the manufacture of three-layer honeycomb panels is given in Table 1.

To manufacture a honeycomb filler, bimetal Al–Ti billets of 130×130×0.180 mm were used, which were previously produced by VDW [5]. From bimetal sheets, strips of 12 mm width were cut, from which in turn in a special equipment, corrugated strips with a step of bending of 10 mm were formed.

In the manufacture of a honeycomb filler, spot welding was used, which was carried out at room temperature in air. Before welding, the contact surfaces of the corrugated strips were cleaned mechanically and degreased. Welding was carried out at constant values of voltage $U_w = 10$ V and current $I_w = 250$ mA, the intensity of heating was determined by the pulse duration $t_w = 0.5\text{--}5.0$ s and their number $N_w = 1\text{--}20$.

Unlike welding of homogeneous material, in spot welding of bimetal strips, there may be some complications due to not only the heterogeneity of the material over thickness, but also various physical and mechanical properties of titanium and aluminium. Titanium has a low electrical and thermal conductivity, very active in relation to the gases contained in the atmosphere. Its welding is carried out at relatively low parameters of current, compression force and heating duration. Aluminium has high thermal conductivity, low electrical resistance and refractory oxide film on the surface. Therefore, the surfaces of parts before welding should be carefully treated so that the oxide film was removed to prevent the formation of lacks of fusion.

As is shown in [5], the optimal variant of welding of bimetal Al–Ti strips when producing a honeycomb filler is welding of the aluminium layer to the titanium layer.

Before VDW of panels, end surfaces of a honeycomb filler and contact surfaces on lids were cleaned with a scraper and degreased with alcohol.

Welding was carried out in the vacuum chamber of the installation P115, equipped with a radiation heating system. The heating temperature was monitored by a chromel-alumel thermocouple, fixed in the

equipment. The pressure to the specimens was applied from the press through the lower stem. The pressure control was carried out using a dynamometer.

Welding was carried out in the following mode: temperature $T_w = 560\text{--}610$ °C, pressure $P_w = 5\text{--}20$ MPa, welding duration $t_w = 20\text{--}30$ min.

The structural characteristics of the foil and welded joints were analyzed with the use of the CAMSCAN 4 electron microscope, equipped with EDX INCA 200 system for energy dispersive analysis of a local chemical composition on plane specimens. Cross-sections were prepared according to the standard procedure using grinding and polishing equipment of Struers Company.

Mechanical properties of the specimens were determined during their tests for compression, which corresponds to the research procedure given in [6, 7].

To carry out mechanical tests of the honeycomb structure on compression, a digital pressure controller of the KOLI Company of the brand KhK3118T1 and a sensor of the CAS Company of the brand MNC-1 with a working interval from 0 to 1000 kg were used.

RESEARCH RESULTS

Taken into account that in the aircraft and space industry, materials with low specific weight are used, we produced experimental LCM specimens of different thicknesses and with different number of layers. In Figure 2, *a* the general appearance of LCM specimen, which consists of four layers (2Al + Ti + Al) is presented. The total thickness of LCM is 480 μm , the specific weight of the produced material is 2.9 g/cm³.

To reduce the weight of LCM, as a reinforcing element, wire or titanium mesh can be used. The overall appearance of the LCM specimen with the use of the mesh of VT1 titanium alloy is shown in Figure 2, *b*. The specimen consists of three layers: aluminium layer, titanium layer (mesh) and aluminium layer. The total thickness of the specimen is 950 μm (two layers of aluminium is 300 μm and titanium is 650 μm), the specific weight of the produced material is 2.24 g/cm³.

Generalized results with the parameters of the produced LCM specimens are given in Table 2. Produced LCM have a fairly wide range of specific weight values, which are predetermined by differences in the content of aluminium and titanium in each of the composites.

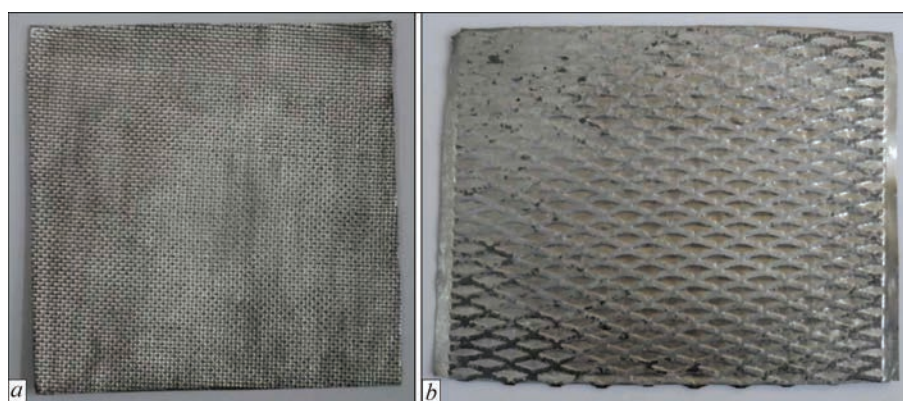


Figure 2. LCM specimens with different thickness and different layer composition: *a* — two aluminium layers, titanium layer, aluminium layer; *b* — aluminium layer, titanium layer (mesh), aluminium layer

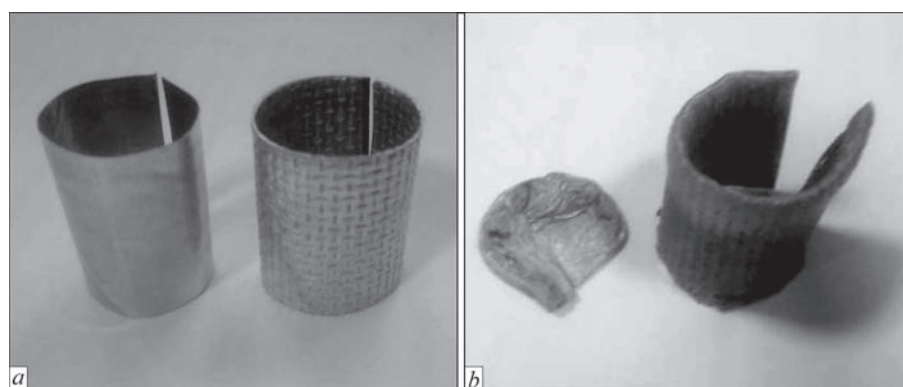


Figure 3. Appearance of aluminium AD1 alloy specimens (left) and Al-Ti LCM (right) in the initial state (*a*) and after heating in the furnace to a temperature of 700 °C for 30 min (*b*)

We have investigated thermal stability of a binary LCM, which consisted of an aluminium and a titanium layer. The carried out studies have shown that as compared to aluminium alloys, it is able to withstand higher temperatures without loss of a design shape, that coincides with the results of other researchers [8]. Figure 3, *a* shows a specimen of aluminium AD1 alloy and LCM, produced from titanium VT1 and aluminium AD1 alloy in the initial state and after heating in the furnace for 30 min at a temperature of 700 °C. As is seen from Figure 3, in the process of heating, the aluminium specimen melts and the LCM specimen retains its design shape.

Obviously, the prospect of using Al-Ti bimetal produced by VDW for the manufacture of three-layer honeycomb panels, as well as the possibility of their operation at elevated temperatures will be determined by the strength and intensity of growth of an inter-

metallic layer in bimetal during the manufacture of honeycomb structures and their operation.

VDW of honeycomb panels was performed at a temperature $T = 560\text{--}600$ °C, pressure $P = 10$ MPa, duration of the process $t_w = 30$ min, vacuum in the chamber was maintained at the level of $1.33 \cdot 10^{-3}$ Pa.

To determine the more specific temperature of welding T-joints of lids with a honeycomb filler, the studies of mechanical properties of three-layer panels, produced at different temperatures of the process were conducted, from the results of which the welding mode was chosen.

For mechanical compression tests, the specimens were selected consisting of a single bimetal honeycomb Al-Ti and lids of AMg2 alloy. The size of a honeycomb filler cell was 10×10 mm, height was 12 mm and cross-sectional area was 18 mm². To produce specimens for each of the studied temperatures, two

Table 2. Parameters of specimens of layered composite materials

Number	LCM composition	Number of layers	Material of layers	Layer thickness, μm		Total thickness, μm	Specific weight of LCM, g/cm^3
				Al	Ti		
1	Al-Ti	2	Al, Ti — foil	150	30	180	3.4
2	Al-Ti-Al	3	Al — foil, Ti — mesh	150	650	950	2.24
3	Al-Al-Ti-Al	4	Al, Ti — foil	150	30	480	2.9
4	Al-Ti-Al-Ti-Al	5		150	30	510	3.21

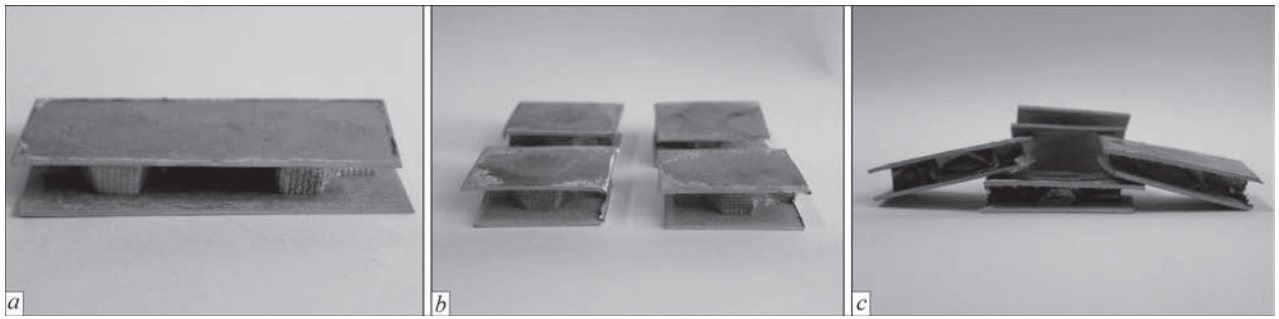


Figure 4. Specimens of the honeycomb panel produced by the method of VDW: *a* — after welding; *b* — elements of a three-layer panel after cutting with an abrasive disc; *c* — after mechanical compression tests

panels were welded, the typical appearance of which is shown in Figure 4, *a*. Then, the panels were cut in half with the use of an abrasive disc (Figure 4, *b*). Upsetting of the honeycombs was set at the level of 50 % of their initial height. It was established that in the specimens produced at a welding temperature of 570 °C, a partial delamination of facial lids occurs already at the stage of their cutting. During the mechanical tests, T-joints are completely destroyed. A poor quality of the joint between the surfaces of facial lids and the ends of a honeycomb filler leads to uneven redistribution of a load, and as a result to a significant decrease in the level of strength of such panels, the average value of which is 2/3 of the strength of the original honeycomb filler (Table 3).

An increase in welding temperature to 580 °C allows increasing the compression strength to 37.2 MPa. At the same time, during deformation of the walls of a honeycomb filler, a single destruction of welding places between filler and lids occurs.

The further increase in welding temperature to 590 °C allows bringing the strength of the three-layer panel to 47.3 MPa, which corresponds to the value inherent in a honeycomb filler after annealing at a tem-

Table 3. Results of mechanical tests on compression of three-layer panel specimens

Welding temperature T_w , °C	Compression strength, MPa	Average compression strength, MPa
570	—	27.1
	—	
	28.0	
580	26.1	37.2
	31.9	
	34.0	
	47.0	
	35.9	
590	52.2	47.3
	43.6	
	44.8	
	48.7	
600	44.3	44.0
	38.8	
	57.6	
	35.2	

perature of 600 °C for 60 min. Moreover, as is seen from Figure 4, *c*, during compression a deformation of the walls of a honeycomb filler without destruction of places of welding filler with facial lids occurs.

The strength of the T-joints produced at a welding temperature of 600 °C is close to the previous results: its slight drop occurs, which is probably related to the diffusion of magnesium of AMg2 alloy to the joining zone.

From the abovementioned, it can be concluded that to produce a high-quality T-joint of a honeycomb filler with facial lids, the optimum welding temperature is 590 °C.

Moreover, according to metallographic examinations of the joints produced at a temperature of 570 °C, some of the specimens are destroyed due to the lack of a physical contact between welded surfaces (Figure 5, *a*). In the specimens produced at a temperature of 590 °C, a sealed joint is formed, in the butt a small number of defects is observed (Figure 5, *b*).

According to the carried out works, the procedure of manufacturing a three-layer honeycomb panel should include the following basic operations:

- diffusion welding of bimetal material;
- cutting of bimetal foil into strips (Figure 6, *a*);
- formation of profiled bands from strips (Figure 6, *b*);
- cleaning and degreasing of the corresponding surfaces and welding of a honeycomb filler;
- cleaning and degreasing of end surfaces of a honeycomb filler block and facial lids of a honeycomb panel;
- VDW of a three-layer honeycomb panel (Figure 6, *c*).

Welding of bimetal Al-Ti material was carried out at a temperature $T_w = 580$ °C, pressure $P_w = 5$ MPa, with the exposure on the mode during $t_w = 20$ min. The produced plates of 130×70 mm were cut into strips of 70×12 mm (Figure 6, *a*), of which, after the formation of profiled strips by spot welding, a honeycomb filler with the size of honeycombs of 10×10×12 mm (Figure 6, *c*) was manufactured.

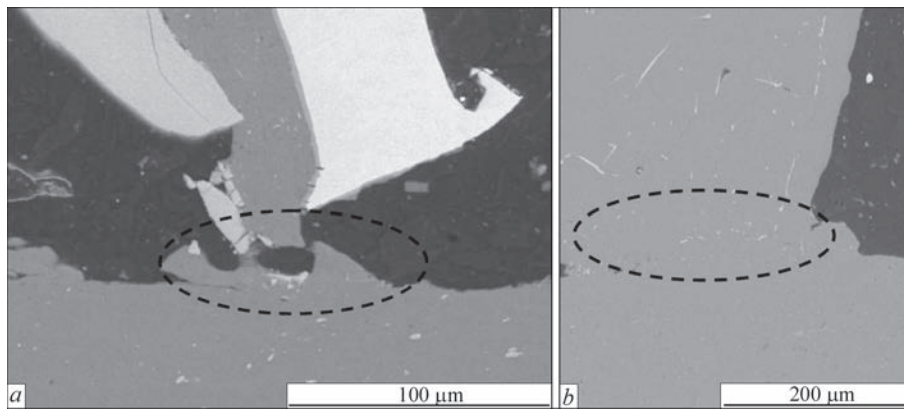


Figure 5. Microstructure of the zone of T-joint specimens produced at a temperature of 570 (a), 590 °C (b)

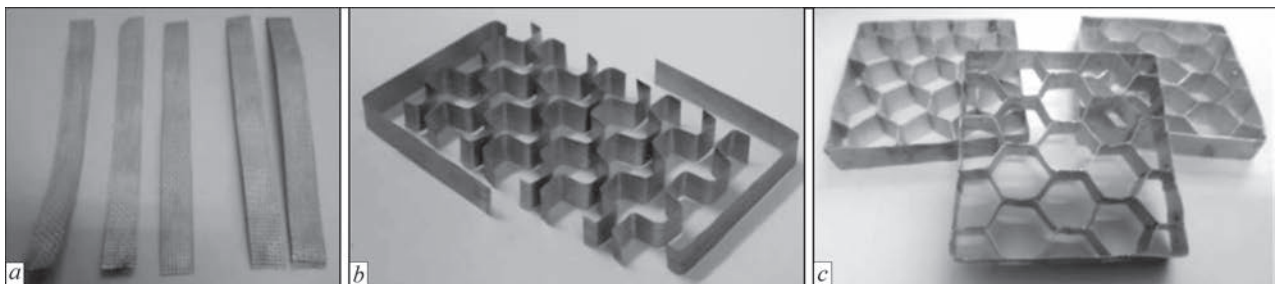


Figure 6. Stages of manufacturing honeycomb filler: a — strips of bimetall Al-Ti material; b — workpieces of profiled strips for spot welding of a honeycomb filler; c — 72×72 mm honeycomb filler

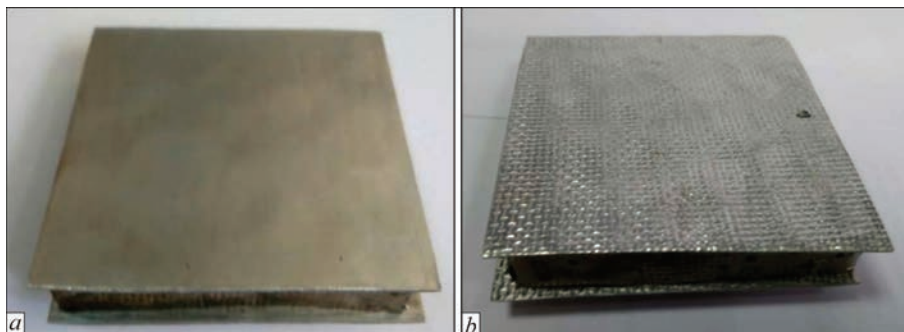


Figure 7. Model specimen of a three-layer honeycomb panel with lids of aluminium AMg2 alloy (a) and honeycomb panel with lids of layered composite Al-Ti-Al-Al material

For welding panel of honeycombs on the base of bimetall Al-Ti material and lids of aluminium AMg2 alloy, the equipment was designed and manufactured, consisting of a matrix and a punch and embedded elements that allowed centering of a panel billet on the center of the matrix and regulating the level of plastic deformation of a product. The procedure of producing welded joints was worked out.

On the basis of the developed technology, a batch of model specimens of a three-layer panel of bimetall Al-Ti honeycomb filler and facial lids of aluminium AMg2 alloy were manufactured (Figure 7, a). A three-layer panel was also produced, which completely consists of LCM (Figure 7, b). A honeycomb filler consists of Al-Ti bimetall, and lids consist of Al-Ti-Al-Al LCM.

As our studies showed, the mass of a three-layer panel produced with lids of aluminium alloy is

46–48 g, and the mass of a three-layer panel with Al-Ti-Al-Al LCM is respectively 24–26 g.

Thus, it can be assumed that the use of LCM for the manufacture of a three-layer honeycomb panel provides a significant reduction in the mass of products.

CONCLUSIONS

1. The fundamental possibility of producing honeycomb three-layer panels with LCM by VDW method is shown.

2. Welding parameters were determined, that allow producing T-joint of a honeycomb filler with LCM based on Al-Ti alloys with lids of aluminium alloy with an average compression strength at the level of 47.3 MPa.

3. It is shown that the use of LCM for the manufacture of three-layer honeycomb panels allows reducing

the mass of products by 2 times as compared to the panels made with lids of aluminium alloy.

REFERENCES

1. Bitzer, T. (1997) *Honeycomb Technology. Materials, Design, Manufacturing, Applications and Testing*. Springer-Science+Business Media Dordrecht.
2. Bashurin, A.V., Mastikhin, E.Yu., Kolmykov, V.I. (2010) Diffusion welding of hollow bimetal panels. *Zagotovitelnye Proizvodstva v Mashinostroenii*, **1**, 13–15 [in Russian].
3. Jafarian, H.R., Mahdavian, M.M., Shams, S.A.A., Eivani, A.R. (2021) Microstructure analysis and observation of peculiar mechanical properties of Al/Cu/Zn/Ni multi-layered composite produced by Accumulative-Roll-Bonding (ARB). *Materials Sci. and Engin.: A*, **805**, 140556. DOI: <https://doi.org/10.1016/j.msea.2020.140556>
4. Falchenko, Iu.V., Petrushynets, L.V., Polovetskii, E.V. (2020) Peculiarities of producing layered metal composite materials on aluminium base. *The Paton Welding J.*, **4**, 11–21. DOI: <https://doi.org/10.37434/tpwj2020.04.02>
5. Falchenko, Iu.V., Petrushynets, L.V., Polovetskyi, Ye.V. (2020) Peculiarities of producing Al–Ti bimetal sheet joints by the method of vacuum diffusion welding. *The Paton Welding J.*, **8**, 25–28. DOI: <https://doi.org/10.37434/tpwj2020.08.04>
6. Zongwen, Li, Jianxun, Ma. (2020) Experimental study on mechanical properties of the sandwich composite structure reinforced by basalt fiber and nomex honeycomb. *Materials*, **13**(8), 1870. DOI: <https://doi.org/10.3390/ma13081870>
7. Seemann, R. (2020) *A virtual testing approach for honeycomb sandwich panel joints in aircraft interior*. Springer Vieweg.
8. Robabeh Jafari, Beitallah Eghbali, Maryam Adhami Materials (2018) Chemistry and physics influence of annealing

on the microstructure and mechanical properties of Ti/Al and Ti/Al/Nb laminated composites. *Materials Chemistry and Physics*, **213**, 313–323. DOI: <https://doi.org/10.1016/j.matchemphys.2018.04.001>

ORCID

L.V. Petrushynets,: 0000-0001-7946-3056,
Yu.V. Falchenko: 0000-0002-3028-2964,
O.O. Novomlynets: 0000-0002-0774-434X,
V.E. Fedorchuk: 0000-0002-9929-3231

CONFLICT OF INTEREST

The Authors declare no conflict of interest

CORRESPONDING AUTHOR

Yu.V. Falchenko
E.O. Paton Electric Welding Institute of the NASU
11 Kazymyr Malevych Str., 03150, Kyiv, Ukraine.
E-mail: falchenko@paton.kiev.ua

SUGGESTED CITATION

L.V. Petrushynets, Yu.V. Falchenko,
O.O. Novomlynets, V.E. Fedorchuk (2022)
Application of a layered composite material based
on aluminium and titanium alloys to produce welded
three-layer honeycomb panels. *The Paton Welding J.*,
7, 17–22.

JOURNAL HOME PAGE

<https://pwj.com.ua/en>

Received: 02.06.2022

Accepted: 15.09.2022

MORE CLIMATE PROTECTION AND LOWER ENERGY COSTS IN THE METAL INDUSTRY

Decarbonization in the metal industry: decarbXpo presents technologies and services for more climate protection and lower energy costs from 20–22 September. This year with a free lecture program for companies.

Reduce both emissions and costs.

Messe Düsseldorf is launching a new type of trade fair: The Expo for Decarbonized Industries > ENERGY STORAGE (decarbXpo) combines the most comprehensive offer of solutions for decarbonising industries and trade crafts with a high quality forum and conference agenda to become a single event.

From 20–22 September, companies will present their technologies and services for reducing both emissions and costs. Companies from the metal industry can expect several highlights:

◆ On 21 September, during the trade fair, ecoMetals Day will take place — an interdisciplinary congress of experts for the transformation of the industry.

◆ On 19 and 20 September, VDMS AG Power to X for Applications is organising their #P2X Conference with a focus on hydrogen applications.

In addition, there will be a comprehensive free-to-attend lecture programme in the forum in Hall 9. Among other things, numerous start-ups will present exciting solutions for the industry.



DOI: <https://doi.org/10.37434/tpwj2022.07.04>

EFFECTIVENESS OF COMBINED GAS-SLAG PROTECTION AT MIG DEPOSITION OF COPPER ALLOYS ON STEEL

T.B. Maidanchuk, V.M. Ilyushenko, A.M. Bondarenko, D.M. Stepchenko

E.O. Paton Electric Welding Institute of the NASU

11 Kazymyr Malevych Str., 03150, Kyiv, Ukraine

ABSTRACT

A complex of investigations was performed to study the technological capabilities for application of combined gas-slag protection in MIG-process of copper alloy deposition on steel. It is shown that at semi-submerged arc surfacing (by semi-open arc) it is possible to control the technological characteristics of the welding arc, namely: increase its spatial stability, improve the pattern of electrode metal transfer (essentially reducing its spattering fraction), as well as provide a high-quality protection of the deposits from oxidation. Application of such a combined protection is particularly rational at a highly efficient process of two-electrode MIG surfacing.

KEYWORDS: copper alloys, combined gas-slag protection, spatial stability of the arc, two-electrode surfacing, deposited metal quality

INTRODUCTION

Copper alloys are widely used in various fields of mechanical engineering. In order to increase the structural strength of products and save precious nonferrous metals, bimetal products steel + bronze are often used. The most common method to produce such parts is the mechanized and automated consumable electrode arc surfacing in shielding gases (MIG-process) [1, 2]. At the same time, to provide minimal penetration of steel and a slight transition of iron into the deposited metal, surfacing is performed on low current densities, which leads to a decrease in the process stability and a significant spattering of the electrode metal. Taken into account the high tendency of bronze (especially aluminium and silicon) to oxidation, a need arises to use more reliable protection of welding pool from air. It is typical that in surfacing of silicon bronzes even applying such an advanced process as CMT Brazing of the Fronius Company with the use of CuSi wire, on the metal surface, a film of a thin layer of silicates and oxides, that are poorly removed from the surface, is observed [3, 4].

The mentioned disadvantages are especially revealed in a high-efficiency two-electrode MIG-process of surfacing, in which the volume of molten metal increases and requires creating additional conditions for its protection from environmental impact. In connection with that, the problem of studying technological capabilities of using a combined gas-slag protection in automated arc processes when the process of melting and transfer of electrode metal occurs in a gas-protective environment and the weld pool metal is additionally protected by molten flux.

It should be noted that in the practice of welding production, the use of combined gas-slag protection is successfully realized in manual welding using coating electrodes and mechanized and automated welding using flux-cored wires [5–7].

RESEARCH MATERIALS AND EQUIPMENT

The studies were carried out using specimens of steel of grade St.20 of 200×300×14 mm. The welding wire is bronze BrKMts3-1 of 1.2 mm diameter. As a shielding gas, argon of the first grade was used. The molten glass-type fluxes of general purpose of grades AN-60SM, AN-20S, AN-26S, as well as the agglomerated flux UV420 TT of the Böhler Thyssen Company were evaluated.

The installation for surfacing is equipped with a mechanism for feeding two wires, which provided the process of surfacing with both one and two electrodes connected to a one power source (the so-

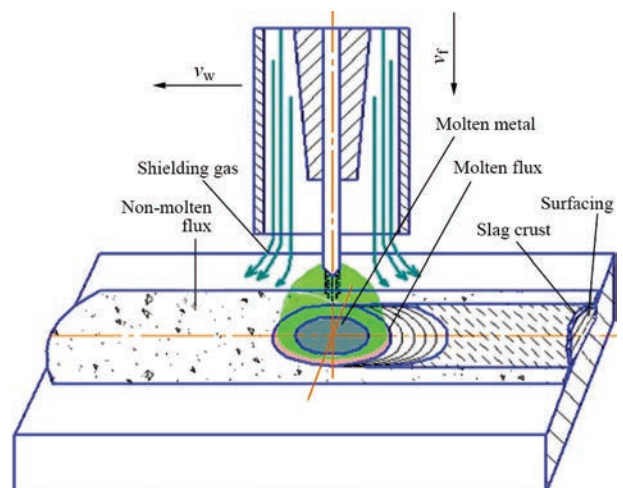


Figure 1. Scheme of surfacing process with a combined gas-slag protection

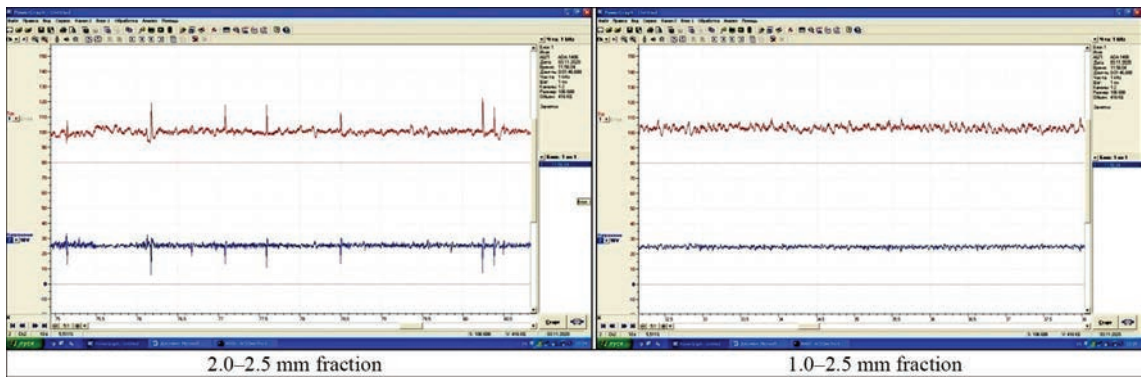


Figure 2. Oscillograms of surfacing processes using flux AN-60SM of different granularity

called split electrode). The power source is rectifier VDU-506. The laboratory equipment is fitted with a registration and measuring complex on the base of an analogue-digital converter ADA-1406, which makes it possible to monitor the actual parameters of the surfacing process and to study the technological properties of welding arc.

The scheme of surfacing process with a combined gas-slag protection is shown in Figure 1.

EXPERIMENTAL STUDIES AND RESULTS

The principal possibility of MIG-process of surfacing bronze with a combined protection (over a flux layer) was evaluated during the one-electrode process. As the experiments showed, during traditional shielding gas consumptions, at the exit from the nozzle, its pressure can blow the flux away, which leads to a deterioration of the quality of deposits. It was determined that boundary argon consumptions should not exceed 15 l/min.

In order to choose the optimal grade of flux, the impact of different fluxes on the stability of MIG-process of surfacing, formation of deposited metal, separation of slag crust and metallurgical quality of deposits (presence of pores) were studied.

Table shows the appearance and geometric dimensions of deposited beads, produced using fluxes of grades AN-60SM, AN-20S, AN-26S and agglomerated flux UV420 TT.

As the experiments showed, in surfacing bronze BrKMts3-1 on steel with additional slag protection, the best results as for deposited bead formation, separation of slag crust and quality of deposited metal were obtained when using manganese-silicate flux AN-60SM. It was found that the highest stability of the process is observed while using fine-grained flux with the grain size of 1.0–2.5 mm (Figure 2).

To determine the optimal amount of flux, the height of its layer was changed in the range 4–8 mm, the rest of the process parameters was not changed ($I_w = 180–200$ A, $U_a = 24–25$ V, $v_w = 10$ m/h, electrode stickout is 12 mm, $Q_{Ar} = 15$ l/min). The best results on the process stability were recorded when using a flux layer of 6.0 mm height, which is evidenced by the oscillograms of current and voltage (Figure 3).

In addition to increased stability of the surfacing process, at the height of the flux layer of 6.0 mm, spattering of electrode metal is also absent and a high quality of bead formation is observed. In this case, the arc is semi-open, a thin film of the slag covers the entire surface of the bead, as a result of which, it has a not oxidized “shiny” appearance, which is typical for bronze (Figure 4).

In addition, when using a combined protection at the same modes, the shape of beads changes: the height of beads increases and they are getting narrow in the cross-section. In our opinion, such effect of flux

Table 1. Appearance and geometric dimensions of beads depending on flux grade

Geometric dimensions of beads					
	Protection	Ar	Ar + AN-60SM	Ar + AN-20S	Ar + AN-26S
Bead width, mm	16–17	14–15	13.5–14	13.5–14	12–13
Bead height, mm	3–3.5	3.5–3.8	4–4.5	4–4.5	4.2–4.6
Penetration depth, mm	0.3–0.6	0.4–0.45	0.4–0.6	0.35–0.45	0.35–0.45

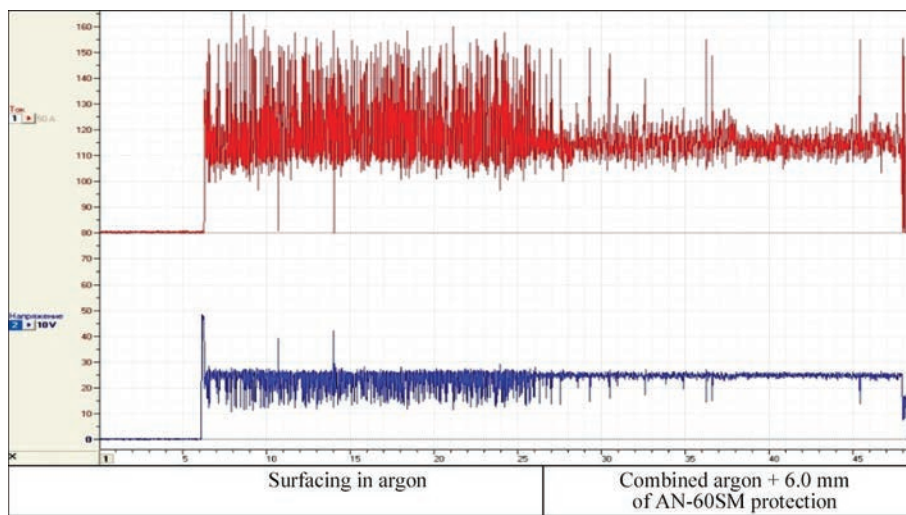


Figure 3. Oscillograms of current (*a*) and voltage (*b*) of the process of surfacing bronze BrKMts3-1 at a combined argon + flux AN-60SM protection

on the formation of deposited beads occurs due to the improvement of a spatial stability of the arc, predetermined by the presence of the film of molten flux on the edges of the pool and in its tail part, which stabilizes the position of the cathode spot on the surface of the welding pool. The quality of beads can also be affected by surface tension on the boundary molten slag–liquid metal–solid backup.

As was noted above, the need in additional protection of molten metal is especially relevant for the two-electrode MIG-process of surfacing bronze. The previously developed and mastered [2] technologies of surfacing bronze by a “split electrode” were focused on the processes with the wires of 2.0–3.0 mm diameter with the use of flux or argon as a welding pool protection.

A complex of studies on the influence of mode parameters on the process of two-electrode surfacing using a wire of 1.2 mm diameter with the use of a combined argon + flux protection was performed. Considering that along with the basic mode parameters (current, voltage on the arc, speed of surfacing), distance between the electrodes has a significant impact on the penetration of steel and the shape of the deposited bead. A number of experiments were performed in order to optimize this parameter for wires of 1.2 mm diameter.

In the proceedings [2], that present the results of argon-arc surfacing of aluminium bronze BrAMts9-2 of 2 mm diameter by a “split electrode”, for the oriented choice of optimal value of the interelectrode distance, it is recommended to take the distance equal to three electrode diameters.

In our experiments, the distance between the electrodes varied from 3.6 to 8.0 mm. The experiments were performed by surfacing of individual beads and

each subsequent bead was deposited after a complete cooling of the plate.

Surfacing mode: $I_s = 200\text{--}240$ A; $U_a = 28\text{--}32$ V; $v_s = 12$ m/h; $Q_{Ar} = 15$ l/min, height of the layer of flux AN-60SM is 6 mm.

Figure 5 shows macrosections of cross-sections of the beads, deposited at a different interelectrode distance. It is clearly seen that with an increase in the interelectrode distance, the shape and degree of penetration of the base metal change. This change is predetermined by the peculiarities of welding arc burning, melting and transfer of electrode metal in the two-electrode process.

At optimal values of an interelectrode distance, an alternate arc burning at each electrode is observed, which provides a scattered heat input across the width of the pool and, accordingly, the minimum penetration of the base metal.



Figure 4. Appearance of deposited beads: *a* — surfacing in argon; *b* — argon + 4.0 mm of flux AN-60SM; *c* — argon + 6.0 mm of flux AN-60SM

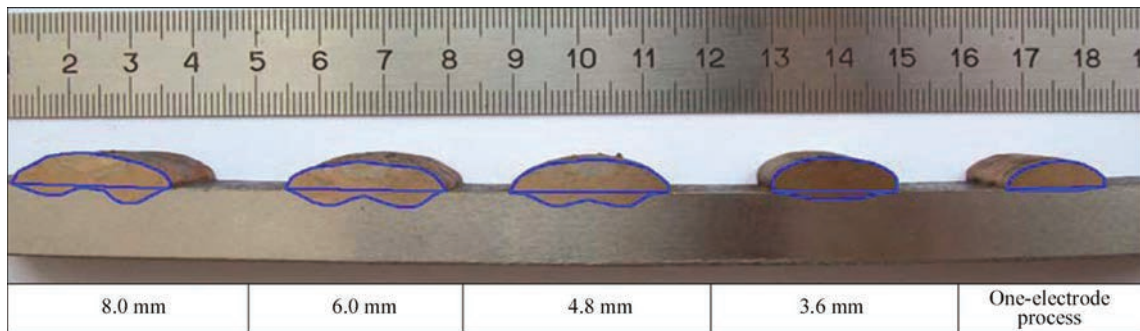


Figure 5. Cross-section of deposited beads at different interelectrode distance

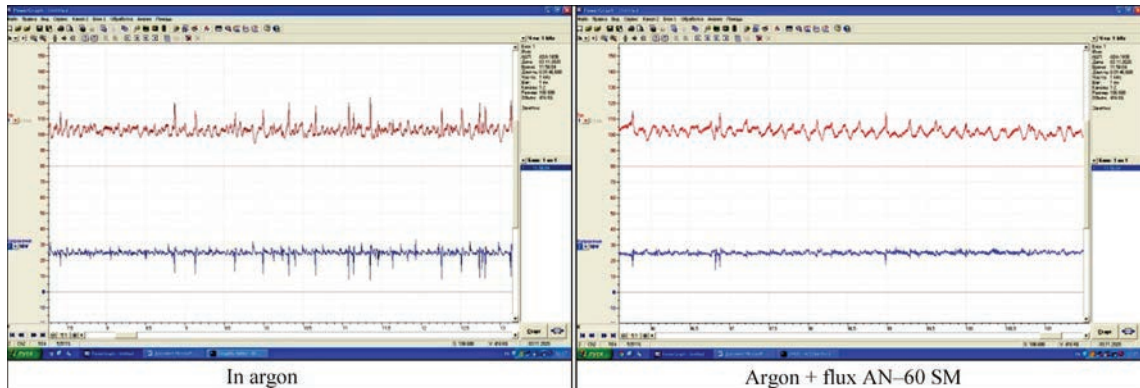


Figure 6. Oscillograms of two-electrode process of surfacing bronze BrKMts3-1 of 1.2 mm diameter on steel in argon and with a combined protection



Figure 7. Transverse macrosection of deposited bead of bronze at optimal modes ($\times 2$)

It should be noted that at an interelectrode distance of up to 4.0 mm, the process of two-electrode surfacing with a combined gas-slag protection is also characterized by an increased stability (Figure 6), which guarantees producing of well-formed deposits.

Considering that the two-electrode process allows improving the efficiency of surfacing by 1.5–1.7 times (up to 3.0–3.2 kg/h for the wires of 1.2 mm diameter, additional slag protection of welding pool provides a high quality of deposited metal (Figure 7).

CONCLUSIONS

1. As a result of experimental studies, it was established that the use of a combined gas-slag protection improves technological properties of the welding arc, namely its spatial stability due to the presence of shielding molten slag, affects the pattern of the

transfer and the degree of electrode metal spattering, provides a high-quality formation of deposited bronze with its typical “shining” surface.

2. The best results of MIG-process of surfacing bronze BrKMts 3-1 using a wire of 1.2 mm diameter with a combined gas-slag protection were obtained when as an additional slag protection, the flux of grade AN-60SM with 6 mm height of the layer was used.

3. The special rationality of using combined gas-slag protection in the two-electrode MIG-process of surfacing copper alloys in order to better protect the volumes of molten metal and welding pool against oxidation, which were increased as compared to the one-electrode process, was shown. The basic parameters of the two-electrode MIG-process of surfacing with a combined protection of the wire of 1.2 mm diameter are optimized. Also, the optimal interelectrode distance was determined, which provides a slight penetration of steel and minimal mixing of base and deposited metals at the selected values of current and speed of surfacing.

REFERENCES

- Gurevich, S.M. (1990) *Handbook on welding of nonferrous metals*. Kyiv, Naukova Dumka [in Russian].
- Ilyushenko, V.M., Lukyanenko, E.P. (2013) *Welding and surfacing of copper and copper alloys*. Kyiv, IAW [in Russian].
- Kittichai Sojiphan, Trinet Yingsamphancharoen, Narawit Paosen et al. (2019) Effects of MIG-brazing current on wetta-

bility and mechanical property of galvanized steel lap joints. In: *Proc. of 12th Int. Conf. on Thailand Metallurgy*, 93–99. DOI: 10.13140/RG.2.2.30625.56162

4. <https://www.fronius.com/en-us/usa/welding-technology/world-of-welding/fronius-welding-processes/cmt>
5. Pokhodnya, I.K. (1990) *Metallurgy of arc welding. Processes in arc and melting of electrodes*. Kyiv, Naukova Dumka [in Russian].
6. Shlepakov, V.N., Kotelchuk, A.S. (2019) Improvement of technological and sanitary-hygienic characteristics of gas-shielded arc welding process. *The Paton Welding J.*, **6**, 29–33. DOI: <https://doi.org/10.15407/as2019.06.05>
7. Bonnel, J.-M., Maurer, M., Rosert, R. (2019) Submerged arc surfacing of high-alloy steels by flux-cored wires. *The Paton Welding J.*, **6**, 3–12. DOI: <https://doi.org/10.15407/as2019.06.01>

ORCID

T.B. Maidanchuk: 0000-0002-2826-8514,
V.M. Ilyushenko: 0000-0002-9047-8512,
A.M. Bondarenko: 0000-0003-0506-4444
D.M. Stepchenko: 0000-0001-9191-5780

CONFLICT OF INTEREST

The Authors declare no conflict of interest

CORRESPONDING AUTHOR

T.B. Maidanchuk

E.O. Paton Electric Welding Institute of the NASU
11 Kazymyr Malevych Str., 03150, Kyiv, Ukraine.

E-mail: pwj_37@ukr.net

SUGGESTED CITATION

T.B. Maidanchuk, V.M. Ilyushenko,

A.M. Bondarenko, D.M. Stepchenko (2022)

Effectiveness of combined gas-slag protection at mig deposition of copper alloys on steel. *The Paton Welding J.*, **7**, 23–27.

JOURNAL HOME PAGE

<https://pwj.com.ua/en>

Received: 17.05.2022

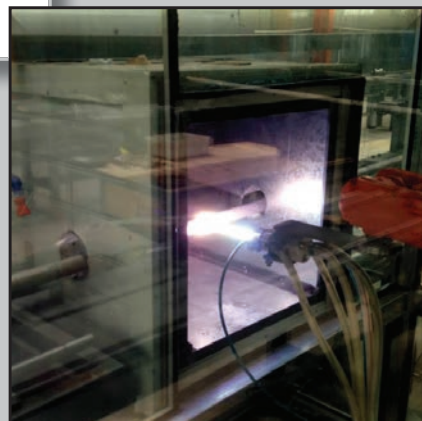
Accepted: 15.09.2022

DEVELOPED in PWI

EQUIPMENT FOR HIGH-PERFORMANCE SUPERSONIC PLASMA SPRAYING OF WEAR-RESISTANT, HEAT-RESISTANT AND HEAT-PROTECTIVE COATINGS



The equipment is designed for applying wear-resistant, corrosion-resistant, heat-shielding and special coatings by spraying powders from metals, alloys, carbides, borides, oxides and metal-ceramic materials. The thickness of applied coatings is from 20–50 μm to 1–2 mm and more.



Parameters	Values
Plasma forming gas	Air + methane, propane-butane (up to 5–10 %)
Plasma temperature, K	3500–7000
Plasma jet speed, m/s	1500–3000
Spray particle speed, m/s	400–800
Maximum spraying capacity, kg/h	15–50
Electric power, kW	40–180
Spray material utilization rate	До 0,8

DOI: <https://doi.org/10.37434/tpwj2022.07.05>

CORROSION RESISTANCE OF PLASMA COATINGS PRODUCED FROM COMPOSITE TiAl-BASED POWDERS WITH THE ADDITION OF NON-METALLIC REFRACTORY COMPOUNDS

Yu.S. Borysov, A.L. Borysova, N.V. Vihilianska, O.P. Gryshchenko, Z.G. Ipatova, K.V. Yantsevych, M.A. Vasytkivska

E.O. Paton Electric Welding Institute of the NASU
11 Kazymyr Malevych Str., 03150, Kyiv, Ukraine

ABSTRACT

The results of the study of the phase composition and corrosion resistance of plasma coatings from composite powders based on intermetallic in TiAl with the introduction of non-metallic refractory compounds (SiC or Si₃N₄) into its composition are presented. The plasma coatings were deposited on the specimens of St3, AMg3 and VT6 alloys. The coatings were studied by the methods of metallographic and X-ray structural phase analysis. The studies of electrochemical properties of the plasma coatings were carried out by the potentiostatic method in a 3 % NaCl solution. As initial materials for plasma spraying, the composite powders TiAl–SiC, TiAl–Si₃N₄, produced by the method of mechanochemical synthesis were used. Using the method of X-ray structural analysis, it was revealed that the phase composition of the plasma coatings for TiAl–SiC system consists of the following phases: TiAl, TiAl₃, TiC, Ti₅Si₃, Ti₃AlC, TiO₂, and for the coating TiAl–Si₃N₄ from the phases Ti₂Al, Ti₅Si₃, TiN, TiO. The average thickness of the coatings was 200 ± 50 μm and the porosity did not exceed 10 %. It was found that the introduction of SiC or Si₃N₄ into the composition of the composite coating leads to a decrease in the corrosion current in a 3 % NaCl solution by about an order of value, and the corrosion resistance of St3, AMg3 and VT6 alloys increases by 12–13, 8–9, and 1.8–2.0 times, respectively. The service life of the plasma coatings made of TiAl composite powders with the addition of SiC and Si₃N₄ was calculated. The studied coatings belong to the class of resistant and are capable to protect metals in a 3 % NaCl solution for a period from 6 to 10 years.

KEYWORDS: intermetallics, titanium, aluminium, non-metallic refractory compounds, composite powder, plasma coatings, corrosion resistance

INTRODUCTION

Intermetallics of Ti–Al system have a number of unique properties such as high melting point, low density, high modulus of elasticity, yield strength, which grows (for TiAl) at an increase in temperature, high values of heat and corrosion resistance. Titanium aluminides (TiAl, Ti₃Al) can be used as structural materials, such as protective coatings in gas and oil refining facilities of the chemical industry, nuclear engineering, where such characteristics as corrosion resistance and resistance to high-temperature oxidation are required [1–8].

Such methods of spraying coatings are used as ion-plasma [9], magnetron spraying [10], electrospark deposition [11]. The results of these works indicate that introducing such elements as carbon, nitrogen and silicon into the composition of the coatings allows improving their protective and also anticorrosion properties.

At the PWI, for thermal spraying of protective coatings based on intermetallics of Ti–Al system, composite powders (CP) with the introduction of non-metallic refractory compounds (NRC) were developed, namely B₄C, BN, SiC and Si₃N₄.

Copyright © The Author(s)

In this work, to study the corrosion properties of the coatings with CP based on TiAl intermetallics, two compositions of TiAl + 12 wt.% SiC and TiAl + 14 wt.% Si₃N₄ with addition of NRC were selected. The choice of these compositions was made on the basis of comparison of corrosion resistance of SiC and Si₃N₄ with other compounds of this group (B₄C, BN).

According to literary sources [12, 13], the beginning of B₄C oxidation is a temperature of 500 °C, and at 800–1000 °C, oxidation transfers to the active phase; BN is actively oxidized at 700–800 °C with the formation of B₂O₃, N₂, while Si₃N₄ silicon nitride has a high chemical resistance: compact specimens are resistant to air for a long time at 1200 °C, and in an oxygen medium, oxidation begins at 1000 °C and only at 1400 °C it runs actively. Regarding silicon carbide, as is known, even in an oxygen medium at 1300 °C, the ratio of weight of the oxidized powder before the initial state is less than 5 %.

Comparing the corrosion resistance of products of interaction of CP components TiAl–NRC (for B₄C and BN they include carbides, nitrides, and for SiC and Si₃N₄ they are silicides, titanium and aluminium nitrides) according to the literary sources [14], silicides have a higher corrosion resistance as compared

to other refractory compounds. This was the reason for choosing CP types in this work.

The aim of this work is the studies of influence of NRC (SiC, Si₃N₄) on corrosion resistance of plasma coatings from TiAl intermetallics and evaluating their protective action on carbon steels and light alloys (aluminium AMg3 and titanium VT6 alloys).

RESEARCH OBJECTS AND EXPERIMENT PROCEDURE

The initial materials for plasma spraying were CP TiAl–SiC and TiAl–Si₃N₄, produced by the method of mechanochemical synthesis with a particles size of 40–63 μm. The coatings were deposited on the specimens of St3, AMg3 and VT6 alloys in the installation UPU-8M for plasma spraying using the following modes: $I = 600$ A, $U = 40$ V, $Q_{Ar+N_2} = 50$ l/min, spraying distance — 80 mm.

The coatings were examined by the methods of metallographic, microdurometric and X-ray structural phase (installation Dron-UM-1, monochromatized CuK_α radiation) analysis.

The electrochemical properties of the plasma coatings were studied by the potentiostatic method in the potentiostat P-5827M at a scanning rate of 0.2 mV/s and a temperature of 18–20 °C. Stationary potentials were measured relative to the silver chloride electrode.

For the studies, the medium of a 3 % NaCl solution was selected. The choice of this electrolyte is predetermined by the fact that the main use of titanium and aluminium based alloys is the protection of parts and units in the aircraft industry [15]. The limited serviceability of individual units is associated with the fact that in them during operation many factors interact, which determines the conditions of operation — high-temperature gas corrosion, corrosion under the influence of Cl⁻ ions. The source of corrosion-aggressive components can be water, containing chloride ions, which enters the engine during injections (up to 1000–1200 injections per year). The presence of Cl⁻ ions leads to local destructions, as well as inhibits the formation of passive films on the metal surface. That is why as an aggressive medium for electrochemical tests, a 3 % NaCl solution was selected. Based on the experimental data, cathode and anode polarization curves were built in the coordinates $E_c = f(\lg i_c)$ where E_c is the potential, V; i_c is the corrosion current, A/cm². According to polarization curves, using the graphic method, the rate of i_c and the potential E_c of the corrosion respective to the extrapolation of Tafel slopes on cathode and anode curves before their mutual intersection were determined. Using the values of corrosion currents, determined from the polarization

curves, the weight and depth index of corrosion of the coatings were calculated by the formulas

$$K_w = \frac{iA1000}{nF}, K_d = K_d \frac{8.76}{\rho},$$

where K_w is the weight index of corrosion, g/(m²·h); A is the atomic weight of metal, g/mol; n is the valence of a metal ion, that went into the solution; F is the Faraday number, 26.8 A·h/mol; K_d is the depth index of corrosion, mm/year; ρ is the methane density, g/cm³; 8.76 is the coefficient for the transition from the weight index of corrosion K_w to the calculation for 1 h to the depth index of corrosion K_d of about a year, calculated from the number of hours per year (24×365 = 8760 h) and divided by 1000.

RESULTS OF THE EXPERIMENT AND THEIR DISCUSSION

Examinations of the microstructure (Figure 1) and microhardness of the deposited plasma coatings indicate that the developed coatings have heterogeneous structure with uniform distribution of phases over depth, any defects and delaminations at the interface with the base are absent. The average thickness of the coatings is 200 ± 50 μm, the porosity is 8–10 %, the microhardness is 5500 ± 600 MPa for TiAl–Si₃N₄, and 6000 ± 100 MPa for the composite coating TiAl–SiC. Using the method of X-ray structural analysis, it was revealed that the phase composition of the plasma coatings for TiAl–SiC system consists of the following phases: TiAl, TiAl₃, TiC, Ti₅Si₃, Ti₃AlC, TiO₂, for the coatings of TiAl–Si₃N₄ system with Ti₂Al, Ti₅Si₃, TiN, TiO (Figure 2). At the same time, the phase composition of the coatings does not depend on the type of the base, on which they are deposited.

The studies of the kinetics of the electrode potentials of the developed plasma coatings made it possible to reveal that the values of the electrode potential are stabilized within 40–60 min during the immersion of the coated specimens into it. The stationary potentials E_{st} of the studied coatings in a 3 % NaCl solution were –0.2 – –0.7 V, depending on the base material. The highest positive potential is observed in the coatings deposited on VT6 alloy (–0.2 V), followed by the coatings deposited on St3 and AMg3 alloy being –0.58 and –0.7 V, respectively. The specified discrepancies in the values of the stationary electrode potential E_{st} can be explained, first of all, by the difference in the chemical composition of the base material. The plotted dependence curves in the coordinates $E_{st} - \tau$ have approximately the same form (Figure 3). Thus, the I region corresponds to a rapid change in E_{st} in the II region, a slow change in E_{st} occurs, and in the III region, the initial equilibrium value of the potential

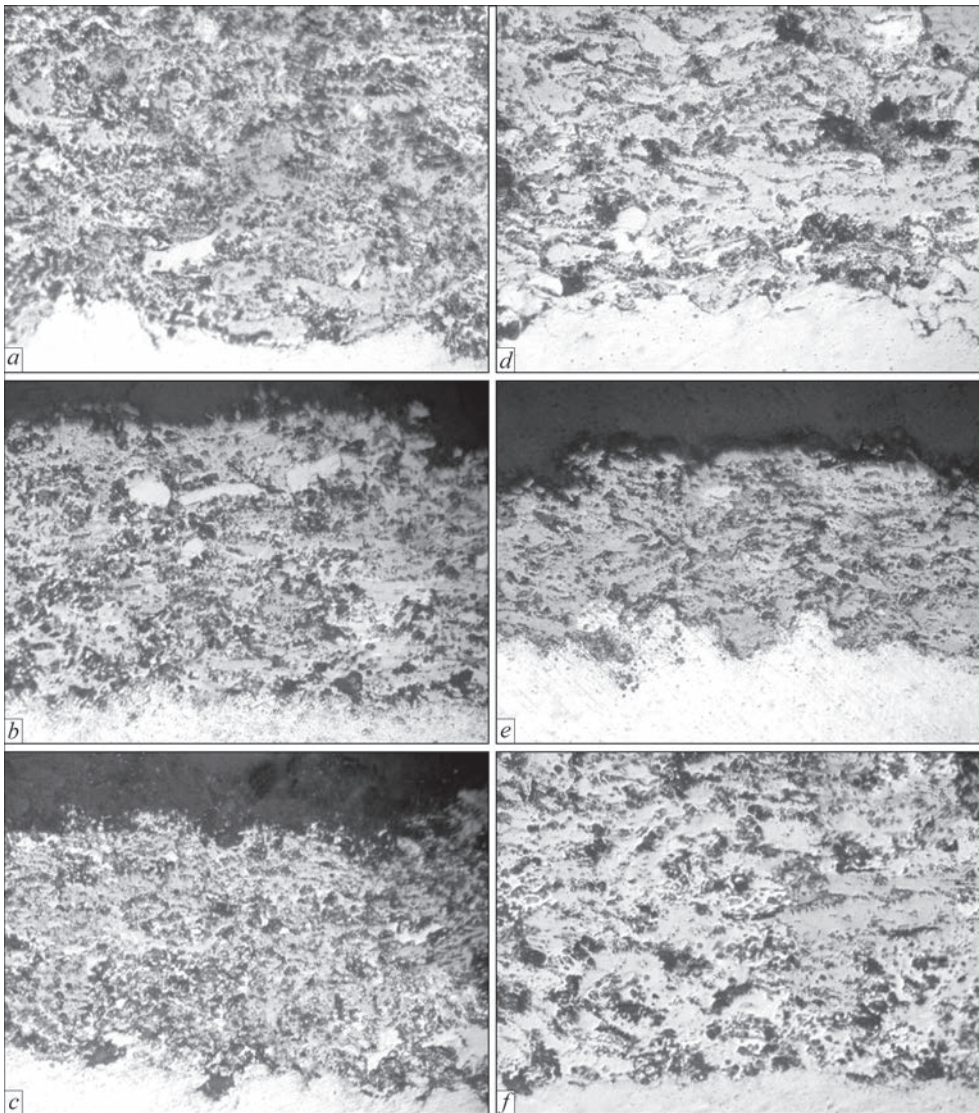


Figure 1. Microstructure ($\times 400$) of plasma coatings of TiAl-SiC system (*a-c*) and TiAl-Si₃N₄ (*d-f*), deposited on St3 (*a, d*), aluminium AMg3 (*b, e*) and titanium VT6 (*c, f*) alloys

is restored very slowly, at which the rate of running anode and cathode processes is equal.

The analysis of the obtained polarization curves (Figure 4) showed that the nature of the corrosion behaviour of the plasma coatings with CP TiAl-SiC, TiAl-Si₃N₄, deposited on different bases, is approximately the same. The comparison of corrosion cur-

rents (Table 1), determined by extrapolation of Tafel regions of the polarization curves, showed that the coatings deposited on titanium VT6 alloy are characterized by the minimum corrosion current i_c , respectively, and its corrosion resistance is the highest.

In the literature, the information about the electrochemical behaviour of the alloy based on intermetallic

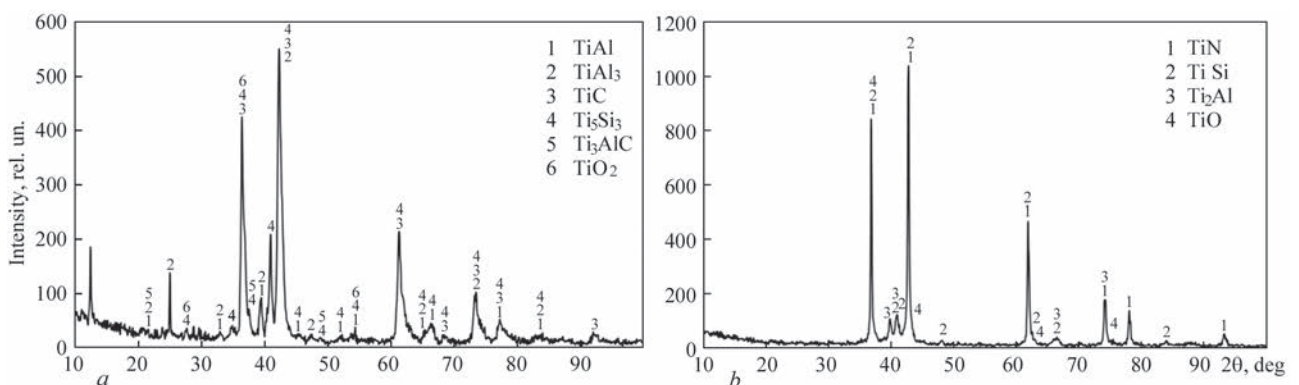


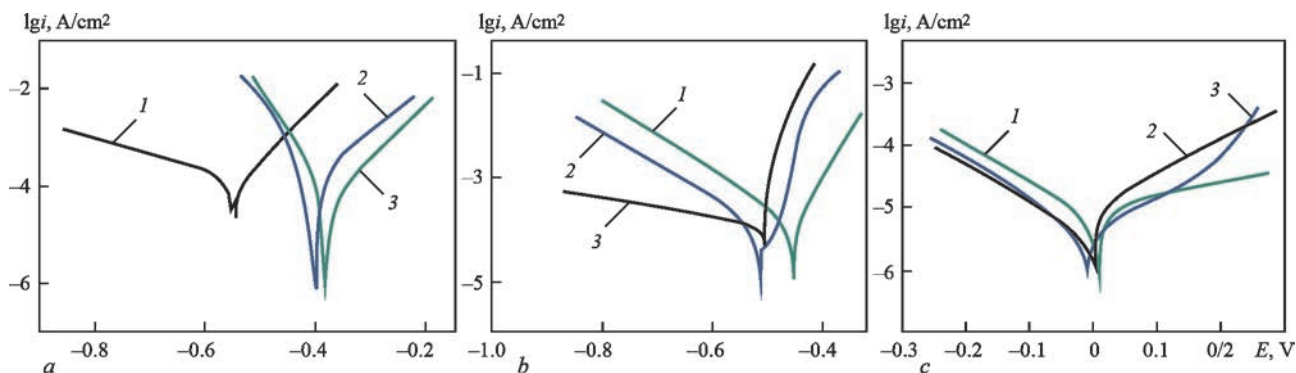
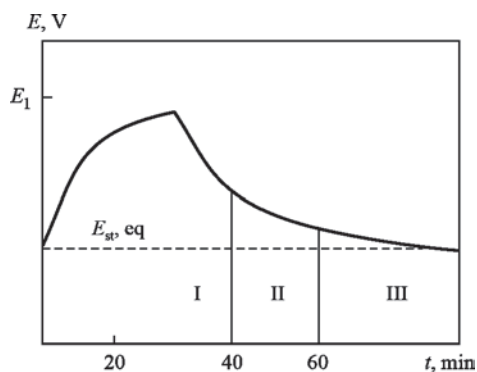
Figure 2. X-ray patterns of plasma coatings in the initial state: *a* — TiAl-SiC; *b* — TiAl-Si₃N₄

Table 1. Results of electrochemical studies of plasma coatings in a 3 % NaCl solution

Base	Coating	Electrochemical characteristics		
		E_{st} , V	E_c , V	i_c , A/cm ²
AMg3 alloy	–	–0.84	–0.5	$2.6 \cdot 10^{-5}$
	TiAl–Si ₃ N ₄	–0.64	–0.46	$4.1 \cdot 10^{-6}$
	TiAl–SiC	–0.7	–0.51	$5.2 \cdot 10^{-6}$
St3	–	–0.48	–0.5	$6.5 \cdot 10^{-5}$
	TiAl–Si ₃ N ₄	–0.58	–0.41	$5.4 \cdot 10^{-6}$
	TiAl–SiC	–0.58	–0.36	$4.4 \cdot 10^{-6}$
VT6 alloy	–	–0.04	0.04	$2.6 \cdot 10^{-6}$
	TiAl–Si ₃ N ₄	–0.2	–0.01	$3.5 \cdot 10^{-6}$
	TiAl–SiC	–0.2	–0.01	$3.2 \cdot 10^{-6}$

of TiAl titanium is available [15], according to which in a 3.5 % NaCl solution, the corrosion current i_c for it is about $5 \cdot 10^{-5}$ A/cm². Electrochemical studies of the plasma coatings (Table 1) showed that the introduction of carbide and nitride additives into TiAl alloy, which leads to the formation of new phases during plasma spraying of CP, produced by the method of mechanochemical synthesis, increases its corrosion resistance in the electrolyte by an order of value ($i_c = 10^{-6}$ A/cm²).

The corrosion potential of the plasma coatings on St3 shifts by 0.1–0.2 V in a more positive direction as compared to the stationary potential, on the polarization curves, inhibition of the cathode process of hydrogen release can be observed. The analysis of anode polarization curves (Figure 4, *a*) indicates that in the region of active dissolution (near the potential of –0.38 V), a linear relationship between the potential and the logarithm of the current density is observed. When the potential is further increased (≈ -0.3 V), the dissolution process is inhibited and the saturation current is achieved, after which the current density remains unchanged when the potential is increased.

**Figure 4.** Polarization curves of plasma coatings with CP TiAl–SiC and TiAl–Si₃N₄ in a 3 % NaCl solution, deposited on St3, AMg3 and VT6 alloys: *a* – 1 – St3; 2 – TiAl–SiC; 3 – TiAl–Si₃N₄; *b* – 1 – AMg3 alloy; 2 – TiAl–SiC; 3 – TiAl–Si₃N₄; *c* – 1 – VT6 alloy; 2 – TiAl–SiC; 3 – TiAl–Si₃N₄**Figure 3.** Change of stationary potential over time for plasma coatings

For the plasma coatings, deposited on AMg3, the corrosion potential is also shifted by 0.2–0.3 V in a more positive direction (–0.5 V), which indicates a uniform dissolution of the base through the pores of coatings of ions Al³⁺. Analysis of anode polarization curves allowed revealing that the electrochemical process occurs in the region of anode dissolution and at a potential close to zero, its inhibition occurs.

In spraying of plasma coatings on VT6 alloy, the corrosion potential enters the passive region in connection with the formation of the protective layer of titanium TiO₂ oxide on the surface.

The plasma coatings, deposited on St3 and AMg3, reduce corrosion currents in the studied electrolyte by one order and negligibly affect the corrosion resistance of VT6 alloy.

After corrosion experiments, an X-ray phase analysis of surface areas on the plasma coatings, exposed to the aggressive environment, was carried out. It was revealed that the phase composition of the coatings, deposited on different metal bases, is slightly different.

Thus, the coatings with CP TiAl–SiC between the main phases of TiC, Ti₃Si₃ and intermetallics of TiAl system on St3 contain iron FeO and Fe₃O₄ oxides, on AMg3 aluminium Al₂O₃ oxide, on VT6 titanium TiO₂ oxide (Figure 5, *a–c*).

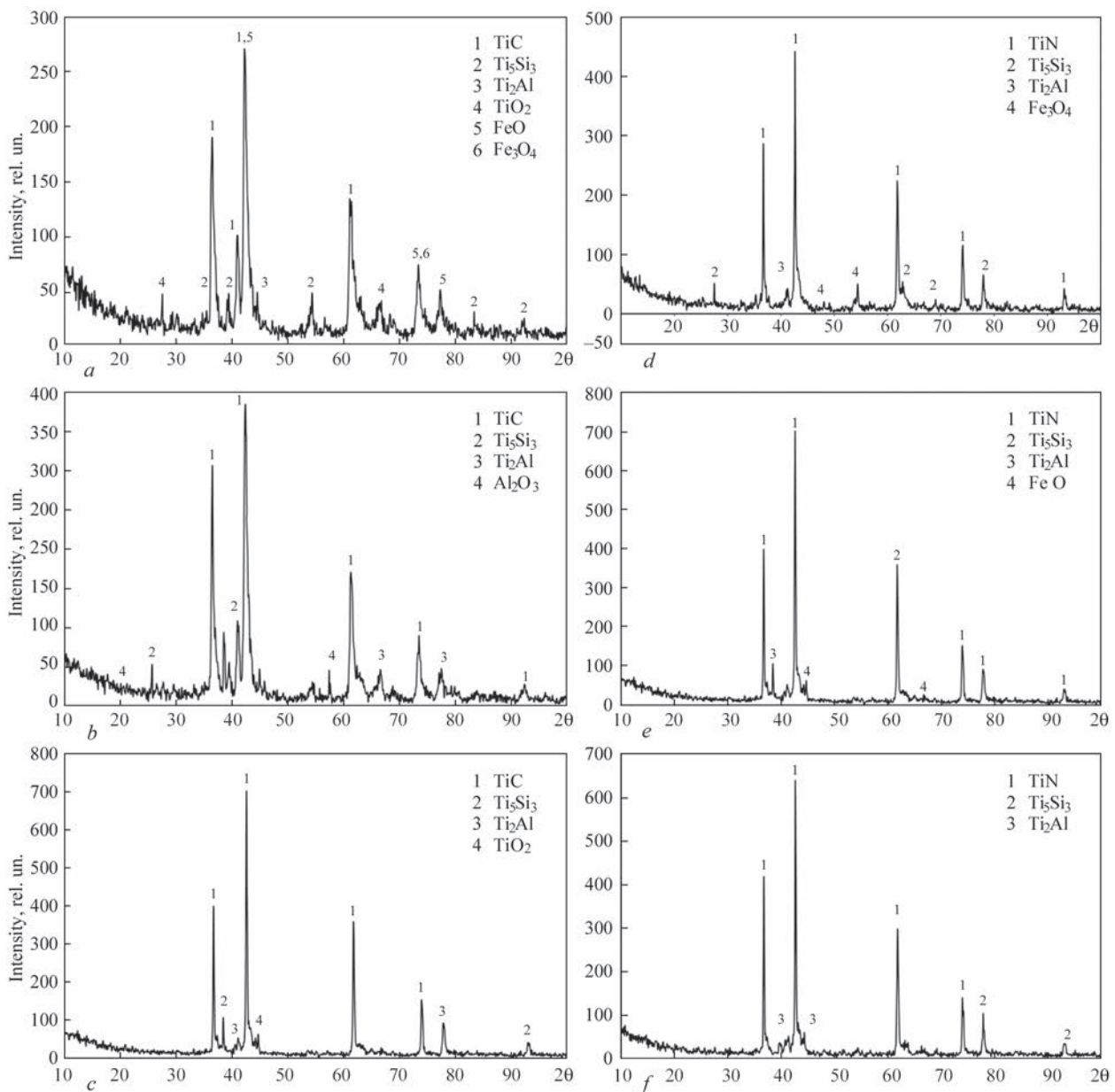


Figure 5. X-ray patterns of the surface of plasma coatings with CP TiAl–SiC (*a–c*), TiAl–Si₃N₄ (*d–e*), deposited on St3 (*a, d*), aluminium AMg3 (*b, e*) and titanium VT6 (*c, f*) alloys, after corrosion tests in a 3 % NaCl solution

For the coatings with CP TiAl–Si₃N₄ on St3, in addition to the main phase composition of TiN, Ti₅Si₃ and intermetallics of Ti–Al system, iron Fe₃O₄ oxide was detected. These results may indicate that the aggressive environment is penetrated into the interface of the coating with the base with the release of corrosion products on the surface of the electrode.

Analysis of corrosion test results showed that the plasma coatings with CP TiAl–SiC and TiAl–Si₃N₄ reduce the rate of corrosion of St3 by 10–16 times, AMg3 alloy by 8–9 times and VT6 alloy by 1.8–2.0 times. An increase in corrosion resistance can be explained by the formation of titanium silicide (Ti₅Si₃) in the plasma coatings. From literary sources it is known that silicides of metals significantly improve the corrosion resistance of coatings and alloys in vari-

ous aggressive environments, which is predetermined by the presence of strong covalent bonds metal-non-metal, and also Si–Si bonds [17, 18].

According to the polarization curves, the plasma coatings deposited on the surface of St3 and aluminium AMg3 alloy affect the rate of anode dissolution both in the active region, as well as in the region of their passive state, the anode process is inhibited (see Figure 4, *a, b*).

The process of anode dissolution of coatings on St3 proceeds mainly according to the reaction $\text{Fe} \rightarrow \text{Fe}^{2+} + 2\text{e}$, Fe²⁺ ions pass into the solution from the base material through the pores in the coating. This is confirmed by the data of XRD, where it was revealed that after corrosion tests, on the surface of the coatings deposited on St3, a layer of corrosion products

Table 2. Resistance and service life of plasma coatings in a 3 % NaCl solution

Coating (base)	Depth index of corrosion K_d , mm/year	Point on the resistance scale	Service life, years
TiAl–Si ₃ N ₄ (AMg3 alloy)	0.058	5	6
TiAl–Si ₃ N ₄ (St3)	0.045	4	7
TiAl–Si ₃ N ₄ (VT6 alloy)	0.042	4	8
TiAl–SiC (AMg3 alloy)	0.055	5	6
TiAl–SiC (St3)	0.049	4	7
TiAl–SiC (VT6 alloy)	0.036	4	10

Notes. 1. For St3 $K_d = 0.5935$; for AMg3 — 0.4925; for VT6 — 0.0667 mm/year. 2. All coatings belong to the group “resistant”.

consisting of iron oxides (FeO, Fe₃O₄) is formed. The process of anode dissolution of the coatings on AMg3 alloy proceeds according to the reaction $Al \rightarrow Al^{3+} + 3e$, on the surface of the coatings, a layer of Al₂O₃ oxide is formed.

The polarization curves for the coatings deposited on VT6 alloy are located quite close to each other, the corrosion potential indicates the passive state of the surface of the specimens as a result of the formation of a film of titanium TiO₂ oxide on them. The corrosion potential, which is close to zero, characterizes the completely passive corrosion resistance of the coating surface [19]. It should be noted that inhibition of anode dissolution occurs both for the alloy itself and for the plasma coating as well (see Figure 4, c).

The values of the corrosion currents, found from the polarization curves, made it possible to calculate the depth index of the coating corrosion. To characterize the corrosion resistance, a ten-point evaluation scale was used, according to which the plasma coatings can be attributed to the group “resistant”. The calculated service life of the plasma coatings indicates the possibilities of their operation in the environment of a 3 % NaCl solution for 6–10 years (Table 2).

In terms of corrosion resistance, the plasma coatings with CP TiAl–SiC are not inferior to the composite coatings produced by sintering of powders of Ti₃Al intermetallics with the addition of silicon carbide and deposited on a titanium alloy by the electrospark method ($i_c = 2.04 \cdot 10^{-6}$ A/cm²) [20].

CONCLUSIONS

1. It was found that the plasma coatings have heterogeneous structure with uniform distribution of phases over depth and the absence of defects and delaminations on the interface with the base. The phase composition of the plasma coatings for TiAl–SiC system consists of the following phases: TiAl, TiAl₃, TiC, Ti₅Si₃, Ti₃AlC, TiO₂, for TiAl–Si₃N₄ system with Ti₂Al, Ti₅Si₃, TiN, TiO. The thickness of the coatings was 200 ± 50 μm.

2. The introduction of non-metallic refractory compounds into the plasma coatings based on TiAl in spraying on the bases of St3 and AMg3 allows increasing their corrosion resistance in a 3 % NaCl solution by an order of value, in spraying on the base of VT6, the corrosion resistance does not increase significantly.

3. Corrosion resistance of the plasma coatings based on TiAl almost does not depend on the nature of a refractory additive (SiC and Si₃N₄), which is introduced, because for both coatings, the formation of Ti₅Si₃ occurs, as a result of which this characteristic increases.

4. The plasma coatings with CP TiAl–SiC, TiAl–Si₃N₄, which are deposited on the bases of St3, AMg3 and VT6, increase their corrosion resistance in a 3 % NaCl solution by 12–13 times, 8–9 times and 1.8–2.0 times, respectively.

5. The plasma coatings can be placed in the following line by increasing their corrosion properties: coatings on AMg3 → coatings on St3 → coatings on VT6.

6. According to the scale of corrosion resistance, the plasma coatings with CP TiAl–SiC and TiAl–Si₃N₄ belong to the “resistant” group. The calculated service life of the coatings indicates the possibility of their operation in the environment of a 3 % NaCl solution for a period from 6 to 10 years.

REFERENCES

1. Sinelnikova, V., Podergin, V., Rechkin, V. (1965) *Aluminides*. Kyiv, Naukova Dumka [in Russian].
2. Kablov, E.N., Lukin, V.I. (2008) Intermetallics based on titanium and nickel for advanced engineering products. *The Patent Welding J.*, **11**, 65–70.
3. Kurzina, I. A., Kozlov, E., Sharkeev, Yu. (2007) Influence of ion implantation on nanoscale intermetallic-phase formation in Ti–Al, Ni–Al and Ni–Ti systems. *Surf. Coat. Tech.*, **201**, 8463–8468.
4. Cinca, N., Guilemany, J. (2012) Thermal spraying of transition metal aluminides: An overview. *Intermetallics*, **24**, 60–72.
5. Yang, D., Tian, B., Cao, Y. (2011) Microstructures and properties of FeAl coatings prepared by LPPS, APS and HVOF. In: *Proc. of ITSC'2011*, 1229–1234.

6. Cinca, N., Guilemany, J. (2013) An overview of intermetallics research and application: Status of thermal spray coatings. *J. of Materials Research and Technology*, 2(1), 1–11.
7. Syrovatka, V.L., Olikier, V.E., Yakovleva, M.S. (2013) Intermetallics of Fe–Al system: Methods of producing, properties, coatings. *Materialovedenie*, 3, 46–53 [in Russian].
8. Grigorenko, S.G. Grigorenko, G.M., Zadorozhnyuk, O.M. (2017) Intermetallics of titanium. Peculiar features, properties, application (Review). *Sovrem. Elektrometal.*, 3, 51–58 [in Russian].
9. Blinkov, P.R., Volkhonsky, V.S., Sergevnnin, N.Yu. (2015) Structure- and phase formation in Ti–Al–Si–N system at forming of nanostructural ion-plasma coatings. *Neorganicheskie Materialy*, 51(11), 34–38 [in Russian].
10. Voronov, A.V., Sergeev, V.P., Sergeev, O.V. et al. (2009) Producing of nanocomposite coatings based on Ti–Al–Si–N system using two magnetrons. *Izv. TPU, Engineering Geosursov*, 315(2), 147–150 [in Russian].
11. Pyachin, S.A., Ershova, A.A., Vlasova, N.M. et al. (2019) Preparation and properties of electrospark coatings from Ti₃Al granules with silicon carbide and boron carbide additives. *Letter Materials*, 9(2), 191–196.
12. Vojtovich, R.F. (1981) *Oxidation of carbides and nitrides*. Kyiv, Naukova Dumka [in Russian].
13. Vojtovich, R.F., Golovko, E.I. (1978) *High-temperature oxidation of metals and alloys*. Kyiv, Naukova Dumka [in Russian].
14. Nikitin, V.I. (1987) *Corrosion and protection of gas turbine blades*. Moscow, Mashinostroenie [in Russian].
15. Zhuk, N.P. (2006) *Course in the theory of corrosion and protection of metals*. Moscow, Alliance [in Russian].
16. Seikh, A.H. (2015) Corrosion behavior in 3,5% NaCl solutions of γ -TiAl processed by electron beam melting process. *Metals*, 5, 2289–2302.
17. Shein, A.B. (2010) Corrosion-electrochemical behavior of metal silicides of iron triad in different electrolytes. *Fizikokhimiya Poverkhnosti i Zashchita Metallov*, 4(46), 403–413 [in Russian].
18. Knyazheva, V.M., Babich, S.G., Kolotyrykin, V.I., Kozhevnikov, V.B. (1991) Metal-like compounds of transition metals as the new class of corrosion-resistant materials and protective coatings. *Zashchita Metallov*, 4(27), 603–616 [in Russian].
19. Tomashov, N.D., Chernova, G.P. (1993) *Theory of corrosion and corrosion-resistant structural alloys*. Moscow, Metallurgiya [in Russian].
20. Burkov, A., Pyachin, S., Vlasova, N. et al. (2018) Improvement of anticorrosion and tribotechnical properties of Ti₆Al₄V alloy by deposition of electrospark Ti–Al–Si–C coatings. *Obrabotka Metallov*, 20(3), 85–96 [in Russian].

ORCID

Yu.S. Borysov: 0000-0002-6019-8464,
 A.L. Borysova: 0000-0002-7376-3370,
 N.V. Vihilianska: 0000-0001-8576-2095,
 O.P. Gryshchenko: 0000-0003-2640-8656,
 Z.G. Ipatova: 0000-0003-2209-408X,
 K.V. Yantsevych: 0000-0002-3975-7727,
 M.A. Vasylykivska: 0000-0001-8311-6428

CONFLICT OF INTEREST

The Authors declare no conflict of interest

CORRESPONDING AUTHOR

N.V. Vihilianska
 E.O. Paton Electric Welding Institute of the NASU
 11 Kazymyr Malevych Str., 03150, Kyiv, Ukraine.
 E-mail: pewinatalsa@gmail.com

SUGGESTED CITATION

Yu.S. Borysov, A.L. Borysova, N.V. Vihilianska, O.P. Gryshchenko, Z.G. Ipatova, K.V. Yantsevych, M.A. Vasylykivska (2022) Corrosion resistance of plasma coatings produced from composite TiAl-based powders with the addition of non-metallic refractory compounds. *The Paton Welding J.*, 7, 28–34.

JOURNAL HOME PAGE

<https://pwj.com.ua/en>

Received: 09.06.2022

Accepted: 15.09.2022

DEVELOPED in PWI

SUPER LARGE PROFILED SINGLE CRYSTALS OF TUNGSTEN AND MOLYBDENUM

PWI grows and delivers tungsten and molybdenum single crystals in the form of 20×160×170 mm size plates and in the form of a body of rotation up to 85 mm in diameter. Size of crystals can be increased to 20×250×300 mm.



DOI: <https://doi.org/10.37434/tpwj2022.07.06>

CURRENT-SUPPLYING MOULD IN ELECTROSLAG TECHNOLOGIES

Yu.M. Kuskov, V.M. Proskudin, V.A. Zhdanov, L.L. Okopnyk

E.O. Paton Electric Welding Institute of the NASU

11 Kazymyr Malevych Str., 03150, Kyiv, Ukraine

ABSTRACT

The technology of electroslag surfacing and remelting, using a current-supplying mould, as well as the features of a mould design are considered. Experience of upgrading the basic three-sectional design into a two-sectional one is described. Ways of development of electroslag surfacing technology with application of current-supplying moulds of different dimensions and cross-sections are shown.

KEYWORDS: electroslag surfacing and remelting, current-supplying mould

INTRODUCTION

It has been about 70 years since a new technological process — electroslag process was officially recognized. During these years, various methods of electroslag welding and surfacing have been developed, which have found a wide application in industry and have already become “conventional”.

As for the method of electroslag surfacing (ESS) in the current-supplying mould (CSM), such recognition and distribution did not occur. It was caused by the difficulties in its practical realization, mainly due to a low life of the applied unit — current-supplying mould.

The aim of the work is to show some difficulties in creating a new type of moulds, their design and technological features, as well as prospects for the development of this technology, taking into account the success achieved in its industrial application.

For the first time, a nonconsumable section electrode — a mould — without any additional electrodes, was presented in the early 1960s by G.V. Ksyondzyk, staff colleague of the PWI of the NAS of Ukraine, in co-authorship with I.I. Frumin and V.S. Shyrin [1, 2] and patented in many countries [3-5]. The division of functions of melting a deposited material and formation of the deposited layer in it were achieved by the use of various sections of the mould electrically isolated between each other in the technological process.

The scheme of the mould is presented in Figure 1. It consists of separate horizontal water cooled sections 2, 6 and 7, separated between each other by electric insulating gaskets 5. To the upper section 2, which conducts an electric current, the voltage from the power source is supplied; the lower section 7 forms a deposited metal; the intermediate section 6 is used to divide the upper and lower sections. It can

also be an element of automatic tracking of the metal pool level 8.

To protect the upper section against the electric erosion, it has a protective heat-resistant conductive lining 4, which is usually made of graphite. Electric erosion is a phenomenon inherent in both CSM, as well as in ordinary moulds used in the technologies of electroslag remelting (ESR) [6]. At the same time, the resistance of new ESR moulds withstands in average 250 melts, but if an average duration of each melt is 2.5 h, it ranges from 150 to 350 melts.

It should be noted that if in the conventional moulds, the current passing on the mould wall, depending on melting parameter ranges from 10–20 to 90 % of the total current [7], then during ESS in CSM, through the current-supplying section, the entire working current passes. Therefore, in this case, electric erosion pro-

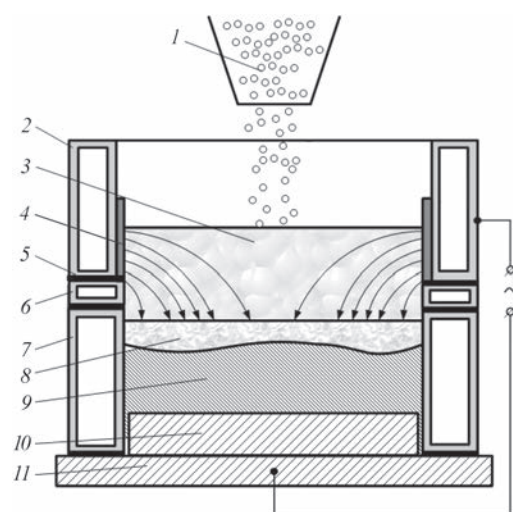


Figure 1. Scheme of ESS with a discrete filler in CSM: 1 — discrete filler; 2, 6, 7 — current-supplying, intermediate and forming sections of the mould, respectively; 3 — slag pool; 4 — protective lining; 5 — insulating gasket; 8 — metal pool; 9 — deposited metal; 10 — product; 11 — bottom plate. Arrows show distribution of current in the slag pool

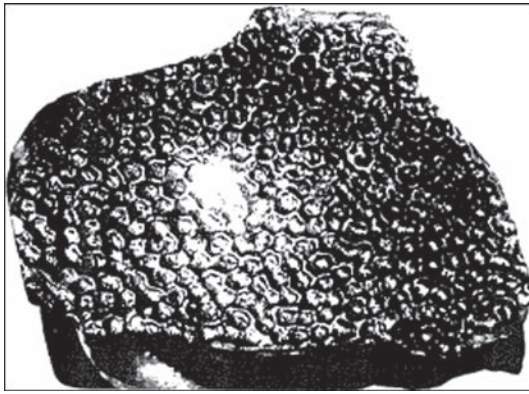


Figure 2. Surface of the slag crust that was in contact with the eroded surface of the wall of the current-supplying section (in the absence of lining): working currents are up to 1 kA, operation time is 1 h ($\times 7$)

cesses should run more intensively. Figure 2 shows the surface of a slag crust that was in contact with an eroded wall surface of the current-supplying section.

One more feature of CSM is that in its current-supplying section, a longitudinal incision is made, which is usually filled with a heat-resistant electric insulating material, as a result of which this section represents a single-turn inductor. The magnetic power lines of this inductor, interacting with the magnetic power lines of welding current, generate a rotary effect in the slag pool (which is also transmitted by friction forces on a metal pool). This additional property of CSM allows getting special advantages in ESS: improving equalizing of temperatures over the volume of the slag pool, providing a uniform distribution of a surfacing filler over the surface of the slag pool, reduction in electric erosion phenomena by decreasing a number of local zones for conducting current to the slag pool.

To start operation of the mould, the slag pool 3 should be created in it. This can be done in two ways:

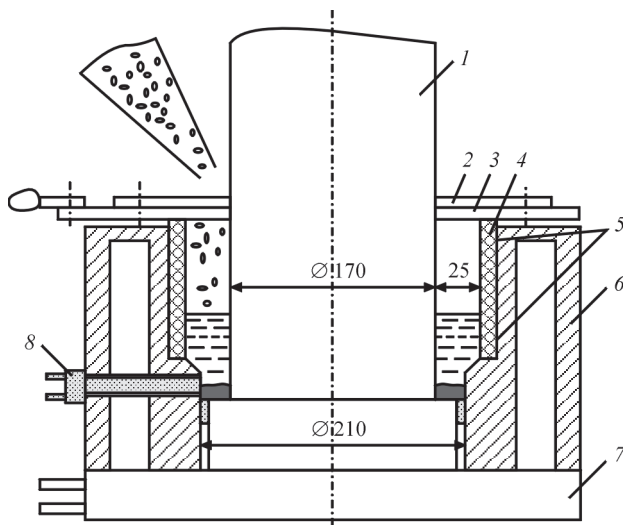


Figure 3. Basic design of two-section CSM: 1 — billet; 2 — steel clamping ring; 3 — copper current-supplying ring; 4 — graphite section; 5 — insulating gaskets; 6 — copper section; 7 — collector; 8 — inductive sensor of metal level

by its formation directly in the mould using an additional non-consumable electrode (solid start), or by pouring a liquid slag into the mould, preliminary molten in a separate capacity (liquid start). In both cases, the volume of the slag should be so that it could cover all three sections. As a conductive medium, it begins to conduct current from the upper (current-supplying) section through the metal pool 8 to the deposited metal 9, the product 10 and the bottom plate 11. Regardless of the electroslag process parameters, a discrete filler 1 is supplied into the slag pool, which during melting in a slag, crystallizes in the lower forming section. In the case of using consumable electrodes in ESS, various electrical circuits of their melting in the slag pool can be used [8].

As is seen from Figure 1 and description of the operation of the mentioned unit, these circuits in design and technological terms are quite simple.

But it should be admitted that in the author's certificate, a rational idea was first and foremost stated on this design. Therefore, with all its simplicity, it took more than ten years to obtain the first encouraging results of operation of the proposed mould. Mostly, this was associated with an increase in its life. Nevertheless, there were problems with the choice of an optimal composition of the flux, open circuit voltage of the power source and the circuit of electrical connection. As an example of optimization of CSM design, in Figures 3 and 4, the variants of creating a two-section CSM for surfacing cylindrical parts are shown.

A distinctive feature of the basic model of such a mould (Figure 3) is the absence of an intermediate section, which is subjected to the most complex thermal conditions, and the use of a graphite bushing as a current-supplying element, isolated from the forming section over the vertical surface and a lower end.

Under such a scheme after pouring the slag into the mould, as a result of a rapid destruction of the insulation, not slag, but arc process begins. The cases of increased erosion destruction of the copper wall of a water-cooled mould and a copper current-supplying ring are observed.

In connection with the obtained result, some design changes were introduced — a graphite bushing was made with a clamp to provide better electrical contact in the current conducting zone and with a boundary vertical section along its length (Figure 4).

The constant rotation of the slag pool could not be achieved due to the appearance of reduction-oxidation reactions in the section area of electric-supplying products, occurring at the border graphite-slag. On the horizontal surface of a copper section in the zone of its close vicinity with the end of a graphite bushing, traces of erosion were noted.

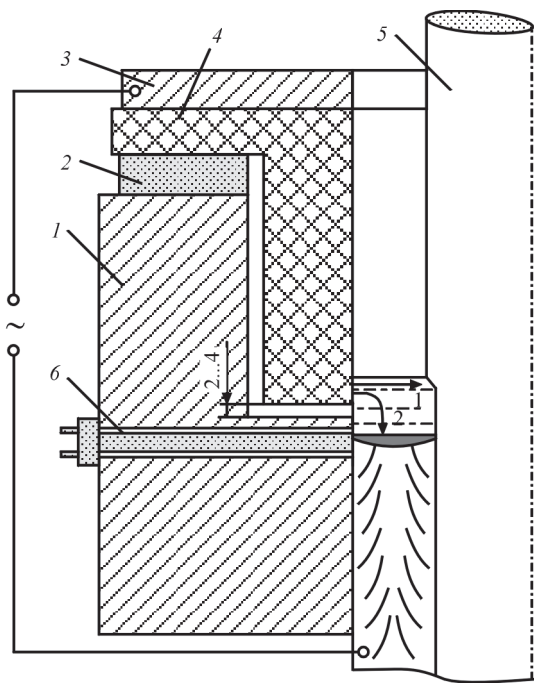


Figure 4. Two-section design of CSM with a clamp on the graphite section: 1 — copper section; 2 — insulating gasket; 3 — copper current-supplying ring; 4 — graphite section; 5 — workpiece; 6 — inductive sensor of metal level; I_1 , I_2 — respectively, horizontal and vertical components of current

The authors of the patent called the unit they developed a “current-supplying mould”, although this name does not fully reflect the physical content of the processes that occur.

The fact is that the voltage is supplied to the mould from the power source. The mould itself (or rather its upper section under voltage), being an element of the electrical circuit power source — upper section — slag pool — metal pool — workpiece — bottom plate, conducts a current passing on it. Therefore, it would be more correct to call this unit a “mould under voltage” or a “current-conducting mould”.

Due to the fact that the original name has already been rooted in the technical literature, the term with the abbreviation CSM should be used, proposed by the authors.

The idea of using ingots during melting or units during surfacing, that simultaneously affect proceeding of the electroslag process and provide the formation of the molten metal is so attractive, that it became used in different variants both in the countries of near and far abroad [9–11].

The “Inteco” Company (Austria) received several patents for melting ingots using CSM [12, 13].

Figure 5 shows one of such methods based on the patent [14]. Its distinctive feature is that during remelting, the voltage is supplied from one power source both to the consumable electrode and also to one of the sections (intermediate) of the mould, which

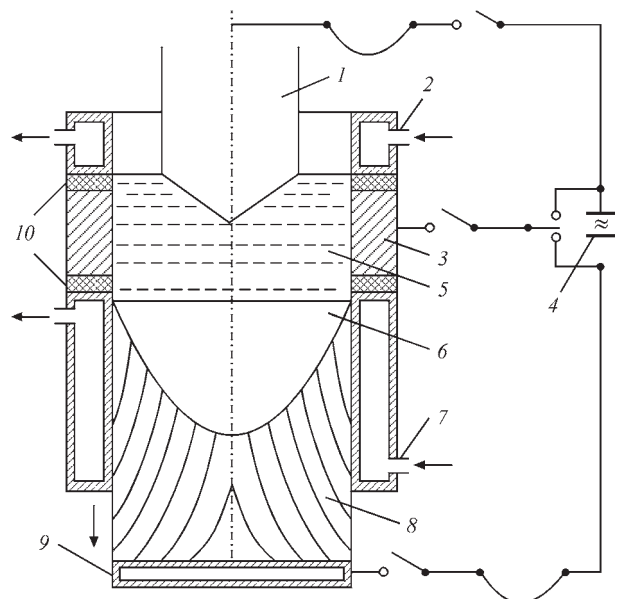


Figure 5. Scheme of section mould based on the patent DE 196 14 182 C1 of Germany: 1 — consumable electrode; 2 — upper section of the mould; 3 — intermediate section of the mould; 4 — power source; 5 — slag pool; 6 — metal pool; 7 — lower section of the mould; 8 — deposited metal; 9 — bottom plate; 10 — electric insulating gaskets

are made of graphite or refractory metals W, Mo, Nb, etc. and isolated from other sections.

This technology received an industrial application during a rapid melting of ingots made from high-speed steels using the method of ESSR (Electro Slag Rapid Remelting) [15].

The further development of ESS technology in CSM was the use of not only electrodes of a large cross-section and a discrete filler in surfacing, but also a filler in the form of a liquid material [16]. At the same time, with an increase in sizes (diameter) of the mould, it is proposed to use a current-supplying section with a large number of vertical sections [17, 18] to provide a uniform penetration of a workpiece surface.

Recently, to expand the capabilities of ESS in CSM, technologies for producing bimetal of a square cross-section were developed [19]. In this case, in the moulds of this type, all the technical features inherent in CSM of a round cross-section are preserved.

Thus, on the basis of the obtained results of a successful industrial testing of ESS technology in CSM using the moulds of two shapes of a working cross-section (round and square), it can be assumed that it became possible to create an operable technology of surfacing and the units for its realization.

REFERENCES

1. Ksendzyk, G.V., Frumin, I.I., Shirin, V.S. (1964) *Current-supplying mould*. USSR author's cert. 264427, fil. 19.11.1964 [in Russian].

2. Ksendzyk, G.V., Frumin, I.I., Shirin, V.S. (1969) *Unit for electroslag remelting*. USSR author's cert. 337026, fil. 25.06.1969 [in Russian].
3. Ksendzyk, G.V., Frumin, I.I., Sirin, V.S. (1979) Patentschrift DE 2746256 C3 BR, C21c 5/52. *Ringformige Kokille für Anlagen zum Electroschmelzen — Umschmelzen bzw. Auftragschweißen von Metallen*. Anmeldetag 14.10.1977, Offenlegungstag 19.04.1979.
4. Ksendzyk, G.V., Frumin, I.I., Shirin, V.S. (1981) *Electroslag remelting and surfacing apparatus*. Pat. 4,305,451 US B22D 27/02. Fil. 23.06.1977, Publ. 15.21.1981.
5. Ksendzyk, G.V., Frumin, I.I., Sirin, V.S. (1981) *Electroslag remelting and surfacing apparatus*. Pat. Specification I 566 819 GB, B22D 11/04, B01F 13/08, B22D 23/06. Fil. 13.09.1977, Publ. 09.07.1981.
6. Artamonov, V.L., Kamensky, Yu.M., Toistev, V.I. et al. (1981) Electric erosion of moulds in ESR and their restoration by cladding. *Spec. Elektrometallurgiya*, **45**, 52–55 [in Russian].
7. (1981) *Electroslag metal*. Eds by B.E. Paton, B.I. Medovar. Kyiv, Naukova Dumka [in Russian].
8. Kuskov, Yu.M., Grishchenko, T.I. (2019) Formation of metal pool in current-supplying mould at electroslag process. *The Paton Welding J.*, **4**, 33–36. DOI: <https://doi.org/10.15407/tpwj2019.04.07>
9. Holzgruber, W., Holzgruber, H. (2000) Innovative electroslag remelting technologies. *MPT Inter.*, **2**, 46–48.
10. Kubin, M., Scheriau, A., Knabl, M. et al. (2016) Investigation of the implication of the current conductive mould technology with respect to the internal and surface quality of ESR ingots. In: *Medovar Memorial Symp. (7–10 June 2016, Kyiv)*, Kyiv, Elmetroll, 174–179.
11. Sokolov, G.N., Mikheev, A.N., Pavlov, A.A. (2002) Electroslag cladding in section mould of edges of rolling mill mandrels. *Svarochn. Proizvodstvo*, **6**, 31–34 [in Russian].
12. Holzgruber, W., Holzgruber, H. (1996) *Verfahren zum Umschmelzen von Metallen Zulinem Strang sowie Vorrichtung da für*. Pat. EP 0 786 531 A1 Europasches Pat. C 22B 9/18, B 22 D 23/10. Anmeldetag 29.01.1996, Offenlegungstag 21.12.1996.
13. Holzgruber, W., Holzgruber, H. (2000) *Wassergekühlte Kokille für das Strangiessen oder Electroschlackeumschmelzen*. Pat. A. T. 406 239 B Republik Osterreich, B 222D 23/10, C21c 5/52. Anmeldetag 09.04.1996, Offenlegungstag 27.03.2000.
14. Holzgruber, H. (1997) *Wassergekühlte Kokille zum Herstellen von Blocken oder Strangen sowie deren Verwendung*. Anmeldetag 11.04.1996. Pat. DE 196 14 182 C1BR, C21C 5/52, C22B 9/193. Veröffentlichungstag 31.07.1997.
15. Alghisi, D., Milano, M., Paziienza, L. (2001) The electroslag rapid remelting process under protective atmosphere of 145 mm billets. In: *Medovar Memorial Symp. (15–17 May 2001, Kyiv)*, Kyiv, Elmetroll, 97–105.
16. Dubodelov, V.I., Pogorsky, V.K., Shnurko, V.K. et al. (2002) Application of magnetodynamic unit in the technology of electroslag cladding of steel mill rolls using a liquid metal. *Advances in Electrometallurgy*, **4**, 7–8.
17. Tomilenko, S.V., Kuskov, Yu. M. (2000) Special features of melting of parent metal electroslag surfacing in a current-supplying solidification mould. *Welding Int.*, **14(11)**, 893–895.
18. Shevchenko, V.E. (2001) *Electroslag technology in production of modern mill rolls*: Syn. of Thesis for Cand. of Tech. Sci. Degree. Kyiv [in Russian].
19. Netyaga, A.V., Kuskov, Yu.M., Proskudin, V.M. et al. (2021) Formation of a layer of high-chromium cast iron in current-supplying mould of a square cross-section at electroslag surfacing. *Suchasna Elektrometal.*, **4**, 16–19. DOI: <https://doi.org/10.37434/sem2021.04.02>

CONFLICT OF INTEREST

The Authors declare no conflict of interest

CORRESPONDING AUTHOR

V.A. Zhdanov

E.O. Paton Electric Welding Institute of the NASU
11 Kazymyr Malevych Str., 03150, Kyiv, Ukraine.

E-mail: vovik19821982@ukr.net

SUGGESTED CITATION

Yu.M. Kuskov, V.M. Proskudin, V.A. Zhdanov, L.L. Okopnyk (2022) Current-supplying mould in electroslag technologies. *The Paton Welding J.*, **7**, 35–38.

JOURNAL HOME PAGE

<https://pwj.com.ua/en>

Received: 19.05.2022

Accepted: 15.09.2022

XVI International Conference

“Problems of corrosion and corrosion protection of materials”

“Corrosion–2022”

15–16 November, Lviv, Ukraine



The Organizing Committee continues the registration of participants and forms a conference abstracts book. Papers containing new, original results will be selected for publication in the journal «Materials Science» (Scopus).

<https://www.ipm.lviv.ua/corrosion2022>

DOI: <https://doi.org/10.37434/tpwj2022.07.07>

PRODUCING HIGH-TEMPERATURE TITANIUM ALLOYS OF Ti–Al–Zr–Si–Mo–Nb–Sn SYSTEM BY ELECTRON BEAM MELTING

S.V. Akhonin¹, V.O. Berezos¹, O.M. Pikulin¹, A.Yu. Severyn¹, O.O. Kotenko¹, M.M. Kuzmenko², L.D. Kulak², O.M. Shevchenko²

¹E.O. Paton Electric Welding Institute of the NAS of Ukraine.
11 Kazymyr Malevych Str., 03150, Kyiv, Ukraine

²I.M. Frantsevich Institute for Problems of Materials Science of the NAS of Ukraine.
3 Acad. Krzhyzhanovskiy Str., 03142, Kyiv, Ukraine

ABSTRACT

A complex of research work was performed on the base of EBM technology to produce high-strength complex titanium alloys of Ti–Al–Zr–Si–Mo–Nb–Sn system with silicon content, higher than the thermodynamically stable value in the solid solution. Alloys of this system are promising for creation of a new class of materials with a high level of heat-resistant characteristics. It is shown that EBM allows producing ingots of high-temperature titanium alloys of Ti–Al–Zr–Si–Mo–Nb–Sn system, which are characterized by sufficient chemical homogeneity and absence of casting defects. It is found that tin presence lowers silicon solubility in the test alloys and intensifies silicide release. Here the structure is also refined. It is found that additional alloying elements influence silicon solubility in titanium, forming complex silicides of (Zr, Ti)₃Si (Ti, Zr)₃Si type in the test alloys. It is shown that the microstructure of the test cast alloys consists of platelike α -phase packets within primary β -grains, having different crystallographic orientation.

KEYWORDS: high-temperature titanium alloy; ingot; electron beam melting; technological modes; chemical composition; cast metal; structure

INTRODUCTION

In the recent decades significant attention is given to development of alloys based on refractory and highly reactive metals. Today, nuclear power engineering, gas turbine construction, aeronautic and aviation engineering require light and strong materials, which can compliment a list of high-temperature alloys based on nickel, cobalt and iron that are traditionally used in these fields. High-temperature titanium-based alloys are one of the ways of solution of this problem. Complex titanium-based alloys are of particular interest. They have high specific strength, heat- and corrosion resistance properties in various media [1–3].

There are high requirements to the critical designation parts, which are constantly improved and become more rigid. This, first of all, relates to the quality of materials being used. Therefore, for the purpose of widespread use of titanium alloys in different structures it is necessary to develop new titanium-based materials with higher operation characteristics as well as improve production of semi-finished products of these alloys in future[4].

Any imperfections of chemical and structural homogeneity in titanium alloys result in decrease of strength and life of the products. Production of titanium alloys is related with the difficulties caused by high titanium sensitivity to interstitial impurities, in

particular, oxygen, nitrogen, hydrogen and carbon and interaction with many chemical elements. This leads to creation of solid solutions or compounds. Moreover one of the main structural imperfections of titanium alloys is the presence of nonmetallic inclusions. High activity results in occurrence of physical-chemical processes of interaction with gases even in solid state. Therefore, non-metallic inclusions, in particular nitrides and oxides, can be generated in a process of ingots melting as well as at various stages of technological redistribution into finished products. Non-metallic inclusions can be introduced in the finished product from charge materials in the process of melting as well as in heat treatment of the finished product. Titanium actively interacts not only with gases, but also with other elements, including alloying components. Therefore, local enrichment of separate volumes of the ingots with alloying elements can result in formation of intermetallic inclusions, for example Ti₃Al, TiAl, TiCr and others [5].

WORK RELEVANCE

Operating temperatures of the modern commercial titanium alloys do not exceed 600 °C that limits their application [6]. Therefore, a problem of improvement of mechanical characteristics of titanium alloys at temperatures exceeding 600 °C is relevant for the moment and requires solution. One of the perspective directions for the problem solution is development

of the titanium composites based on Ti–Al–Zr–Si–Mo–Nb–Sn system with silicon content exceeding thermodynamically stable value in solid solution. Such composites have a multiphase structure where strengthening of titanium matrix with refractory compound of Ti_3Si_3 takes place in a natural way in a process of solidification. The alloys of this system are perspective for development of a new class of materials with high level of heat-resistant characteristics [7–11].

Today not all the methods of titanium ingots manufacture allow obtaining quality metal and violation of a technological process of titanium alloy production results in detection in the ingots of defects reducing metal quality. The main factor affecting the material quality, in particular, ones having low technological plasticity, is a high quality of output ingot. An electron beam melting (EBM) can provide proper quality of obtained ingot with uniform, not coarse structure and good chemical homogeneity. The EBM allows a wide range regulation of melting rate due to independent heat source that in turn allows regulation of duration of metal staying in liquid state. The EBM is a technology that permits providing almost complete removal of refractory inclusions of high and low density. Thus, the EBM allows rising a quality of titanium alloy ingots.

Therefore, now mastering of the technology of melting of high-temperature complex titanium alloys of Ti–Al–Zr–Si–Mo–Nb–Sn system using EBM is a relevant problem.

MATERIALS AND INVESTIGATION METHODS

Most of the titanium alloys contain high amount of alloying elements that somewhat complicates their production using electron beam melting. Melting in vacuum promotes random evaporation of alloying elements with high vapor tension. So, melting of the ingots of complex titanium alloys using EBM provokes a problem of assurance of set chemical composition



Figure 1. Process of melting of ingot of Ti–Al–Zr–Si–Mo–Nb–Sn system titanium alloy of 110 mm diameter in electron beam unit

of an ingot [13]. In this case aluminium is referred to such elements. And concentration in the ingot of elements with vapor density lower than vapor density of titanium (Nb, Mo, Zr and Si) can even somewhat rise. PWI of the NASU has carried out the fundamental investigations of the processes of evaporation of components from a melt in vacuum [12]. They were used to calculate a predicted chemical composition of the ingots based on the results of which a calculation of weight of the charge ingot components was carried out. An alloying component with high density of vapor (Al) was charged taking into account compensation of evaporation losses. The charge ingot for melting of ingots of high-temperature complex titanium alloys of Ti–Al–Zr–Si–Mo–Nb–Sn system was formed in a nonconsumable bucket. Electron beam installation UE-208M (Figure 1) [14] was used for melts.

To master the technology of melting of high-temperature complex titanium alloys of Ti–Al–Zr–Si–Mo–Nb–Sn system using EBM there were used earlier mastered technological schemes of charging of a consumable billet and melting modes [15].

Technological parameters of melting of Ti–Al–Zr–Si–Mo–Nb–Sn system ingots of 110 mm diameter

Melting rate, kg/h	30
Height of portion simultaneously poured in a mold, mm	10
Power, kW:	
in a mold	20
in an intermediate crucible	90

The composition of metal of the obtained ingots was determined using inductively-coupled plasma method in optical emission spectroscopy (ICP-OES) on ICP-spectrometer ICAP 6500 DUO. Content of oxygen and nitrogen was determined by a method of melting of analyzed sample of chips in vacuum in a graphite crucible, heating of which was performed using 900–1000 A current on RO-316, TN-144, RH-3 type devices of LECO Company (USA).

Quality of the ingot surface as for presence of pores, cavities, non-metallic inclusions, and cracks was determined visually without magnifying devices. An ultrasonic testing method was used to determine in the titanium ingots of internal defects in form of non-metallic inclusions, pores or inhomogeneities.

The structural investigations of metal of the obtained cast ingots were performed on the transverse templates, from which the samples for metallographic investigations were cut out. The sections of investigated alloys were made using the method of mechanical grinding with abrasive paper of different grain size and polishing of the samples by abrasive paste with chemical etching by a reagent of the following composition: 70 % H_2O , 25 % HNO_3 , 5 % HF .



Figure 2. Ingots of Ti-Al-Zr-Si-Mo-Nb-Sn system titanium alloys of 110 mm diameter after EBM: *a* — 812-208 melt; *b* — 814-208 melt; *c* — 815-208 melt

The structure of alloys was examined using optical and electron microscopy methods. Metallographic investigations were carried out using optical microscope Jenaphot-2000 by the method of scanning electron microscopy on scanning microanalyzer JEOL Superprobe-733. Standard Vickers method was used for measurement of hardness at room temperature according to the State Standard 2999–75 at 30 kg loading.

INVESTIGATION RESULTS AND THEIR DISCUSSION

In order to provide high physicochemical characteristics of the experimental titanium alloys at room and elevated temperatures a complex alloying was performed for the purpose of hardening of solid solution by α -phase and dispersed particles of secondary phase, in particular silicides. Following the specification a series of melts was carried out (Figure 1) and cast ingots of high-temperature complex titanium alloys of Ti-Al-Zr-Si-Mo-Nb-Sn system of 110 mm diameter and 1000 mm length (Figure 2) with different content of alloying elements were obtained, namely 812-208 melt — Ti-5Al-5Zr-0.8Si-0.3Mo-0.1Nb alloy;

814-208 melt — Ti-6.5Al-5Zr-0.5Si-1.5Sn-0.1Nb alloy; 815-208 melt — Ti-6.5Al-5.5Zr-0.8Si-0.6Mo-0.5Nb-1.7Sn alloy.

A side surface of the obtained cast ingots after cooling in vacuum to temperature below 300 °C is clean, increased concentration of impurity elements on the surface in form of oxidized or alpha layer is absent. Depth of the surface defects of corrugation type makes 2–3 mm, defects in forms of tears, cracks or lack of fusion are absent.

In order to evaluate quality of metal of the obtained ingots there were carried out the investigations of chemical composition of the samples taken on ingot length from upper, middle and lower parts. The results of analysis of chemical composition of metal of the obtained ingots showed that the distribution of alloying elements on ingot length is uniform.

As a result mechanical processing of the side surface was performed and upper and bottom parts of the ingots were cut (Figure 3). The templates were cut out for performance of metallographic investigations and production of the samples for mechanical properties testing (Figure 4).



Figure 3. Appearance of ingots of Ti-Al-Zr-Si-Mo-Nb-Sn system titanium alloys of 110 mm diameter after side surface machining: *a* — 812-208 melt; *b* — 814-208 melt; *c* — 815-208 melt

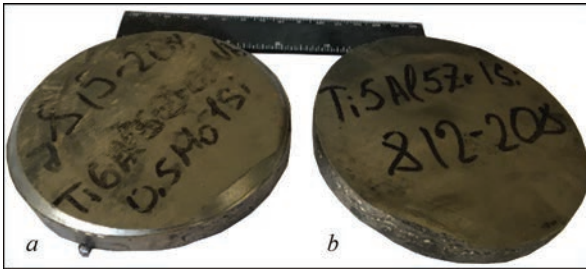


Figure 4. Cut templates of ingots of 815-208 (a) and 812-208 (b) melts for samples manufacture

Melted alloys corresponding to their composition can be referred to pseudo- α -alloys: they consist of α -phase and small amount of residual β -phase, the structure also contains silicides (Figures 5, 6).

Microstructure of the investigated cast alloys represents itself the batches of lamellar α -phase in the

limits of primary β -grains that have different crystallographic orientation. Formation of the structure takes place in the process of cooling, namely internal volume of β -grains is filled with chaotic α -plates as well as collected in the batches (α -colonies), that indicates inhomogeneity of the cast structure. The intermetallics start to segregate first of all on structural defects, boundaries of grains and α -plates stimulating their growth. Primary silicides and silicide layers are formed at decrease of silicon solubility in β -phase according to the diagram of phase equilibrium of Ti-Si system as a result of liquation processes at ingot solidification (Figure 7) [16].

Fine silicides at the boundaries of α -plates are formed in the process of eutectoid transformation and further decrease of silicon solubility in the titanium

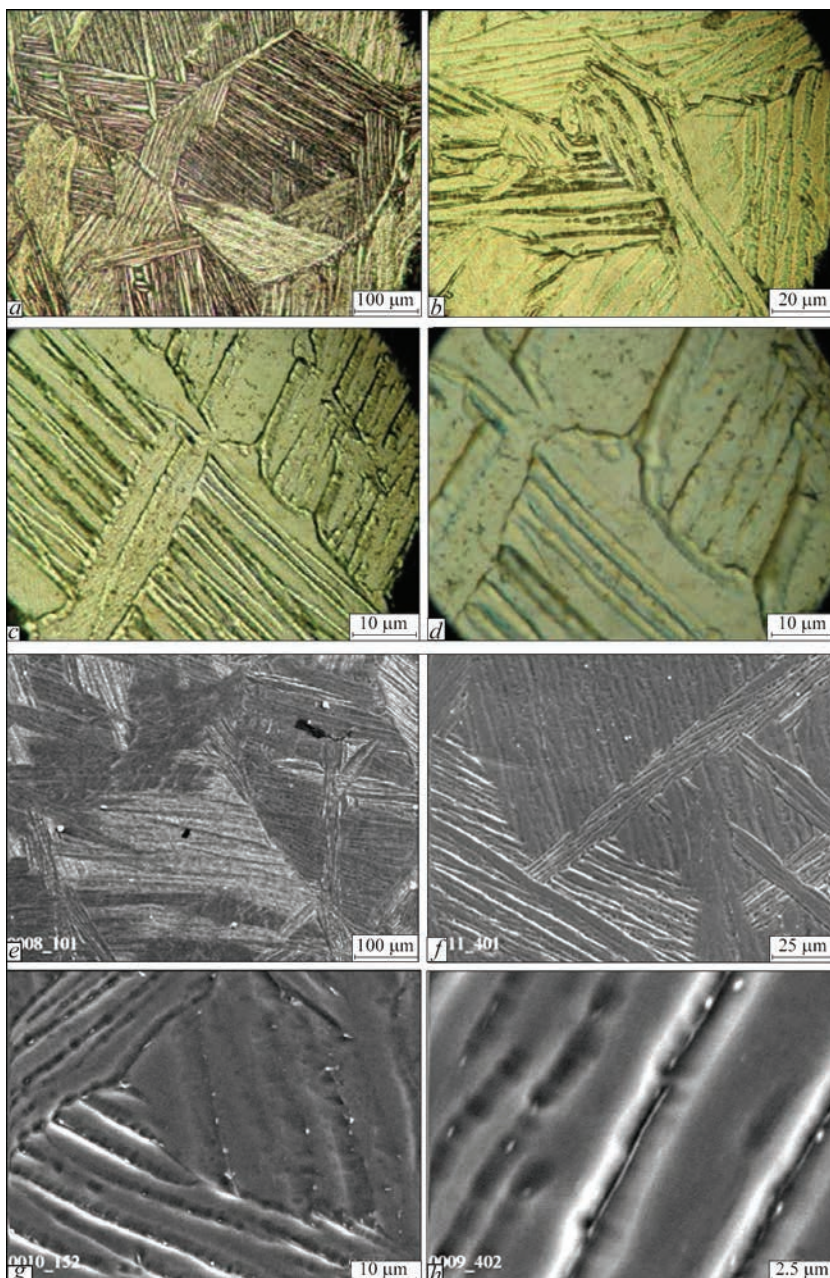


Figure 5. Optical (a–d) and scanning electron (e–h) microscopy of cast alloy Ti-5Al-5Zr-0.8Si-0.3Mo-0.1Nb (melt 812-208)

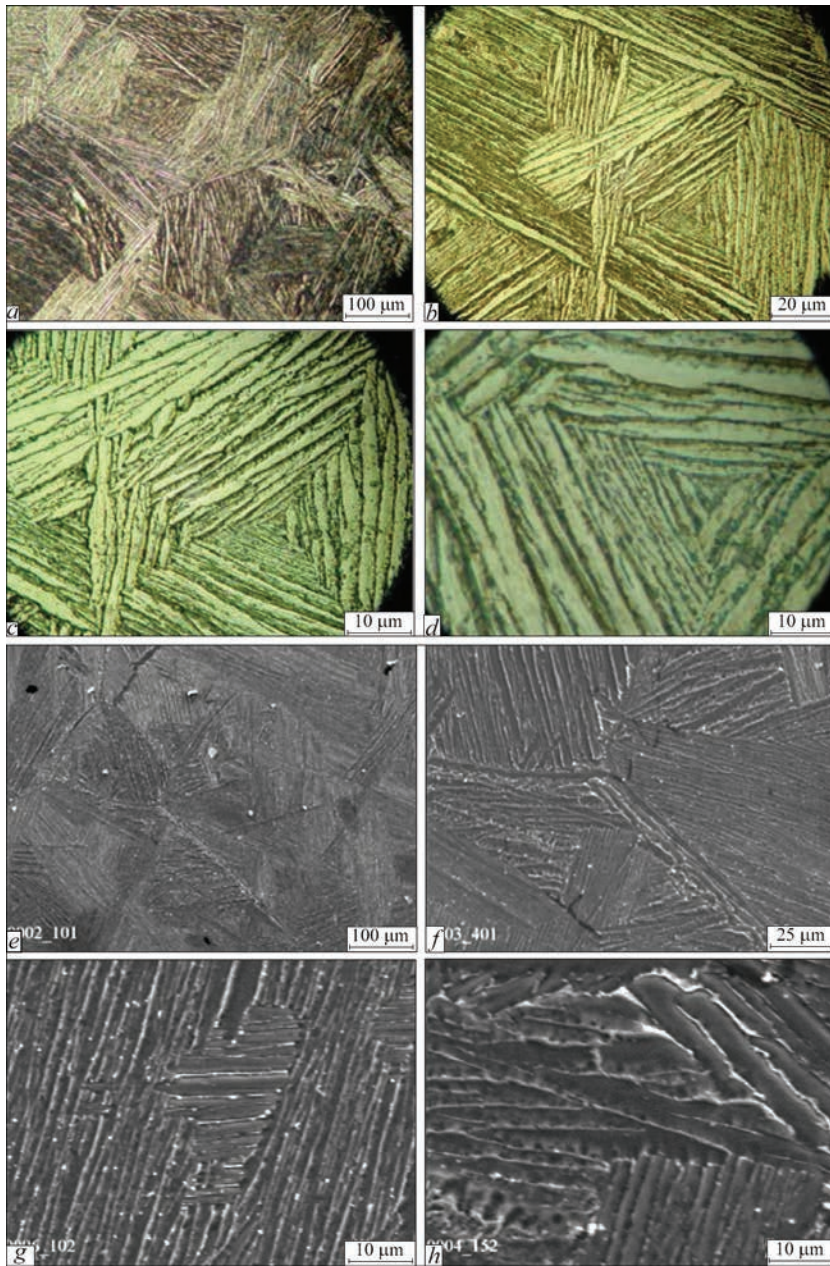


Figure 6. Optical (*a-d*) and scanning electron (*e-h*) microscopy of cast alloy Ti-6.5Al-5.5Zr-0.8Si-0.6Mo-0.5Nb-1.7Sn (melt 815-208)

α -matrix. Figure 8 shows a distribution of the main alloying elements in the cast alloy of 812-208 melt. It can be seen that except of titanium the silicides and their interlayers at the grain boundaries also contain zirconium, i.e. in the investigated alloys there is formation of the complex silicides of $(Zr, Ti)_5Si_3$ and $(Ti, Zr)_3Si$ type, which were earlier found in Ti-Zr-Si-Nb system alloys [17]. Zirconium and silicon are in solid solution as well as in hardening silicide phase that is distributed along the boundaries of former β -grains and α -plates. Thus, alloying elements have significant effect on silicon solubility in titanium.

Aluminium has uniform enough distribution in the structure. It is virtually completely located in the solid solution, almost absent at the boundaries of grains and

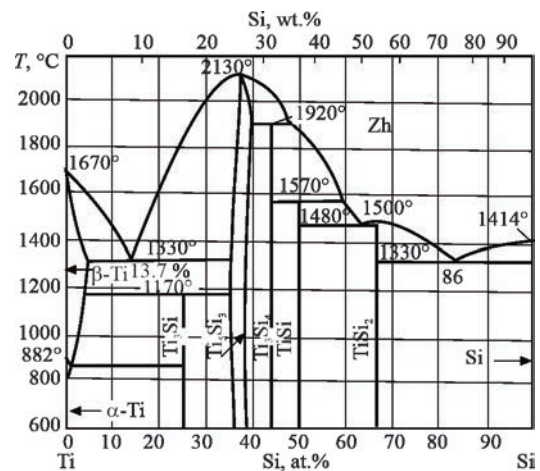


Figure 7. State diagram of titanium-silicon system

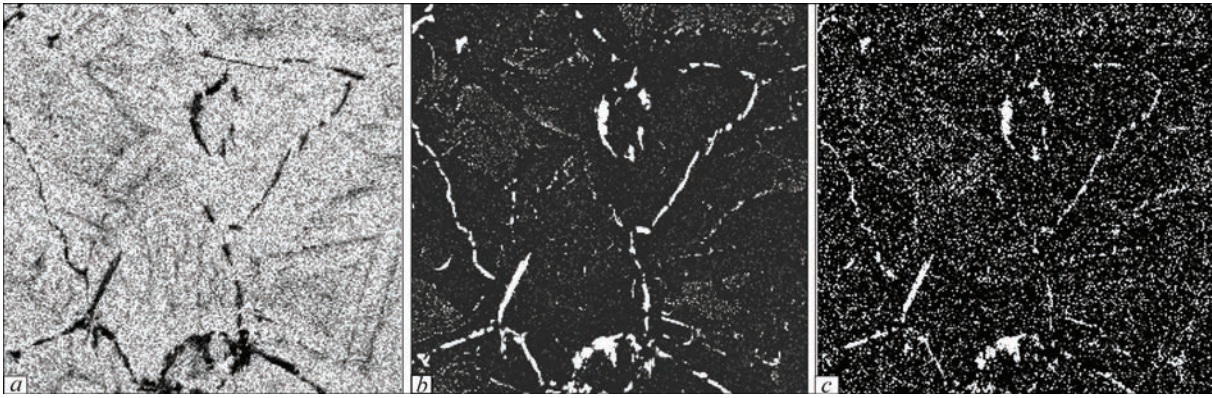


Figure 8. Distribution of doping elements (*a* — Al; *b* — Si; *c* — Zr) in cast alloy Ti–5Al–5Zr–0.8Si–0.3Mo–0.1Nb (815-208 melt)

present in smaller quantity sometimes in the spaces of α -plate batches in the places, where, probably, residual β -phase is present. The size of grains and plates of α -phase depends on silicon content as well as additional alloying in investigated cast titanium alloys. For quantitative evaluation of the lamellar structure the following parameters are used D (β -grain size), d (size of α -plates colonies) and b (width of α -plates). The average size of the grains of cast alloys makes approximately 300–500 μm , alloy 815-208 has finer structure elements (α -plates and their colonies) in comparison with alloy 812-208. Thus, in alloy 812-208 the width of α -plates makes 3–5 μm and in alloy 815-208 it is 2–3 μm (see Figures 5, 6).

In the structure of alloy 812-208 the amount of silicides on the boundaries of former β -grains and between α -plates is smaller than in alloy 815-208. Composition of the latter differs by additional content of tin, which is often used for titanium alloys doping for the purpose of increase of their heat resistance. Addition of tin promotes slowdown of processes of redistribution of the alloying elements between α - and β -phases that rises thermal stability of high-temperature alloys [18].

CONCLUSIONS

1. Performed set of works showed that the electron beam melting allows obtaining metal of ingots of high-temperature Ti–Al–Zr–Si–Mo–Nb–Sn system titanium alloys being characterized with sufficient chemical homogeneity and absence of defects of cast origin (pores, cavities, inclusions of low and high density).

2. It is shown that microstructure of examined cast alloys represent itself the batches of lamellar α -phase in the limits of primary β -grains that have different crystallographic orientation.

3. It is determined that additional alloying elements have significant effect on silicon solubility in titanium. They form complex silicides of (Zr, Ti)₅Si₃ and (Ti, Zr)₃Si type in the investigated alloys.

4. It is shown that presence of tin reduces solubility of silicon in the investigated alloys and therefore increases precipitation of silicides, at that the structure is also refined.

REFERENCES

- Garmata, V.A., Petrunko, A.N., Galitsky, N.V. et al. (1983) *Titanium*. Moscow, Metallurgiya [in Russian].
- Khorev, A.I., Khorev, M.A. (2005) Titanium alloys, their application and prospects of development. *Materialovedenie*, **7**, 25–34 [in Russian].
- Khorev, A.I. (2007) Theory and practice of producing of titanium alloys for prospective structures. *Tekhnologiya Mashinostroeniya*, **12**, 5–13 [in Russian].
- Antonyuk, S.L., Molyar, A.G., Kalinyuk, A.N. et al. (2003) Titanium alloys for aircraft industry of Ukraine. *Advances in Electrometallurgy*, **1**, 9–13.
- Babenko, E.P., Dolzhenkova, E.V. (2014) Examination of fracture causes of VT23 alloy large-sized product. *Metallurgicheskaya i Gornorudnaya Promyshlennost*, **3**, 82–85 [in Russian].
- Iliin, A.A., Kolachev, B.A., Polkin, I.S. (2009) *Titanium alloys. Composition, structure, properties: Handbook*. Moscow, VILS-MATI [in Russian].
- Firstov, S.O. (2004) *New generation of titanium-based materials*. In: *Fracture mechanics of materials and strength of structures*. Ed. by V.V. Panasyuk. Lviv, PMI, 609–616 [in Ukrainian].
- Wu, T., Beaven, P., Wagner, R. (1990) The Ti₅(Al, Si)–Ti₅(Si, Al)₃ eutectic reaction in the Ti–Al–Si system. *Scripta Metallurgica*, **24**, 207–212.
- Salpadoru, H.H., Flower, H.M. (1995) Phase equilibria and transformations in a Ti–Zr–Si system. *Metall. Mater. Transact.*, **26A(2)**, 243–257.
- Kuzmenko, M.M. (2008) Structure and mechanical properties of cast alloys of Ti–Si system. *Fizyko-Khimichna Mekhanika Materialiv*, **44(1)**, 45–48 [in Ukrainian].
- Firstov, S.O., Kulak, L.D., Kuzmenko, M.M., Shevchenko, O.M. (2018) Ti–Al–Zr–Si system alloys for high temperature operation. *Fizyko-Khimichna Mekhanika Materialiv*, **54(6)**, 30–35 [in Ukrainian].
- Paton, B.E., Trigub, N.P., Akhonin, S.V., Zhuk, G.V. (2006) *Electron beam melting of titanium*. Kyiv, Naukova Dumka [in Russian].
- Akhonin, S.V., Severin, A.Yu., Berezos, V.A. et al. (2016) Peculiarities of melting of titanium alloy VT19 ingots in electron beam cold hearth installation. *Sovrem. Electrometall.*, **2**, 23–27 [in Russian].

14. Akhonin, S.V., Pikulin, A.N., Berezos, V.A. et al. (2019) Laboratory electron beam unit UE-208M. *Sovrem. Electrometall.*, **3**, 15–22 [in Russian]. DOI: <https://doi.org/10.15407/sem2019.03.03>
15. Akhonin, S.V., Firstov, S.A., Severin, A.Yu. et al. (2019) Electron beam melting of heat-resistant titanium composites of Ti-Si-Al-Zr-Sn. *Sovrem. Electrometall.*, **2**, 7–12 [in Russian]. DOI: <http://dx.doi.org/10.15407/sem2019.02.02>
16. (2000) *State diagrams of binary metallic system: Handbook*, Vol. 3. Ed. by N.P. Lyakishev. Moscow, Mashinostroenie [in Russian].
17. Shevchenko, O.M., Kulak, L.D., Kuzmenko, M.M., Firstov, S.O. (2020) Influence of zirconium alloying on structure and hardness of quenched cast biocompatible Ti-18Nb-1Si alloy. *Metalofizyka i Novitni Tekhnologii*, **42(2)**, 237–249 [in Ukrainian].
18. Solonina, O.P., Glazunov, S.G. (1976) Titanium alloys. Heat-resistant titanium alloys. Moscow, Metallurgiya [in Russian].

ORCID

S.V. Akhonin: 0000-0002-7746-2946,
 V.O. Berezos: 0000-0002-5026-7366,
 O.M. Pikulin: 0000-0001-6327-3848,
 A.Yu. Severyn: 0000-0003-4768-2363,
 O.O. Kotenko: 0000-0002-0930-9536,

M.M. Kuzmenko: 0000-0001-8108-7088,
 L.D. Kulak: 0000-0001-7861-0931,
 O.M. Shevchenko: 0000-0001-6726-7269

CONFLICT OF INTEREST

The Authors declare no conflict of interest

CORRESPONDING AUTHOR

S.V. Akhonin
 E.O. Paton Electric Welding Institute of the NASU
 11 Kazymyr Malevych Str., 03150, Kyiv, Ukraine.
 E-mail: akhonin.sv@gmail.com

SUGGESTED CITATION

S.V. Akhonin, V.O. Berezos, O.M. Pikulin, A.Yu. Severyn, O.O. Kotenko, M.M. Kuzmenko, L.D. Kulak, O.M. Shevchenko (2022) Producing high-temperature titanium alloys of Ti-Al-Zr-Si-Mo-Nb-Sn system by electron beam melting. *The Paton Welding J.*, **7**, 39–45.

JOURNAL HOME PAGE

<https://pwj.com.ua/en>

Received: 11.04.2022

Accepted: 15.09.2022

DEVELOPED IN UKRAINE

xBeam Metal Printing

Allows no longer have to choose between fine accuracy, defect-free metal structure and high productivity. The new patented solutions are based on the exclusive ability of gas-discharge electron beam gun to generate hollow conical electron beam providing unique physical conditions for precisely controllable metal deposition and forming of desired metal structure in produced 3D metal part.

Advantages.

xBeam 3D Printing has a set of technical, technological and commercial benefits that help it to stand out from any other in metal additive manufacturing (more information in «The Paton Welding Journal» #9_2022).

<https://xbeam3d.com/>



METALLURGICAL PROCESSES IN THE WELD METAL IN ELECTRON BEAM WELDING OF 01570 ALUMINIUM ALLOY

V.V. Skryabinskiy¹, V.M. Nesterenkov¹, M.O. Rusynyk¹, A.V. Mykytchyk²

¹E.O. Paton Electric Welding Institute of the NASU

11 Kazymyr Malevych Str., 03150, Kyiv, Ukraine

²SC “International Center for Electron Beam Technologies

of the E.O. Paton Electric Welding Institute of the NAS of Ukraine”

68 Antonovych Str., 03150, Kyiv, Ukraine

ABSTRACT

Scandium and zirconium content was determined in different areas of welded joints of stamped semi-finished products of 01570 aluminium alloy produced by electron beam welding. It was found that dissolution of not only secondary, but also of a part of primary Al₃(Sc, Zr) intermetallics, contained in the base metal, takes place in the weld pool. The quantity of scandium dissolved in the liquid metal, is determined by the time of the pool existence. Further on, scandium is completely or partially fixed in an oversaturated solid solution, depending on the rate of hardening during the weld metal cooling. At 0.10–0.12 % concentration of scandium dissolved in the weld pool, its complete transition into an oversaturated solid solution ensures hardening at not less than 5·10² °C/s rate. It is shown that approximately 50 % of scandium contained in 01570 alloy, participates in hardening of stamped semi-finished products. The remaining scandium is present in the composition of primary intermetallics.

KEYWORDS: electron beam welding; aluminium alloy; hardening; artificial aging; intermetallics

INTRODUCTION

The 01570 alloy is the most strength among other thermally non-strengthened wrought aluminium alloys of Al–Mg system [1]. By the level of strength properties, wrought semi-finished products of 01570 alloy in the annealed state approach the level of properties of wrought semi-finished products of thermally strengthened aluminium alloys in the state after hardening and artificial aging. It should be noted that heat treatment in the form of annealing for 01570 alloy is strengthening. The chemical composition of the alloy is given in Table 1. In casting of the alloy ingots, a fixation of scandium in an oversaturated solid solution, i.e., hardening occurs. At a subsequent annealing, a decomposition of an oversaturated solid solution of scandium in aluminium with the precipitation of secondary strengthening fine-dispersed particles of Al₃Sc phase occurs. In this connection, as far as concerns 01570 alloy, annealing will be further on called artificial aging. Both for alloys of Al–Sc and Al–Mg–Sc systems in general, as well as for 01570 alloy, in particular, artificial aging at 350 °C of 1 h duration provides the highest increase in strength properties [1, 2]. This heat treatment mode appeared to be better to increase the strength of welded joints of semi-finished products of 01570 alloy [3]. Artificial aging of welded

joints produced by electron beam welding (EBW) improves hardness of the weld metal above the level of hardness of the base metal of stamped semi-finished products, and ruptured specimens cut out from aged welded joints are destroyed over the base metal outside the heat-affected zone. This fact gave reason to assume that with an artificial aging in the weld metal, a higher quantity of fine-dispersed secondary Al₃Sc intermetallics precipitated than initially in the base metal.

To form this excess quantity of particles, three conditions should be fulfilled.

First, an additional scandium is required, that has not previously participated in strengthening of the metal. This scandium is formed in the metal at the stage of producing ingots in the form of primary Al₃Sc precipitates.

Secondly, along with a complete dissolution of secondary intermetallics in the weld pool metal, it is necessary to dissolve primary intermetallics at least partially. Due to the fact that after artificial aging, the hardness of the weld metal becomes higher than the hardness of the base metal, such dissolution takes place. It is important to note that the greatest increase in hardness (i.e., more full dissolution of primary intermetallics) occurs at a low welding speed, when the

Table 1. Chemical composition of 01570 alloy (GOST 4784–2019), wt. %

Al	Mg	Mn	Sc	Zr	Ti	Si	Fe	Cu	Zn
Base	5.3–6.3	0.2–0.6	0.17–0.27	0.05–0.15	0.01–0.05	<0.2	<0.3	<0.1	<0.1

time of staying the metal in the liquid state in the area of exposure to the electron beam increases [4].

Third, during cooling of the weld metal dissolved in a liquid metal, scandium should be fixed in a solid oversaturated solution. The complete transition of scandium from the melt into an oversaturated solid solution grows with an increase in the rate of hardening [5]. And in EBW of 01570 alloy, it was found that a decrease in welding speed from 16.8 to 2.8 mm/s and, accordingly, reduction in the rate of hardening from $1 \cdot 10^4$ to $5 \cdot 10^2$ °C/s does not decrease, but on the contrary increases the hardness of the weld metal. Therefore, it can be assumed that all or almost all scandium, dissolved in a liquid weld pool metal transfers into a solid solution and further on, during aging, it is released in the form of secondary Al_3Sc intermetallics.

The main factor that restrains the widespread use of aluminium-magnesium alloys with scandium is a high cost of scandium. To reduce the consumption of scandium while maintaining high service characteristics, in aluminium-magnesium alloys, zirconium is introduced. Zirconium is introduced into 01570 metal together with scandium. It dissolves in Al_3Sc intermetallic, replacing atoms of scandium, maintaining and stabilizing its properties [6]. In alloys of Al-Mg system, the optimal content of scandium and zirconium is considered to be 0.22–0.24 and 0.10–0.12 %, respectively. If the specified content is elevated, the excess scandium and zirconium in the alloy are in the form of primary $Al_3(Sc, Zr)$ intermetallics, deteriorating the service characteristics of the alloy [7]. For example, in Al–Mg–Sc–Zr alloy at 77 K, primary $Al_3(Sc, Zr)$ phases are responsible for arising of cavities and cracks on their interface with a matrix at cryogenic temperature [8]. At a decrease in the specified content, the possibilities of scandium and zirconium are not fully used.

Concerning quantities of these primary intermetallics, the literature gives contradicting data. Previously, the developers of 01570 alloy wrote that the bulk part of scandium remains in an oversaturated solid solution [1, 9] (from this part, at a subsequent thermomechanical treatment, strengthening secondary intermetallics Al_3Sc are formed), and some negligible part of it is precipitated from the melt in the form of relatively large primary intermetallics [10]. In [11] it is asserted that to form a strengthening phase (secondary intermetallics), 50 % of scandium and zirconium is spent, which is introduced into 01570 alloy. The rest of these elements are contained in primary intermetallics.

The aim of the work is to study the features of metallurgical processes occurring in the weld pool in EBW of 01570 alloy, determining the quantity of

scandium and zirconium, which goes to the formation of secondary intermetallics in the weld metal and the minimum rate of hardening required for a complete transition of scandium into an oversaturated solid solution during cooling of the weld.

RESEARCH METHODS AND EQUIPMENT

The studies were conducted on the plates of 01570 alloy with a thickness of 30 mm. The plates were welded in the electron beam welding installation UL-209M with ELA 60/60 power source at an accelerating voltage of 60 kV.

On cross-sections with the help of Rockwell device, the hardness of the weld metal and near-weld area was measured. The measurements were carried out during loading on a steel ball of 600 N on a scale B. The mechanical properties of the weld metal were determined by the rupture test of standard cylindrical specimens with the diameter of working part being 4.0 mm and clamps of 9.0 mm diameter.

The test specimens were cut out from the weld metal along the welding direction so that the working parts of the specimens and the adjacent areas consisted of the weld metal. The scheme of cutting out specimens is shown in Figure 1.

The microstructure of the specimens was investigated on transverse sections with the use of the electron microscope Carl Zeiss Sigma 300 at an accelerated voltage of 15 kV.

To determine the chemical composition of different areas of the base metal, weld and intermetallic particles, X-ray spectral microanalyzer Oxford Instruments XMAX-350 (attached analyzer PEM Carl Zeiss Sigma 300) and software for calculating results were used.

EXPERIMENTAL INVESTIGATIONS AND RESULTS

The plates of stamped semi-finished products of 01570 alloy were welded in the lateral position using a horizontal beam. The welding modes are given in Table 2. As the beam scanning amplitude increases

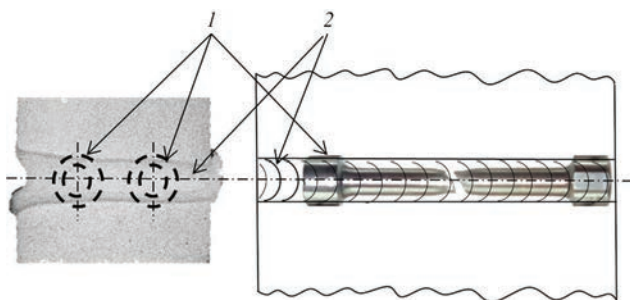


Figure 1. Scheme of cutting out specimens for tensile tests of weld metal: 1 — specimens; 2 — weld

Table 2. EBW modes for welding plates of 1570 alloy of 30 mm thickness

Welding mode	U_b , kV	v_w , mm/s	I_b , mA	Amplitude of beam scanning, mm	Weld width, mm	Rate of hardening of weld metal, °C/s
1	60	2.8	95	1.5	3.5	$5 \cdot 10^2$
2		16.8	260	Same	Same	$1 \cdot 10^4$
3		2.8	130	4.0	7.0	Was not measured
4		6.0	220	Same	Same	Same
5		12.0	310	»	»	»
6		16.8	350	»	»	»

from 1.5 to 4.0 mm, the width of the weld increased from 3.5 to 7.0 mm (Figure 2).

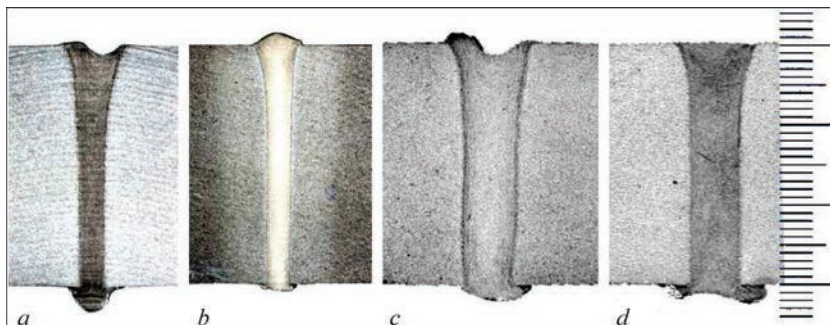
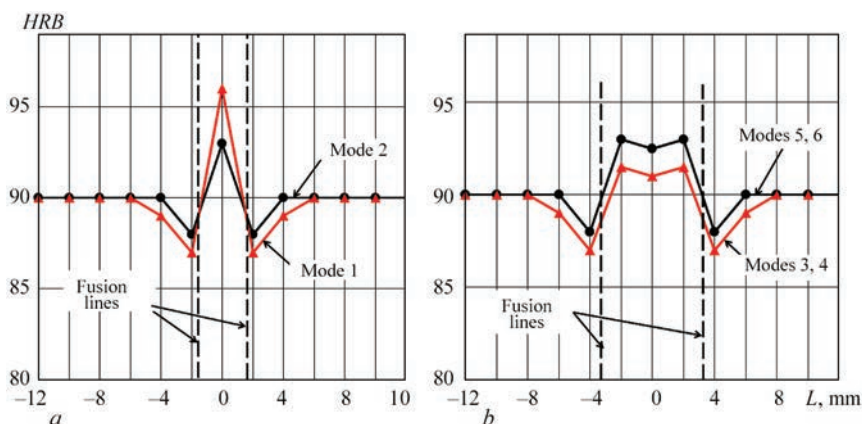
For measurements of hardness and mechanical tests after welding, the plates of 01570 alloy were artificially aged at a temperature of 350 °C during 1 h.

The results of measuring hardness of welded joints showed that for all the studied welding modes, the hardness of the weld metal is by 2–6 *HRB* units higher than the hardness of the base metal (Figure 3). The highest hardness (about 96 *HRB*) is in the narrow welds produced at a welding speed of 2.8 mm/s (mode 1). In the case of an increase in the width of the weld from 3.5 to 7.0 mm (mode 3), its hardness is reduced to 91–92 *HRB*. The hardness of the weld metal produced at a welding speed of 16.8 mm/s (modes 2 and 6) is almost independent of their width and is about 93 *HRB*.

Figure 4 shows intermetallics in the base metal (a) and in the metal of welds, produced at a speed of 16.8 mm/s (b) and 2.8 mm/s (c). On the photos against the backdrop of the dark matrix, light, apparently, primary intermetallics are seen, containing scandium and zirconium with the size from 1.0 to 15.0 μm . The inclusions of a rounded shape (Figure 4, d, e) or in the form of irregular polyhedra (Figure 4, f) are encountered. Their chemical composition is wt.%: Al — 60–62, Sc — 21–22, Zr — 17–18.

Fine (1–3 μm) primary intermetallics are distributed in the matrix relatively uniformly, and larger ones (5–15 μm) are chaotic.

At magnifications $\times 500$ and $\times 1800$, it is impossible to detect nanosized secondary $\text{Al}_3(\text{Sc}, \text{Zr})$ intermetallics, which are contained in the base metal. Therefore, the quantity of scandium and zirconium contained in

**Figure 2.** Transverse macrosections of welded joints of plates of stamped semi-finished product of 01570 alloy with a thickness of 30 mm: a — mode 1; b — 2; c — 3; d — 6**Figure 3.** Distribution of hardness in the transverse sections of welded joints of 01570 alloy after artificial aging with an amplitude of electron beam scanning of 1.5 mm (a) and 4.0 mm (b)

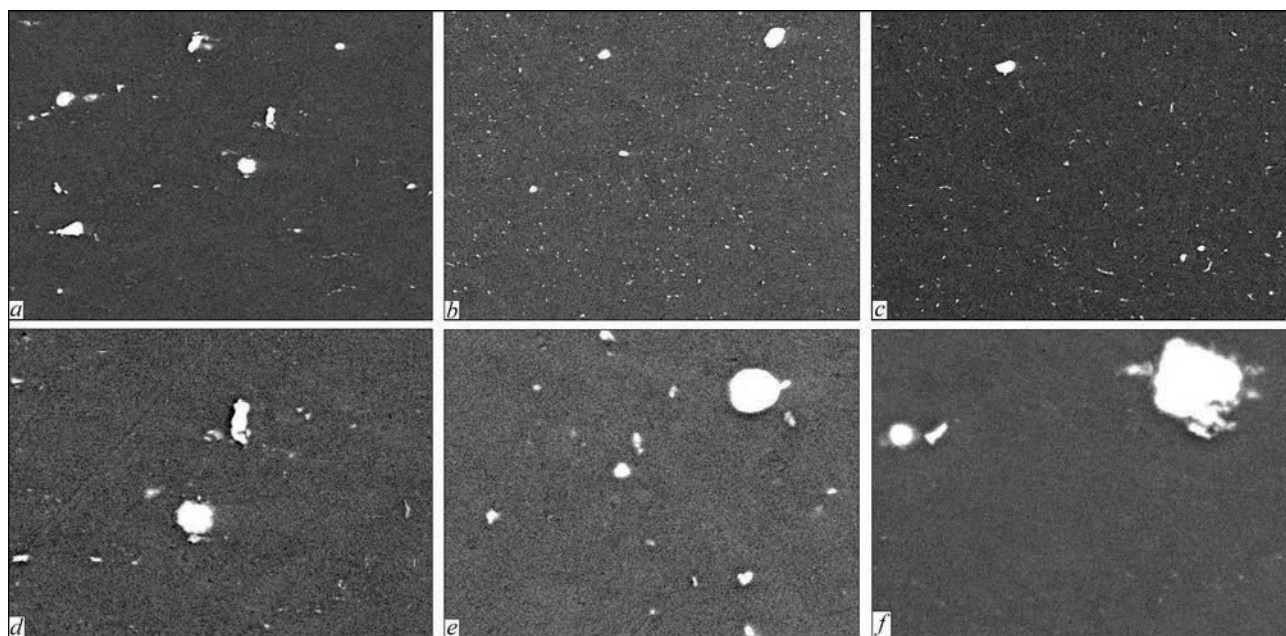


Figure 4. $\text{Al}_3(\text{Sc}, \text{Zr})$ intermetallics in the base metal of 01570 alloy (*a, d*) and in the weld metal in EBW on the mode 2 (*b, e*) and on the mode 1 (*c, f*): *a-c* — $\times 500$; *d-g* — $\times 1800$

them was determined in the regions of matrix, which do not contain primary intermetallics. The content of scandium and zirconium in different areas of welded joints is shown in Table 3.

Secondary intermetallics of the base metal contain about 0.10 % of Sc and 0.07–0.90 % of Zr. This means that in strengthening of stamped semi-finished products of 01570 alloy, not more than a half of the most expensive alloying element — scandium participated. And in a solid solution of the weld metal, scandium content increased and amounts to 0.11 % during welding at a speed of 16.8 mm/s (mode 2) and 0.12 % at a welding speed of 2.8 mm/s (mode 3). Zirconium content in a solid solution of welds amounts to about 0.1 %.

The mechanical properties of the weld metal of 01570 alloy produced at different welding speeds after artificial aging are shown in Table 4. When the welding speed grows from 2.8 to 16.8 mm/s, the strength and ductility of the weld metal increase. The ultimate strength of the weld metal increases from 375 to 385 MPa, the conditional yield strength grows from 230 to 240 MPa, and the relative elongation rises from 15 to 25 %.

RESEARCH RESULTS AND THEIR DISCUSSION

Let us consider the results of measuring hardness, obtained on the specimens produced on the modes 1 and 2 (see Table 2, welds of 3.5 mm width). From Figure 3, *a* it is seen that the hardness of all artificially aged welds is higher than the hardness of the base metal. Moreover, in welding at a speed of 2.8 mm/s, the hardness is higher than at a speed of 16.8 mm/s.

Such an increase in hardness can be explained as follows. During the EBW process, nanosized secondary $\text{Al}_3(\text{Sc}, \text{Zr})$ intermetallics, contained in the base metal, are completely dissolved in a liquid metal of the weld pool. In addition, in the metal of the pool, a partial dissolution of relatively large primary intermetallics occurs. The longer the period of the weld pool existence, the larger part of refractory primary intermetallics succeeds in dissolving in a liquid metal. Therefore, at a low welding speed (2.8 mm/s), the content of scandium dissolved in a liquid metal is higher than at a high welding speed (16.8 mm/s). This is confirmed by an X-ray spectral analysis of a solid solution of the weld metal. In a solid solution of the weld metal, produced at speeds of 2.8 and 16.8 mm/s, scandium is contained in the quantities of 0.12 and 0.11 %, respectively. As was mentioned above, for the welds of 3.5 mm width, produced at welding speeds of both 2.8 as well as 16.8 mm/s, the rates of hardening are sufficient for all scandium dissolved in the weld metal, to be completely fixed in a solid solution during cooling. Further, at an artificial ageing of welded joints in the welds produced at a welding speed

Table 3. Content of scandium and zirconium in different areas of welded joints, wt. %

Place of determination	Sc	Zr
Primary intermetallics	21–22	17–18
Base metal in the areas that do not contain primary intermetallics	0.10	0.07–0.09
Solid solution of the weld metal:		
Mode 2	0.11	0.10
Mode 3	0.12	0.10

Table 4. Mechanical properties of welded joints of 01570 alloy, produced at different welding rates after artificial aging

Welding speed, mm/s (welding mode)	σ_r , MPa	σ_y , MPa	δ , %	ψ , %
2.8 (3)	$\frac{374.2-378.0}{375.4}$	$\frac{229.5-231.1}{230.3}$	$\frac{14.7-15.4}{15.1}$	$\frac{38.3-41.5}{40.1}$
6 (4)	$\frac{375.6-376.2}{375.8}$	$\frac{226.1-232.4}{229.2}$	$\frac{14.6-15.2}{14.9}$	$\frac{26.4-28.3}{27.2}$
12 (5)	$\frac{377.2-384.1}{382.6}$	$\frac{232.2-232.3}{232.3}$	$\frac{17.7-18.3}{18.1}$	$\frac{20.9-21.8}{21.2}$
16.8 (6)	$\frac{379.8-386.4}{384.2}$	$\frac{236.6-239.7}{238.5}$	$\frac{19.1-26.0}{23.5}$	$\frac{41.5-42.0}{41.8}$

of 2.8 mm/s, more strengthening secondary $Al_3(Sc, Zr)$ intermetallics are precipitated than in the welds in welding at a speed of 16.8 mm/s, which causes their higher strengthening. A partial dissolution of primary $Al_3(Sc, Zr)$ intermetallics, contained in the base metal is the reason that the hardness of both welds became higher than the hardness of the base metal.

Further, it was determined what is happening when the volume of the weld pool is increased. The hardness of the welds produced on the modes 1 and 2 (see Table 2, welds of 3.5 mm width) with the hardness of the welds, produced on the modes 3 and 6 (see Table 2, welds of 7.0 mm width) was compared. From Figure 3, it is seen that in this case, the hardness of the aged weld metal after welding at a speed of 16.8 mm/s remained at a level of 93 *HRB*, and at a speed of 2.8 mm/s, it decreased from 96 to 91–92 *HRB*. Such a decrease in hardness can only be explained by a reduction in the rate of hardening. As the width of the weld (i.e., the volume of the weld pool) increases, the time of the metal existing in the liquid state grows. I.e., in welding on the mode 3, in a liquid pool, dissolved no less, but most probably more both secondary as well as primary $Al_3(Sc, Zr)$ intermetallics, as compared to welding on the mode 1.

In this case, the rate of cooling the weld metal and, accordingly, the rate of its hardening could only decrease. Thus, the rate of hardening was not sufficiently high for the full transition of scandium from the melt into an oversaturated solid solution and after aging, the density of precipitates of strengthening secondary $Al_3(Sc, Zr)$ particles in the welds of 7.0 mm width (mode 3) appeared to be lower than in the welds of 3.5 mm width (mode 1). Thus, it can be concluded that the rate of hardening of $5 \cdot 10^2$ °C/c is minimal for the full transition of scandium dissolved in a liquid metal into an oversaturated solid solution. At least, this assertion should be fair at 0.11–0.12 % concentration of scandium in the melt, as it was in our studies.

The results of mechanical tests of the metal of the artificially aged welds are confirmed by the results obtained during the measurement of hardness. The

higher the hardness of the weld metal, the higher its strength characteristics.

CONCLUSIONS

1. In the process of EBW of 01570 alloy in the weld pool, a dissolution of not only secondary but also of a part of primary $Al_3(Sc, Zr)$ intermetallics occurs, contained in the base metal. The quantity of scandium dissolved in a liquid metal is determined by the time of the pool existence. Depending on the rate of hardening during cooling of the weld metal, scandium is fully or partially fixed in an oversaturated solid solution.

2. At 0.10–0.12 % concentration of scandium dissolved in the weld pool, its full transition to an oversaturated solid solution is provided by hardening at a rate of at least $5 \cdot 10^2$ °C/c.

3. In strengthening of stamped semi-finished products, about 50 % of scandium contained in 01570 alloy, is involved. The remaining scandium forms a composition of primary intermetallics of 1–15 μm size, nonuniformly distributed over the metal structure.

REFERENCES

1. Filatov, Yu.A. (2014) Alloys of Al–Mg–Sc system as the special group of wrought aluminium alloys. *Tekhnologiya Lyogkikh Splavov*, **2**, 34–41 [in Russian].
2. Drits, M.E., Toropova, L.S., Anastasieva, G.K. et al. (1984) Influence of homogenizing heatings on properties of alloys of Al–Sc and Al–Mg–Sc systems. *Izv. AN SSSR, Metall*, **3**, 196–201 [in Russian].
3. Skryabinskiy, V.V., Nesterenkov, V.M., Rusnyk, M.O., Strashko, V. (2020) Effect of mode of electron beam welding, heat treatment and plastic deformation on strength of joints of aluminium 1570 alloy. *The Paton Welding J.*, **5**, 10–15. <https://patonpublishinghouse.com/eng/journals/tpwj/2020/05/02>
4. Nesterenkov, V.M., Skryabinskiy, V.V., Rusnyk, M.O. (2021) Effect of thermal cycles in electron beam welding of aluminium 1570 alloy on mechanical properties of welded joints. *The Paton Welding J.*, **5**, 40–45. <https://patonpublishinghouse.com/eng/journals/as/2021/05/06>
5. Berezina, A.L., Segida, E.A., Monastyrskaya, T.A., Kotko, A.V. (2008) Influence of crystallization rate on abnormal oversaturation of Al–Mg–Sc alloys. *Metallofizika i Novejshie Tekhnologii*, **30**(6), 849–857 [in Russian].
6. Davydov, V.G., Elagin, V.I., Zakharov, V.V., Rostova, T.D. (1996) About of doping of aluminium alloys with scandium

and zirconium additives. *Metallovedenie i Termicheskaya Obrabotka Metallov*, **8**, 25–30 [in Russian].

7. Zakharov, V.V., Fisenko, I.A. (2013) On economy of scandium in its doping of aluminium alloys. *Tekhnologiya Lyogkikh Splavov*, **4**, 52–60 [in Russian]. <https://cyberleninka.ru/article/n/ob-ekonomii-skandiya-pri-legirovanii-im-alyuminievyh-splavov/viewer>
8. Zhao, W.T., Yan, D.S., Li, X.Y. et al. (2006) Tensile property of Al–Mg–Sc–Zr alloy at cryogenic temperature. *AIP Conf. Proc.*, **824**, 169–175. <https://aip.scitation.org/doi/abs/10.1063/1.2192348?journalCode=apc>
9. Filatov, Yu.A. (2013) Aluminium alloys of Al–Mg–Sc system for welded and brazed structures. *Tekhnologiya Lyogkikh Splavov*, **2**, 36–42 [in Russian]. <https://cyberleninka.ru/article/n/alyuminievye-splavy-sistemy-al-mg-sc-dlya-svarnyh-i-payanyh-konstruktsiy/viewer>
10. Elagin, V.I. (2004) History, successes and problems of doping of aluminium alloys with transition metals. *Tekhnologiya Lyogkikh Splavov*, **3**, 6–29 [in Russian].
11. Valuev, V.V. (1988) Microstructure of large-sized ingots of 01570 aluminium alloy. *Metallovedenie i Termich. Obrab. Metallov*, **6**, 15–17 [in Russian].

ORCID

V.V. Skryabinskyi: 0000-0003-4470-3421,

V.M. Nesterenkov: 0000-0002-7973-1986,
M.O. Rusynyk: 0000-0002-7591-7169,
A.V. Mykytchuk: 0000-0002-9761-9429

CONFLICT OF INTEREST

The Authors declare no conflict of interest

CORRESPONDING AUTHOR

V.M. Nesterenkov

E.O. Paton Electric Welding Institute of the NASU

11 Kazymyr Malevych Str., 03150, Kyiv, Ukraine.

E-mail: nesterenkov@technobeam.com.ua

SUGGESTED CITATION

V.V. Skryabinskyi, V.M. Nesterenkov,

M.O. Rusynyk, A.V. Mykytchuk (2022)

Metallurgical processes in the weld metal in electron beam welding of 01570 aluminium alloy. *The Paton Welding J.*, **7**, 46–51.

JOURNAL HOME PAGE

<https://pwj.com.ua/en>

Received: 12.04.2022

Accepted: 15.09.2022

WORLD TRADE FAIR FOR WELDING ENGINEERING —
JOINING, CUTTING, SURFACING

LET'S JOIN
THE WORLD!

11. – 15. September, 2023

REGISTER NOW!

www.schweissen-schneiden.com

DVS GERMAN WELDING SOCIETY

MESSE ESSEN

SCHWEISSEN & SCHNEIDEN
No. 1 IN THE WORLD

SUBSCRIPTION-2023



«The Paton Welding Journal» is Published Monthly Since 2000 in English, ISSN 0957-798X, doi.org/10.37434/tpwj.

«The Paton Welding Journal» can be also subscribed worldwide from catalogues subscription agency EBSCO.

If You are interested in making subscription directly via Editorial Board, fill, please, the coupon and send application by Fax or E-mail.

12 issues per year, back issues available.

\$384, subscriptions for the printed (hard copy) version, air postage and packaging included.

\$312, subscriptions for the electronic version (sending issues of Journal in pdf format or providing access to IP addresses).

Institutions with current subscriptions on printed version can purchase online access to the electronic versions of any back issues that they have not subscribed to. Issues of the Journal (more than two years old) are available at a substantially reduced price.

SUBSCRIPTION COUPON	
Address for journal delivery	_____
Term of subscription since	_____ 20 _____ till _____ 20 _____
Name, initials	_____
Affiliation	_____
Position	_____
Tel., Fax, E-mail	_____

The archives for 2009–2020 are free of charge on www://patonpublishinghouse.com/eng/journals/tpwj



ADVERTISING

in «The Paton Welding Journal»

External cover, fully-colored:

- First page of cover (200×200 mm) — \$700
- Second page of cover (200×290 mm) — \$550
- Third page of cover (200×290 mm) — \$500
- Fourth page of cover (200×290 mm) — \$600

Internal cover, fully-colored:

- First/second/third/fourth page (200×290 mm) — \$400

Internal insert:

- (200×290 mm) — \$340
- (400×290 mm) — \$500

- Article in the form of advertising is 50 % of the cost of advertising area
- When the sum of advertising contracts exceeds \$1001, a flexible system of discounts is envisaged
- Size of Journal after cutting is 200×290 mm

Address

11 Kazymyr Malevych Str. (former Bozhenko Str.), 03150, Kyiv, Ukraine

Tel.: (38044) 205 23 90

Fax: (38044) 205 23 90

E-mail: journal@paton.kiev.ua

www://patonpublishinghouse.com/eng/journals/tpwj